

# DUAL ENERGY/SPECTRAL CT PARADIGM OF IMAGING

- TODAY'S CT IMAGING
  - SINGLE SLICE TO SPIRAL/SLIP RING /MULTI DETECTOR
  - ISOTROPIC VOXEL-MULTI-PLANE-2D/3D RECON.
- NEW PARADIGM OF MATERIALS CHARACTERIZATION
  - “DUAL ENERGY CT”- APPLICATION OF TWO X-RAY PHOTON ENERGYS
  - NEW SPECTRAL TISSUE ANALYSIS-”DECOMPOSTION”
- BREAKING THE HOUNSFIELD “BARRIER”

# DUAL ENERGY/SPECTRAL CT TODAYS POLAR VORTEX



JUST LIKE WINTER CT IS EVOLVING



# Godfrey Hounsfield: Intuitive Genius of CT

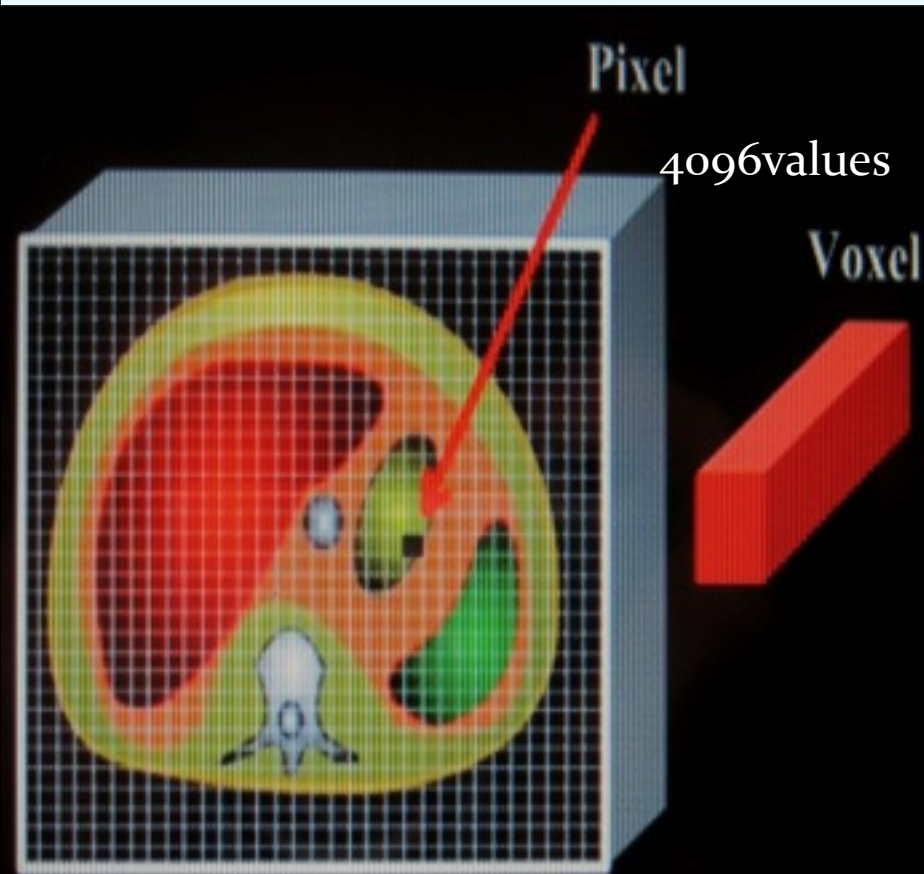


"IT IS AMAZING WHAT CAN BE DONE WITH A HACKSAW AND A MICROMETER."

Dr. G. HOUNSFIELD - 28 JULY 1972



# THE “HU” BARRIER / PARADIGM (amount of attenuation per voxel)



CT Image: Pixel and Voxel





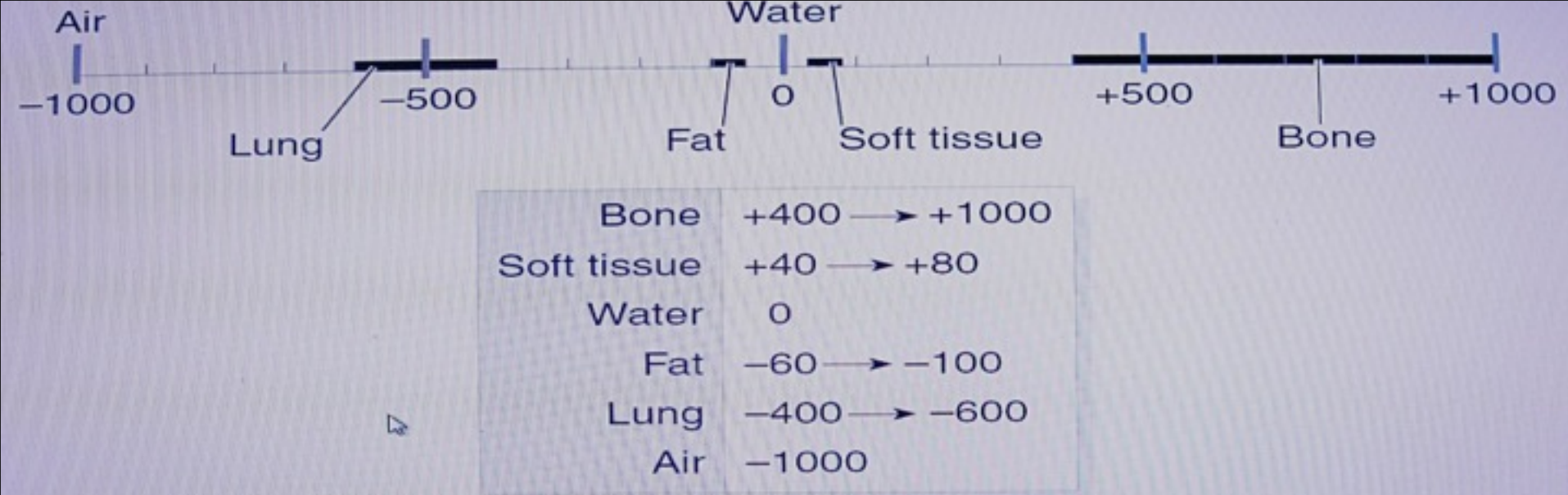


## Image Formation

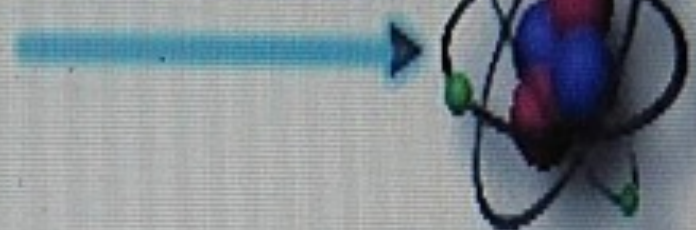
**Voxel (volume element)** - for each image slice, there is an x, y and z dimension. These are coming close to isotropic (the same in each dimension). A typical voxel would be created from a 35 cm FOV, 512 x 512 matrix and 0.6 - 10.0 mm thick slice.



# Attenuation

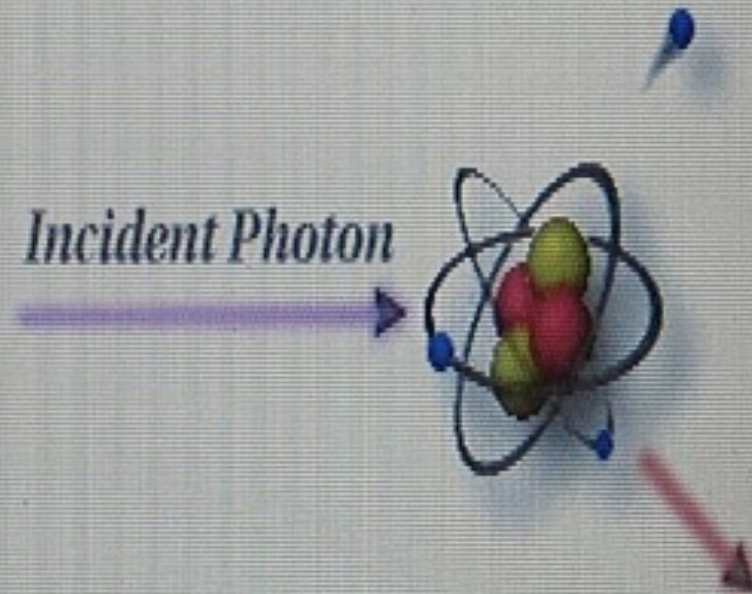
- When x-ray photons interact with matter, the quantity is reduced from the original x-ray beam
- Attenuation is the result of interactions between x-ray and matter that include absorption and scatter
  - Photoelectric absorption
  - Compton scattering
  - Coherent scattering
- Differential absorption increases as kVp decreases

*Incident Photon*



**Compton Scatter**

*Incident Photon*





# Material Characterization

- Materials better differentiated by applying two X-ray spectra and analyzing attenuation differences.
- Technique works well for compounds with large atomic numbers differences between them as it takes advantage of the photoelectric effect  $\sim Z^3$ , and k edge of iodine

# THE APPLIED TUBE ENERGY=KVP

## KILO ELECTRON VOLT =KEV

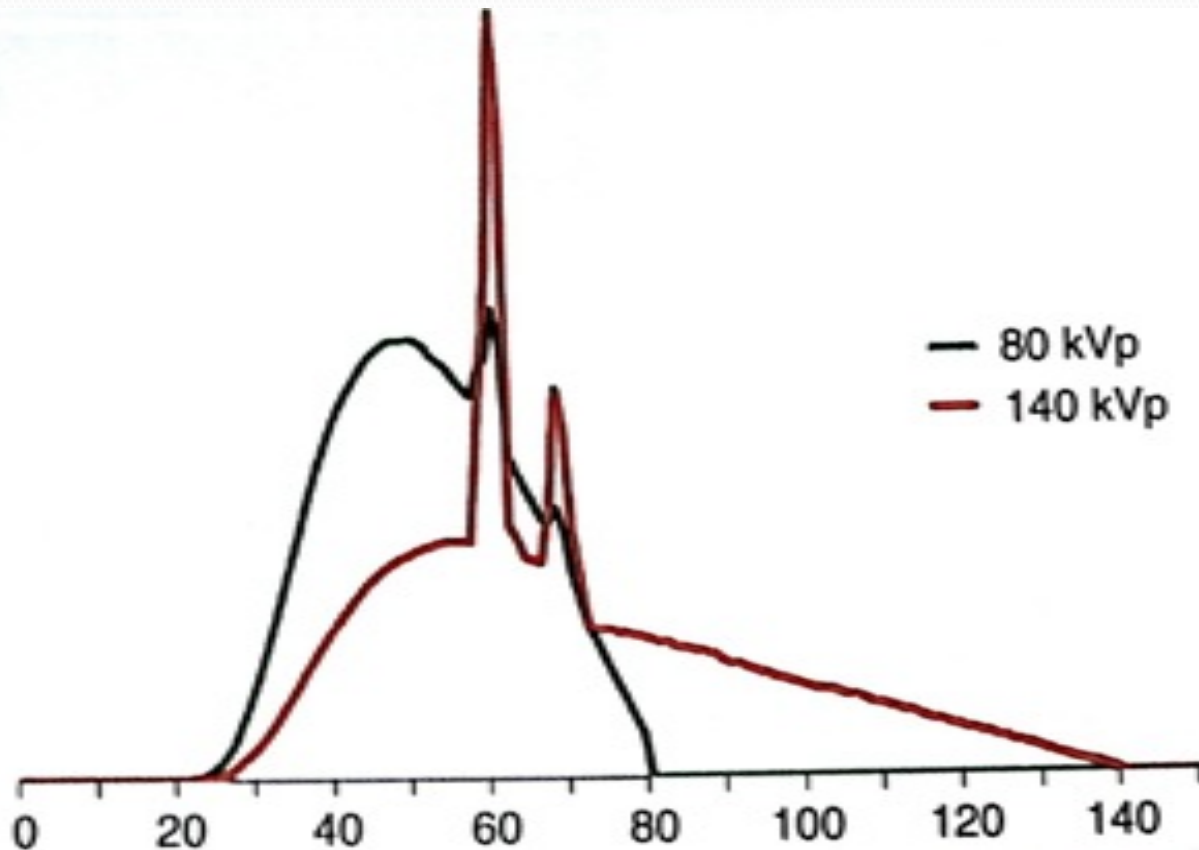
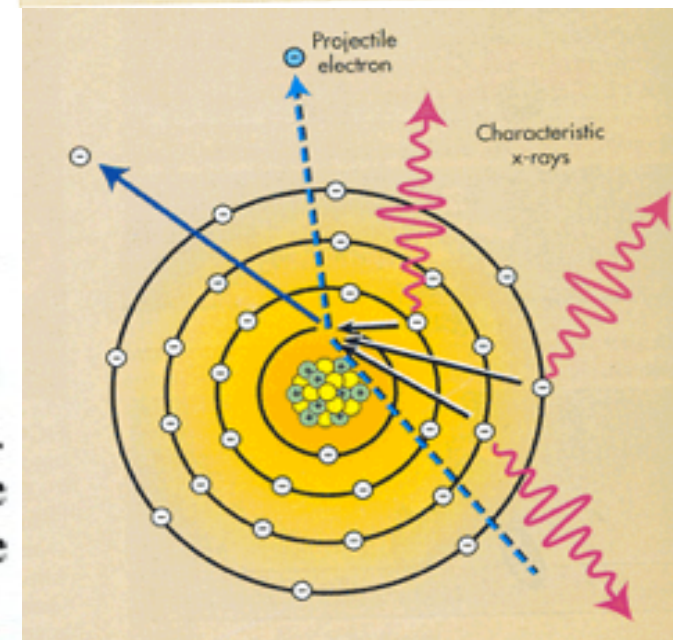
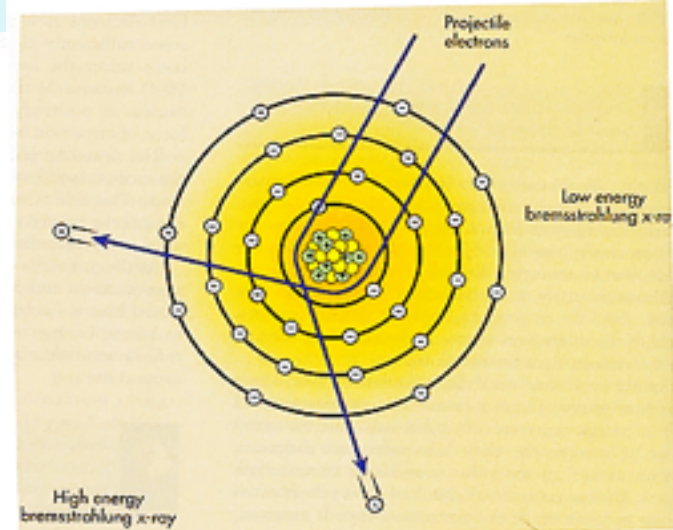


**Fig. 1** Spectra of the Straton tube at 140 and 80 kV potential. The *peaks* represent the characteristic lines of the tungsten anode and the continuous spectrum is a result of Bremsstrahlung. The mean photon energies are 53 and 71 keV, respectively

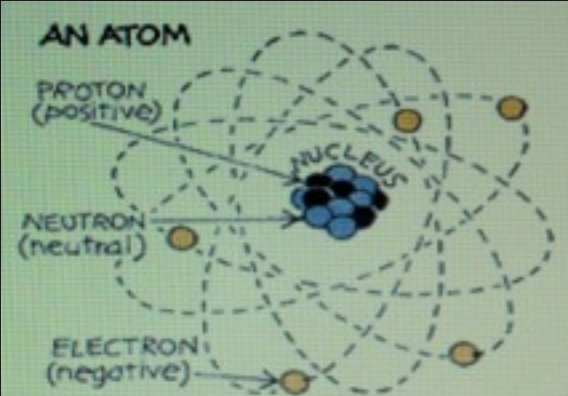




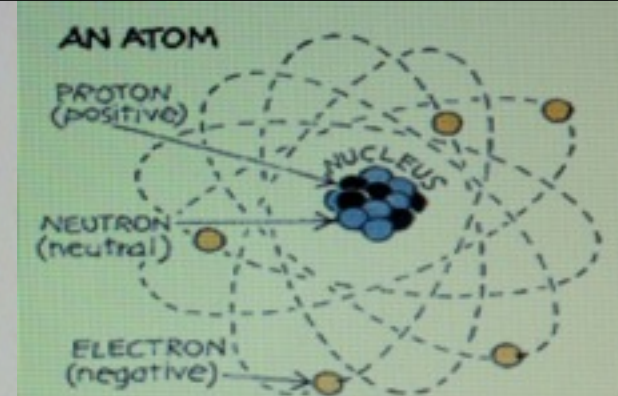
# IODINE Z#53 HAS HIGH ATTENUATION VALUE RELATIVE TO BODY TISSUES

## Human Body Tissue

Substance	Atomic #	Density (kg/m <sup>3</sup> )
Fat	6.3	910
Soft Tissue	7.4	1000
Water	7.5	1000
Muscle	7.6	1000
Bone	13.8	1850



# K-edge



**K-edge** describes a sudden increase in the attenuation coefficient of photons occurring at a photon energy just above the binding energy of the K shell electron of the atoms interacting with the photons. The sudden increase in attenuation is due to photoelectric absorption of the photons. For this interaction to occur, the photons must have more energy than the binding energy of the K shell electrons. A photon having an energy just above the binding energy of the electron is therefore more likely to be absorbed than a photon having an energy just below this binding energy.

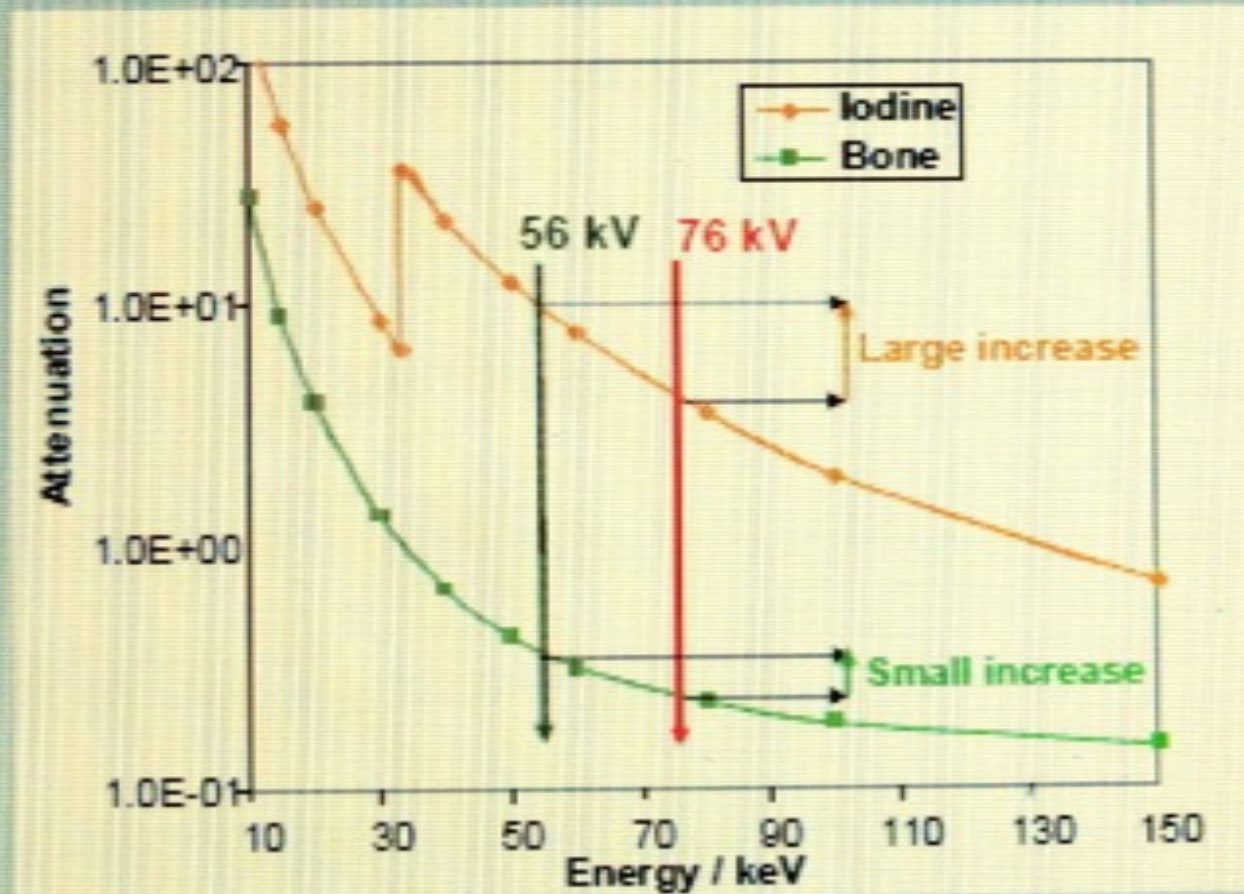
## Use

The two X-ray contrast media iodine and barium have ideal K shell binding energies for absorption of X-rays, 33.2 keV and 37.4 keV, respectively, which is close to the mean energy of most diagnostic X-ray beams. Similar sudden increases in attenuation may also be found for other inner shells than the K shell; the general term for the phenomenon is absorption edge.<sup>[1]</sup>



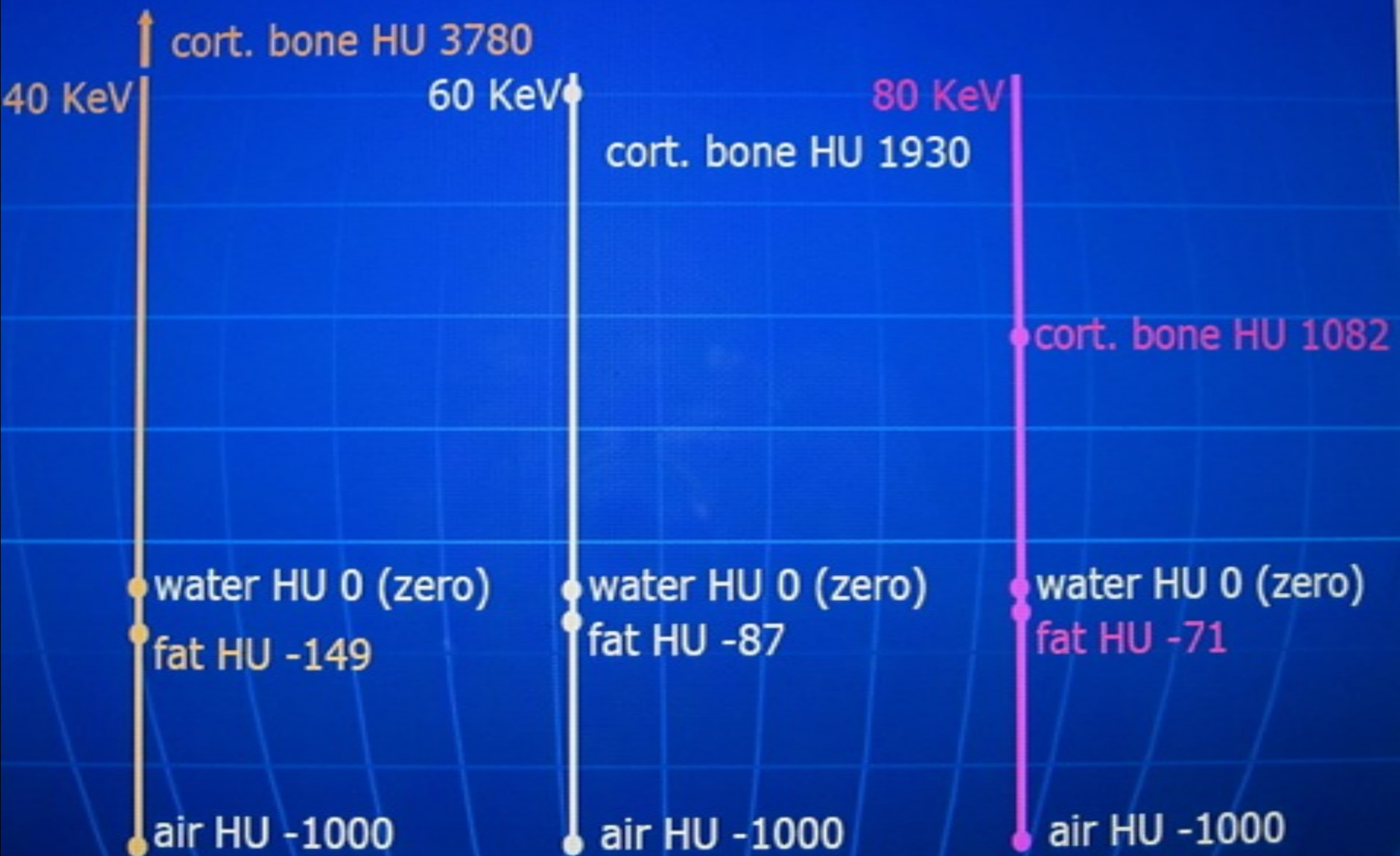
# Principle of Dual Energy CT

- Many materials show different attenuation at different mean energies



- Reason: different attenuation mechanisms (Compton vs photo effect)

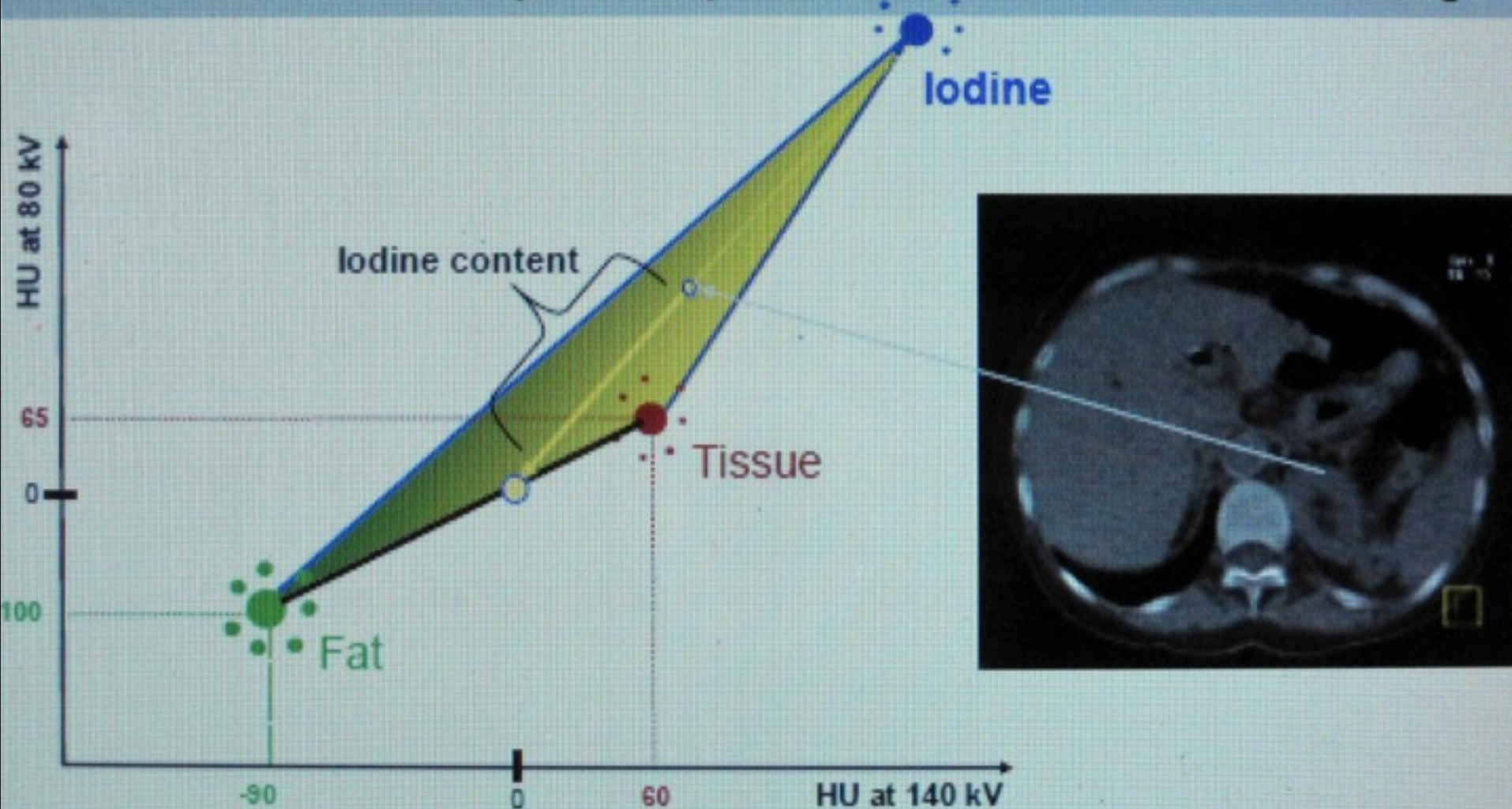
# HU depend upon the X-ray energy





# Applications of Dual Energy CT

- Three material decomposition: **quantification of iodine – iodine image**



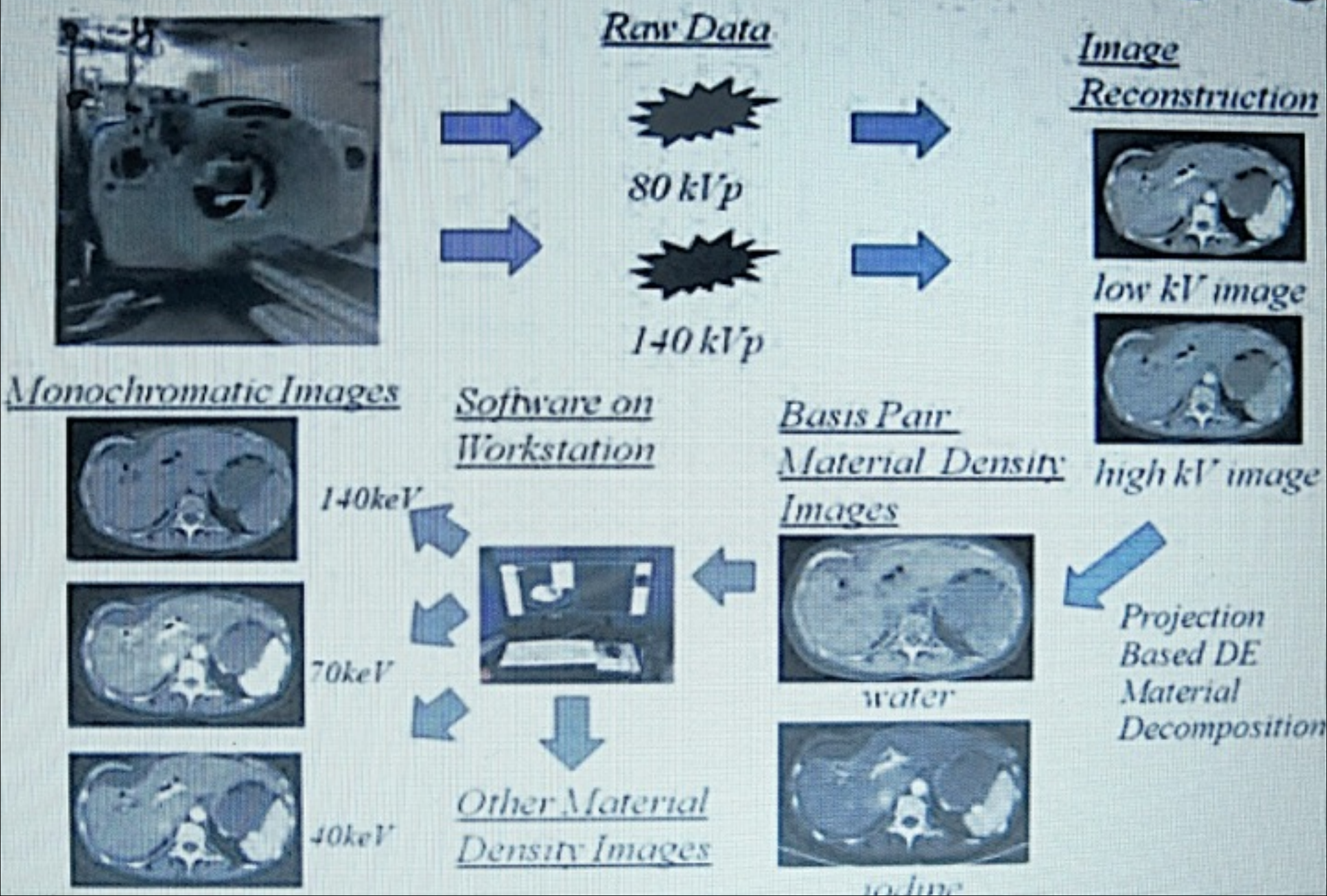
- Removal of iodine from the image: **virtual non-contrast image**

# Virtual non-contrast imaging

- DECT allows for a virtual non-enhancing scan by identifying iodine contrast and subtracting it from the image
- DECT can eliminate need of non-contrast scan and decrease additional radiation exposure
- Able to look at calcium in vessels
- Allows for quantification of iodine content



# Overview of Dual Energy Imaging





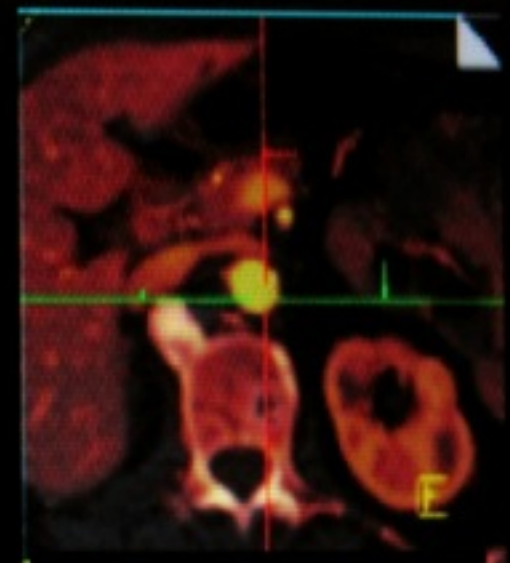
- Most promising application: 3-material decomposition  
→ Calculation of a virtual non-contrast image, Iodine quantification



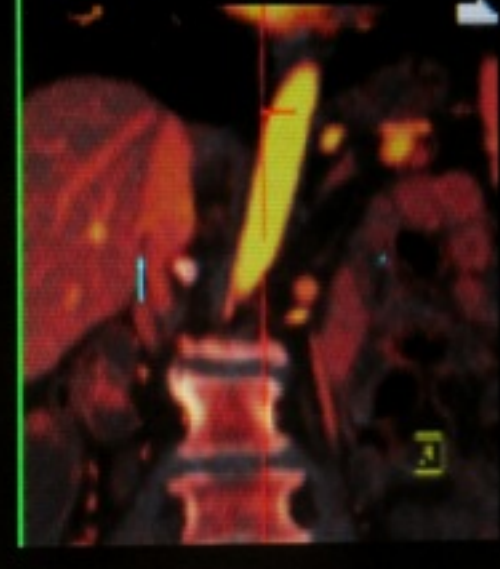
Mixed image 80kV+140kV



Virtual unenhanced image



Iodine overlay image





# Objectives

- How does it work?
  - Approach by vendor
- What is it good for?
  - Established applications
  - Emerging applications



# How to acquire data at two energies? Varies by vendor

- GE - FAST kVp switching
- Philips - Two layer detector
- Siemens - Two x-ray tubes
- Toshiba - Two sequential rotations



# Dose Penalty?

- YES - difficult to obtain dual energy CT images at same dose as single average 120kVp scan
- BUT - if standard practice is C-/C+ scans, a single pass dual energy CT scan may provide virtual non-contrast images
- Small dose increase may justify the additional information obtained

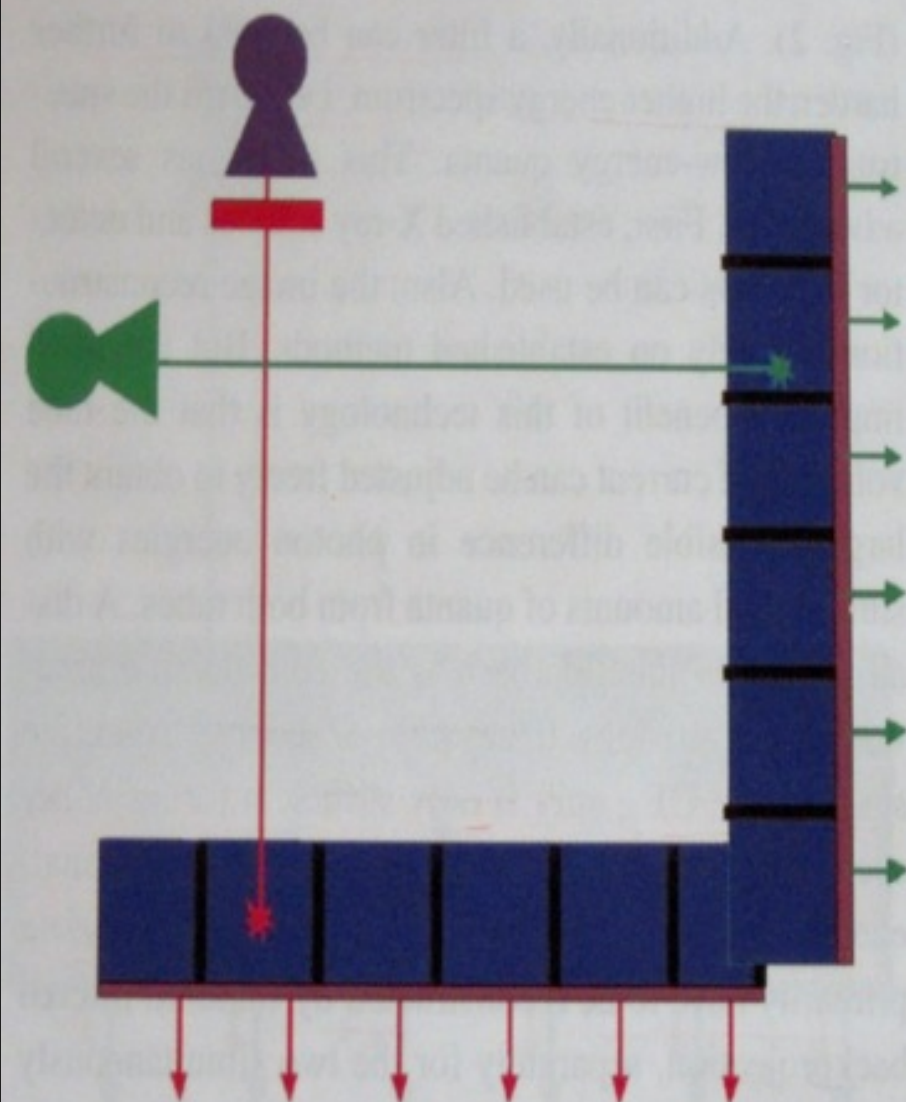
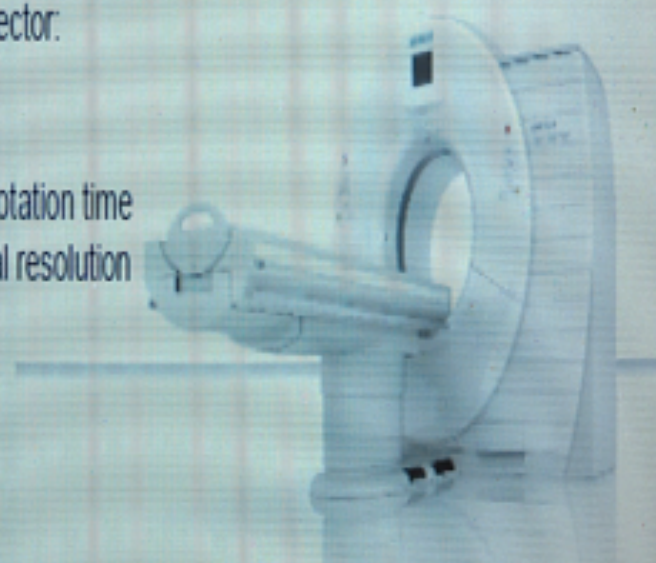
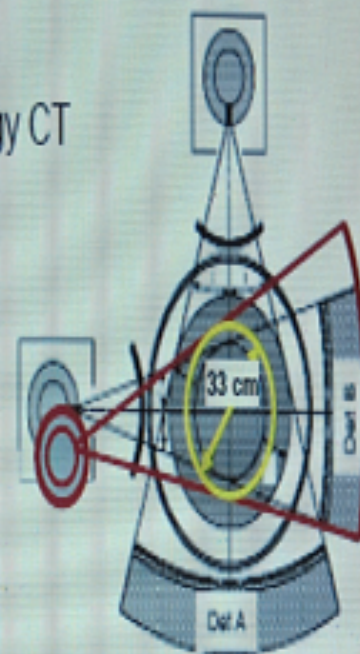


**Fig. 2** Sketch of a dual-source CT system. Two tubes and detectors are mounted orthogonally. To obtain dual-energy datasets, the tubes are operated at different tube voltages, e.g., 80 and 140 kV (*green* and *violet*). Additionally, a filter (indicated in *red*) can be applied to harden the high-energy spectrum

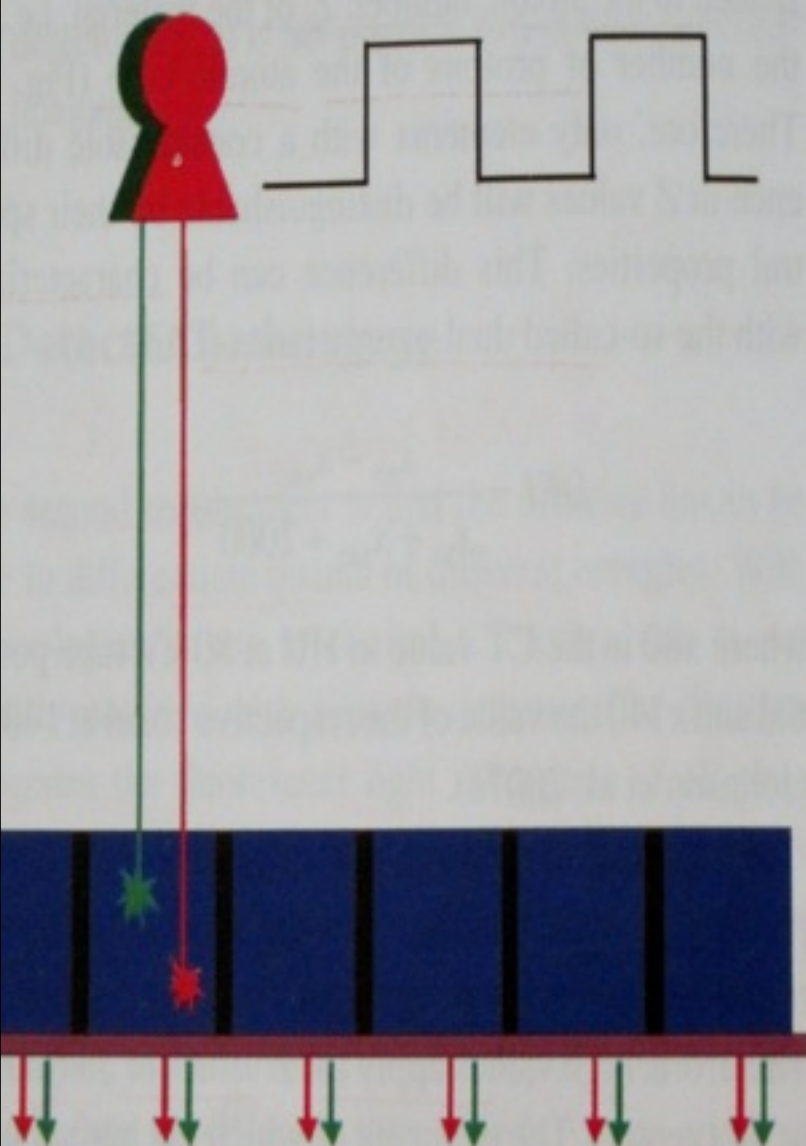
## SOMATOM Definition Flash Latest Generation of Dual Energy CT

### System Design

- Two X-ray tubes at 95°, each with 100 kW
- Two 128-slice detectors, each with 64x0.6mm collimation and z-flying focal spot
- SFOV A/B-detector: 50/33 cm
- 0.28 s gantry rotation time  
75 ms temporal resolution

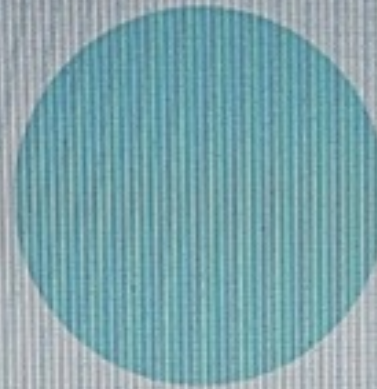




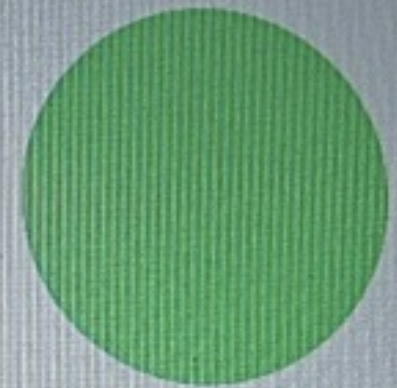


4 Sketch of a rapid kV switching system. There is only one and detector, but the tube voltage is switched rapidly between levels. Optimally, the current is adjusted at least inversely

80KV

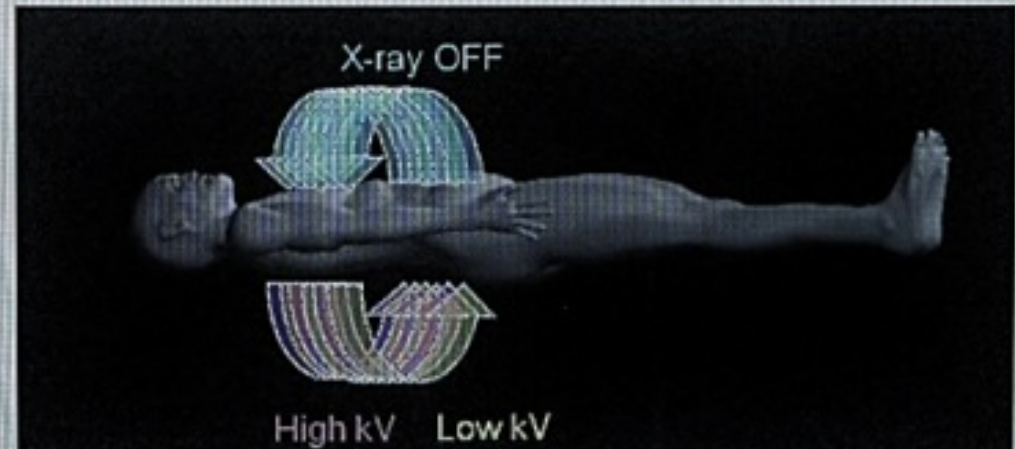


135KV



Scan information - dual energy helical:

- » One helical scan is made during which energy switches between low and high kV
- » To completely cover the region by both energies a low pitch is used
- » Exposure can be turned off at the front side of the patient to minimize dose to the breast area
- » When kV is switched also the mA can be adjusted to achieve identical noise levels in both scans
- » Dual energy helical scans can be made for all rotation speeds under 1s



# Dual Source vs. Spectral Imaging KVP switching

## Dual Source



## Spectral Imaging



NO KVP SETTINGS

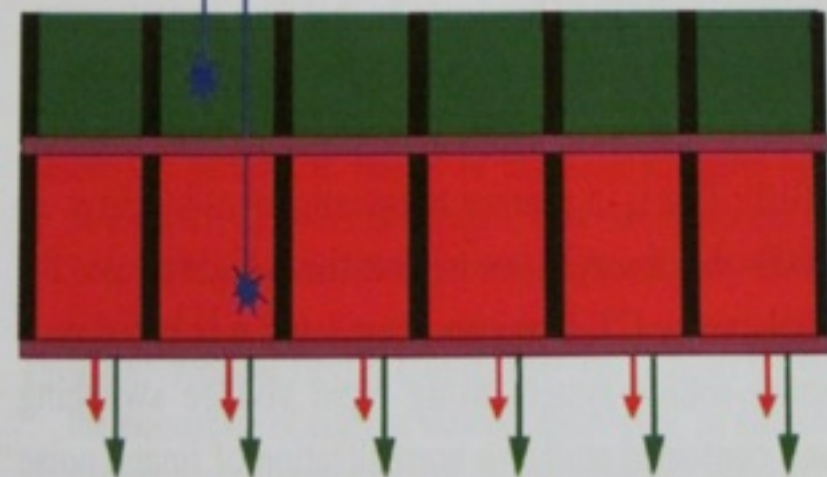
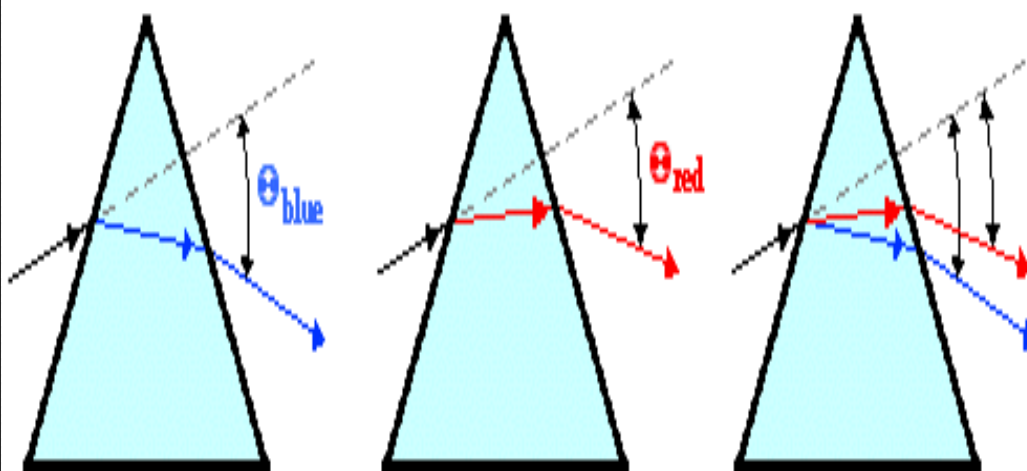
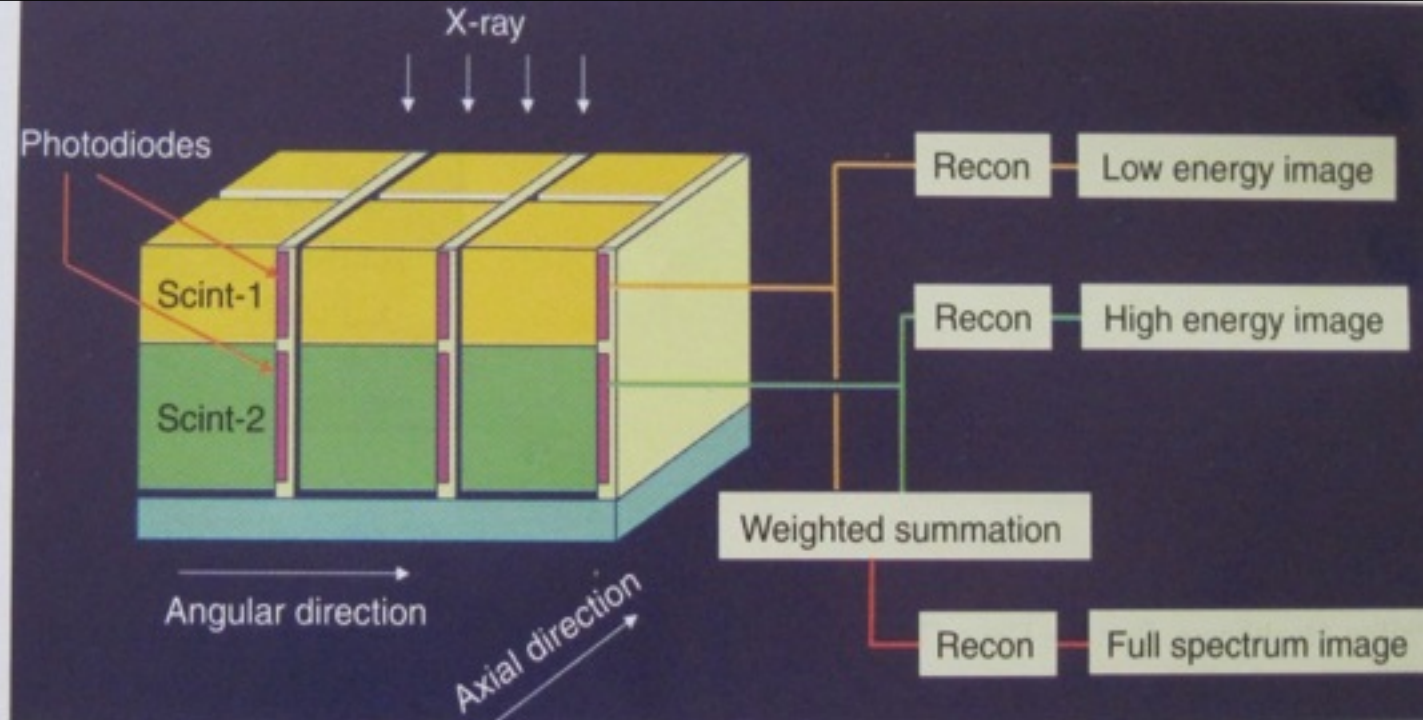


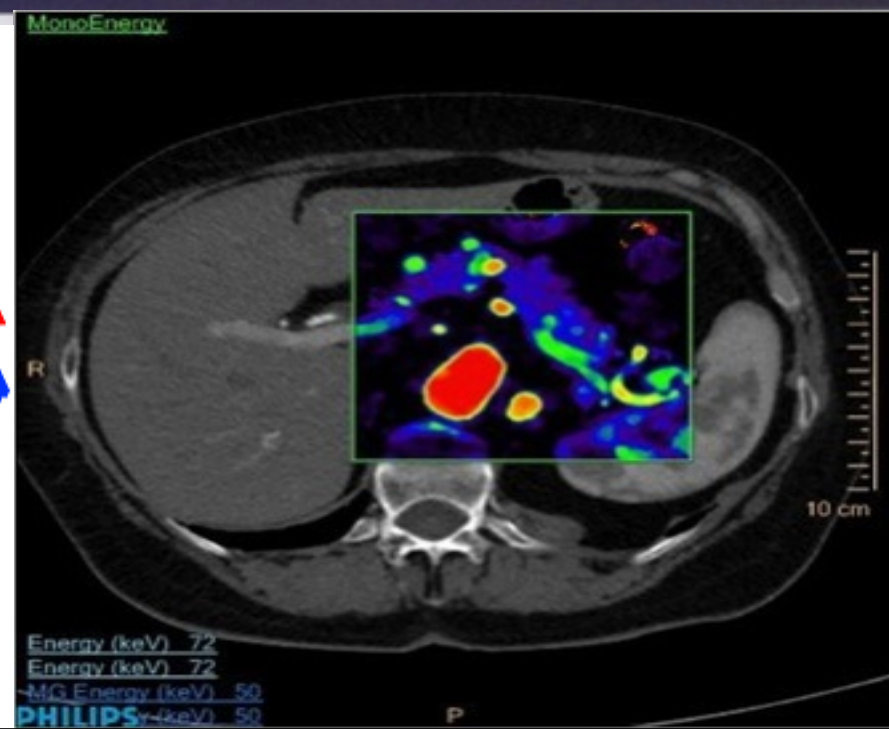
**Fig. 6** Sketch of a layer detector system. There is only one X-ray tube running at constant voltage. The dual-energy information is derived from two layers of the detector with different sensitivity profiles. The *top layer* may, e.g., use CsI or ZnSe as the scintillator so that it is more sensitive to low-energy quanta, while the *bottom layer* may consist of  $Gd_2O_3S$  as the standard material



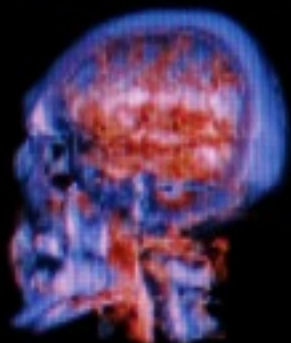
**Fig. 1** A schematic illustration of the dual-layer detection system (only a few detector elements are shown). The photodiodes are parallel to the x-ray direction, attached to the sides of the two types of scintillator elements



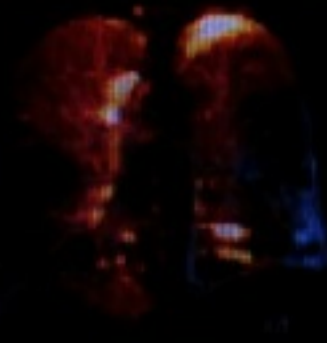
Blue light refracts more than red light due to the difference in wavelength. This causes blue light to deviate from its original path by a greater angle than the red light.



# Spectra of Dual Energy Applications



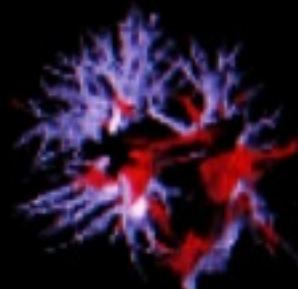
**Direct Angio**



**Lung PBV**



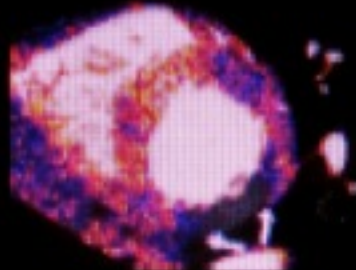
**Virtual Unenhanced**



**Lung Vessels**



**Hardplaque Display**



**Heart PBV**



**Calculi Characterization**



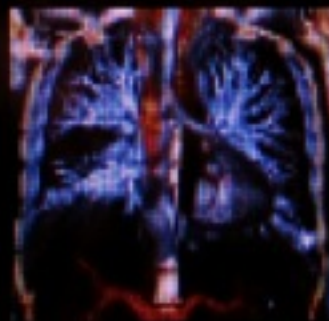
**Brain Hemorrhage**



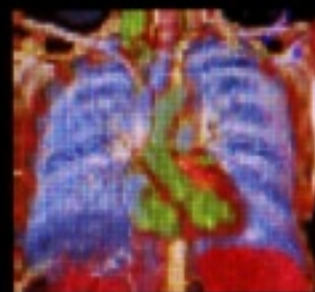
**Musculoskeletal**



**Gout**



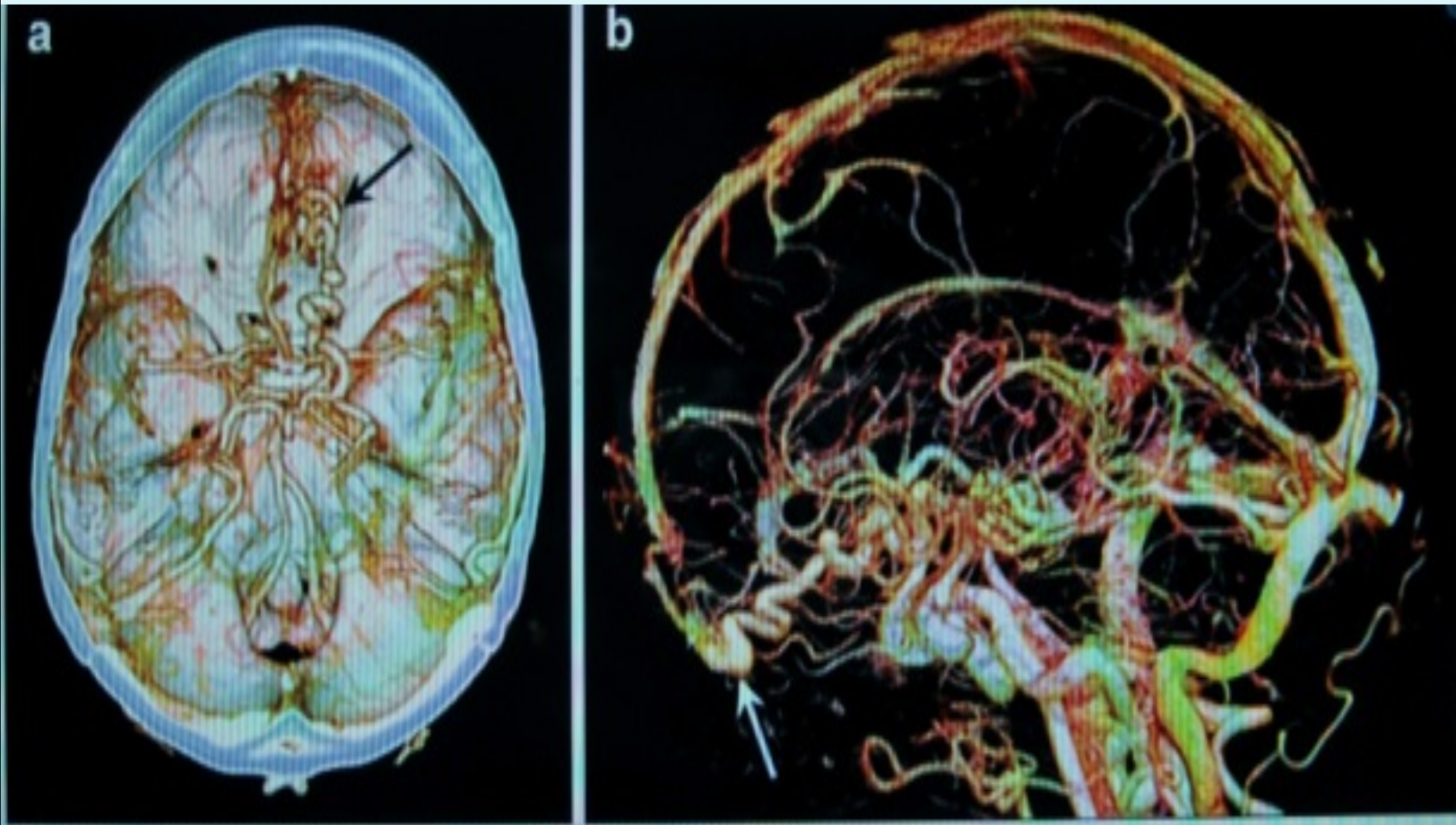
**Lung Nodules\***



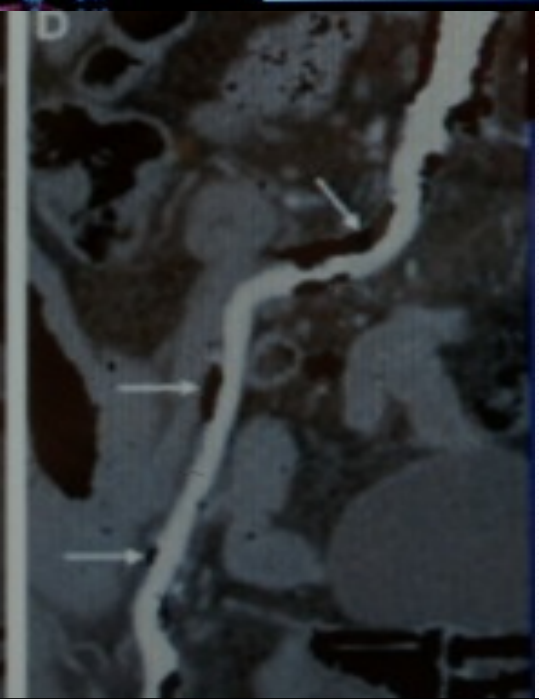
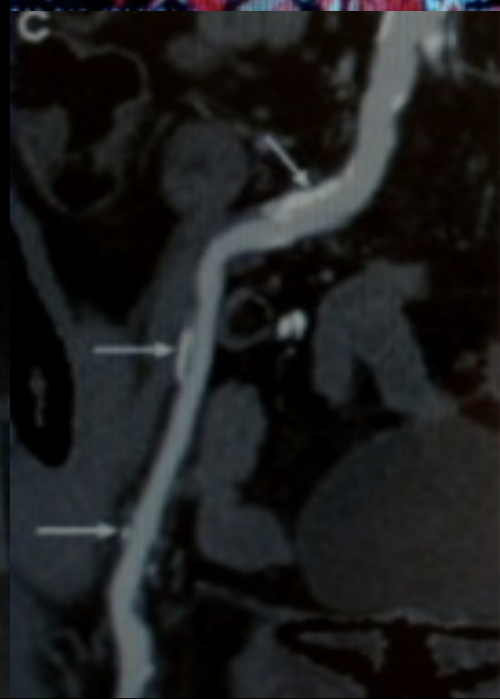
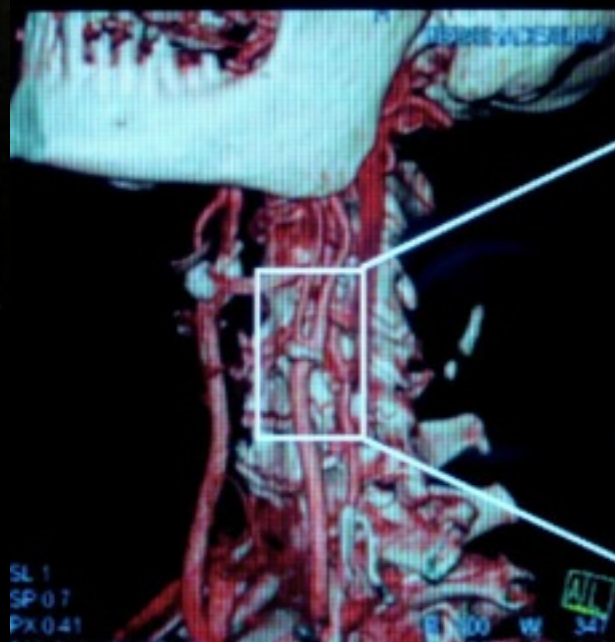
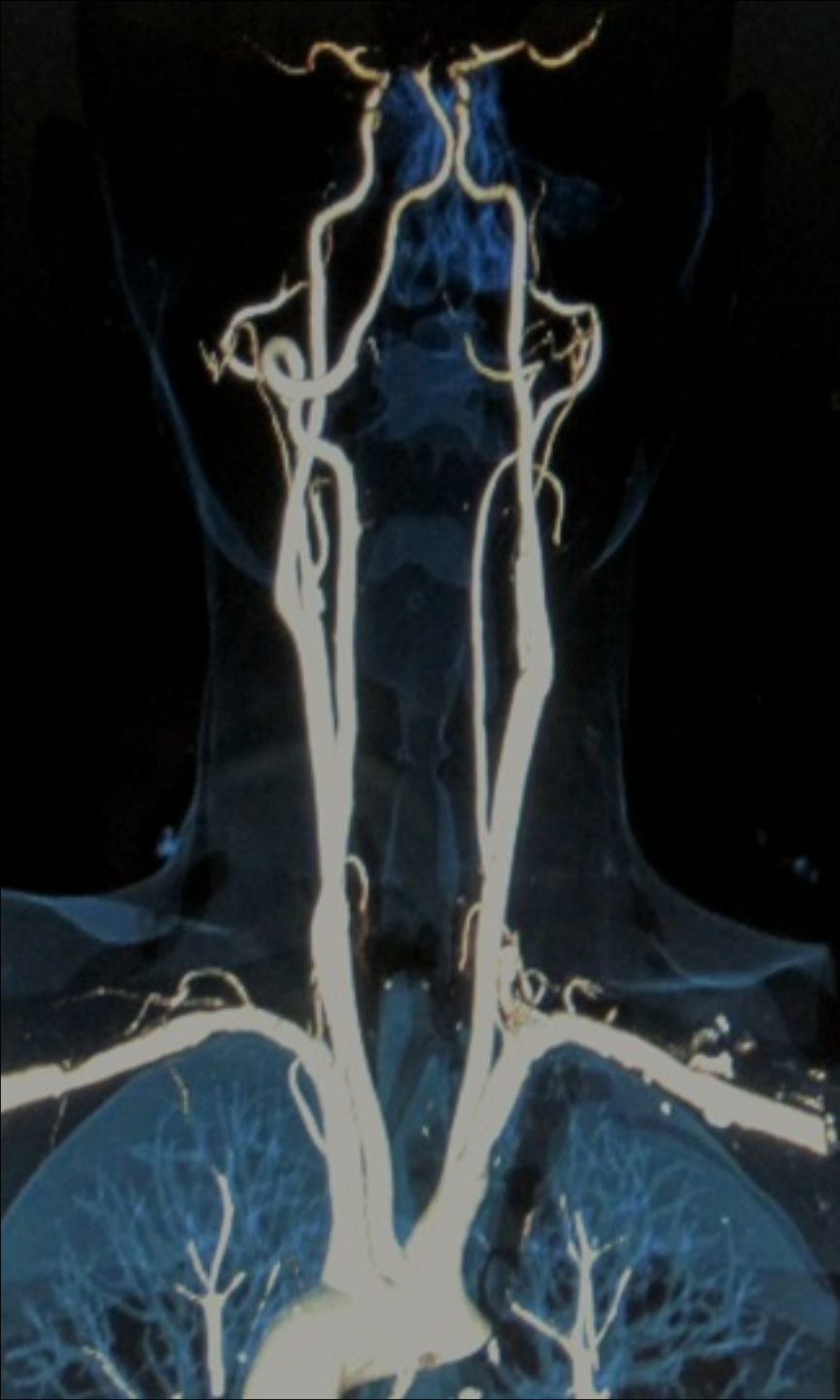
**Xenon\***



# HEAD/ NECK DUAL ENERGY CT



Volume rendering of dual-energy cranial CT angiography demonstrates arteriovenous malformation in the right frontal lobe (A, black arrow). Automated bone removal is precisely achieved using dual-energy (B), allowing improved delineation of the malformation together with drainage into the superior sagittal sinus





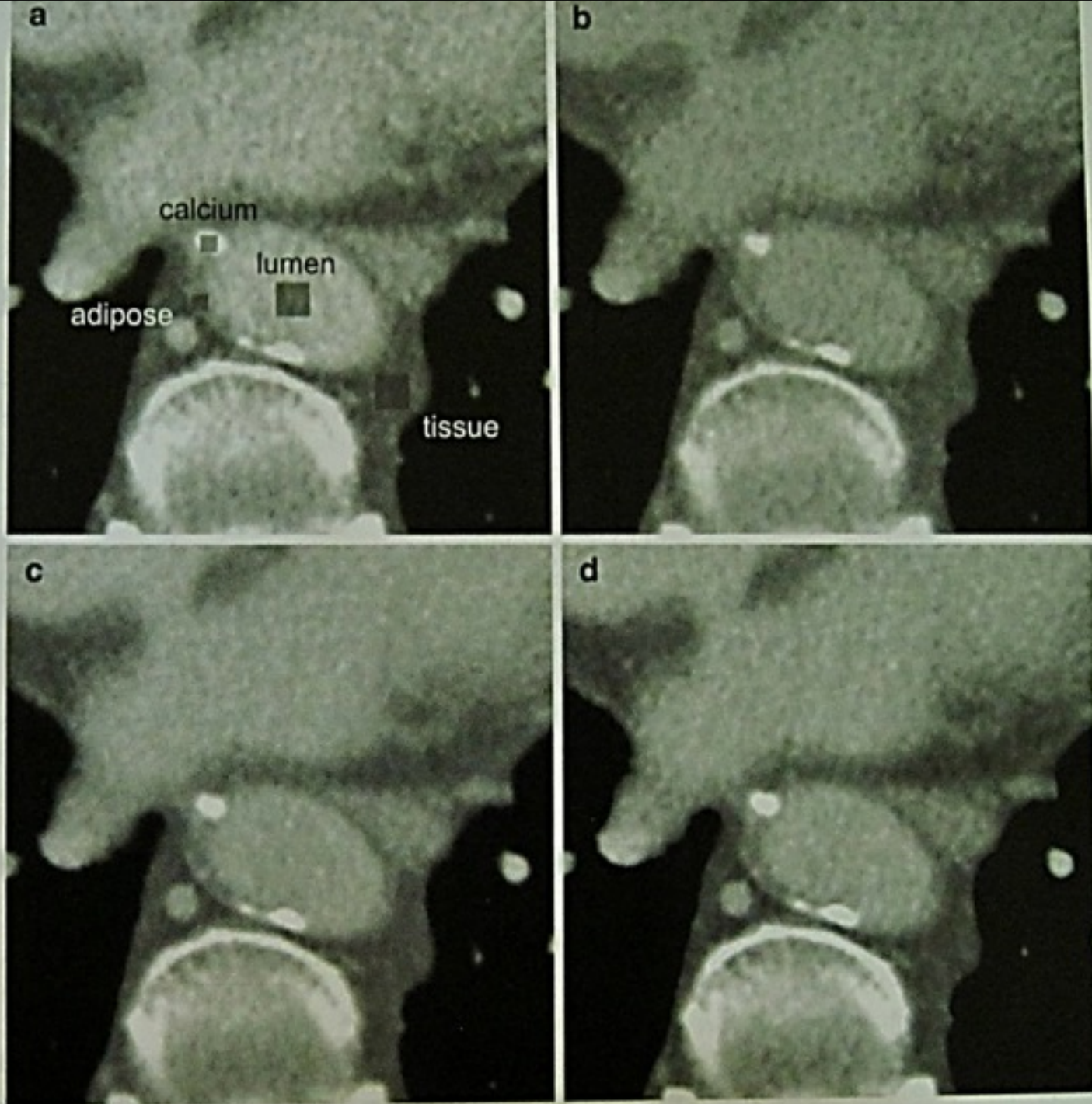


**Fig. 2** CT image showing the contrast between selected tissues (adipose, calcium, lumen, soft tissue) in the 80 kV (a), 140 kV (b), weighted average (c) and cancellation (d) image, respectively. The cancellation image (d) provided the highest contrast between the various plaque components



# Dual-Energy CT in the Evaluation of Intracerebral Hemorrhage of Unknown Origin: Differentiation between Tumor Bleeding and Pure Hemorrhage

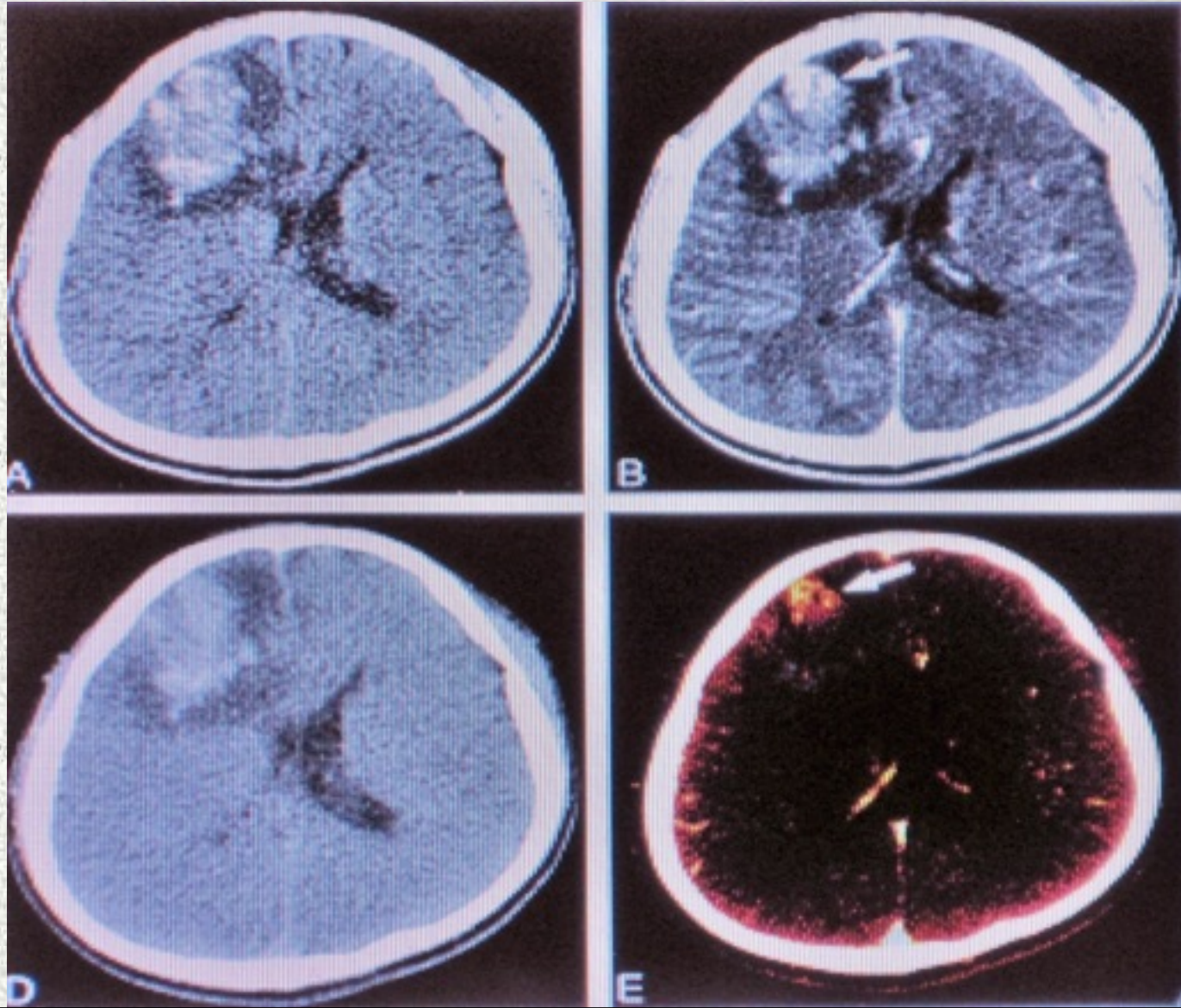
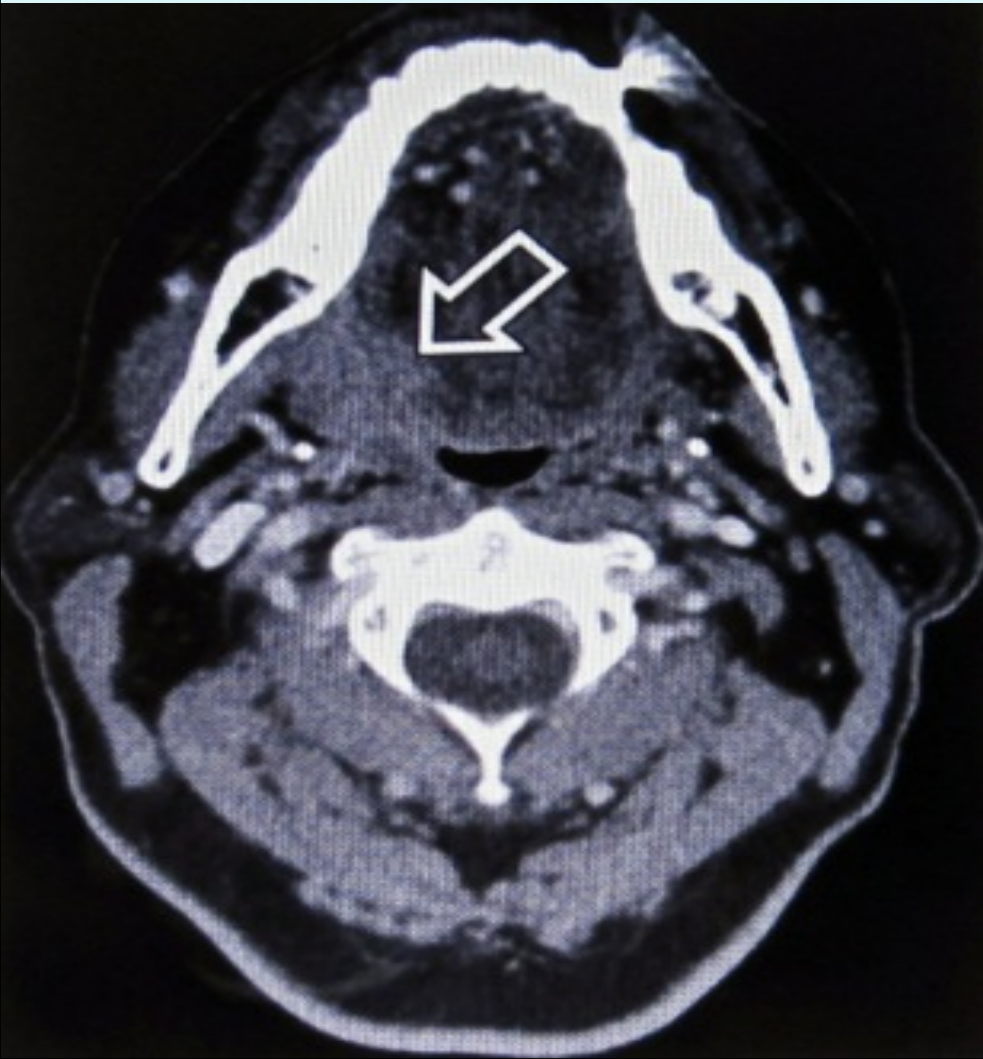




# IMAGE DECOMPOSITION

140KVP ----- 80 KVP



# DUAL ENERGY CHEST CT





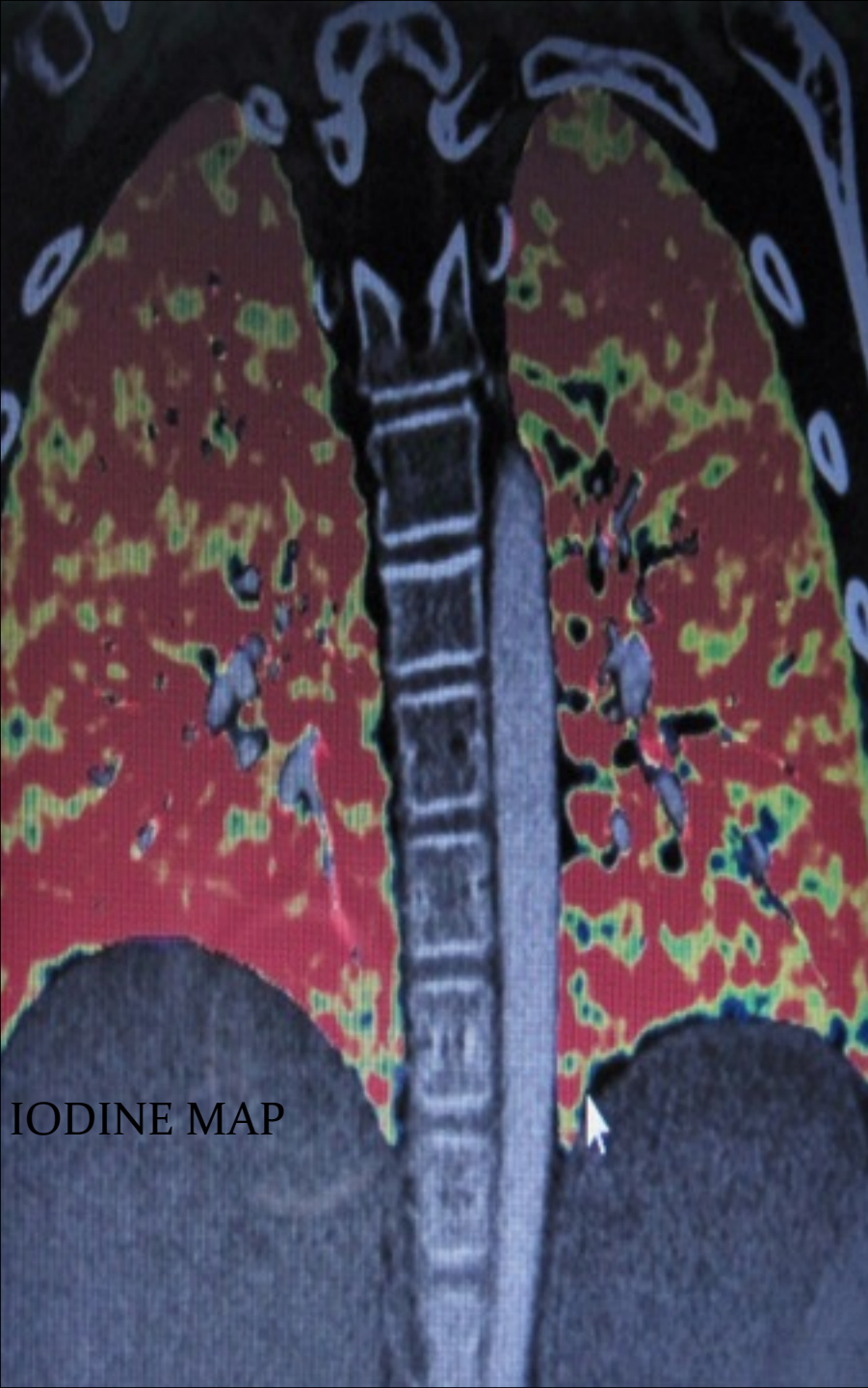
# DECT in assessing PE

- Using DECT, pulmonary vasculature can be assessed
- Degree of iodine enhancement representing lung perfusion iodine blood maps can be seen on an image without having to compare it with an unenhanced CT image

# Decreasing Contrast Volume with DECT

- Significant reduction in contrast volume injected without compromising the dose-length product
  - Median 28 cc in DECT protocol vs 62 cc in standard protocol ( $p < 0.001$ )
- Image reconstruction at 50 keV for evaluating the vascular bed and 70 keV for the pulmonary parenchyma







- **Quantification of iodine to visualize perfusion defects in the lung**
- **Avoids registration problems of non-dual energy subtraction methods**

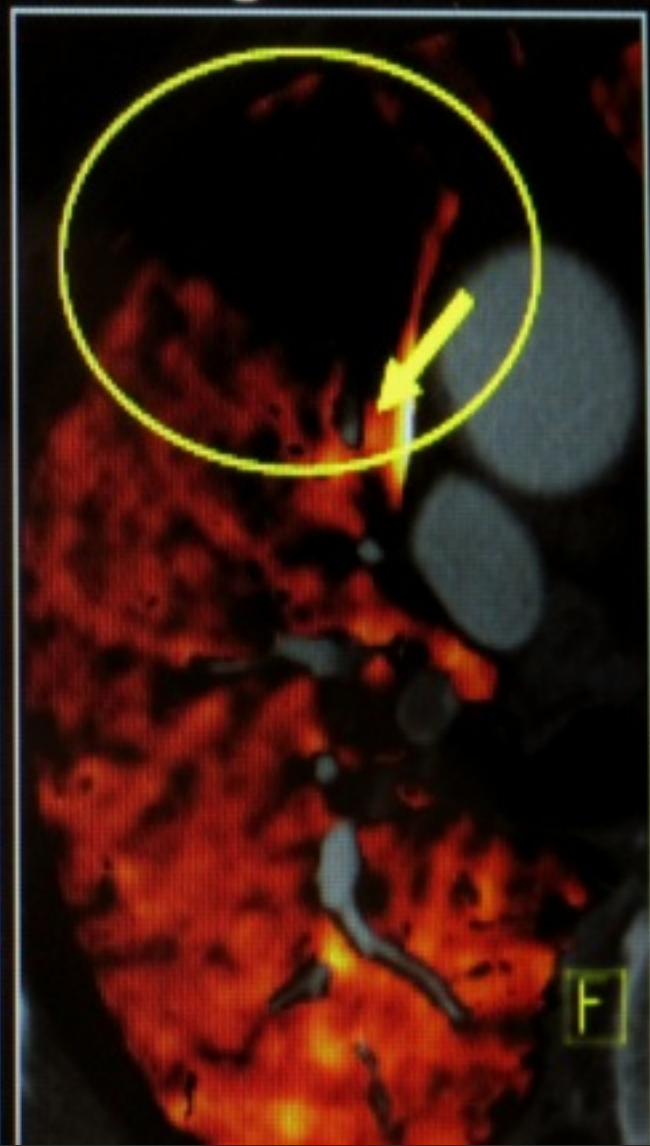
80/140kV Mixed Image



Iodine Image

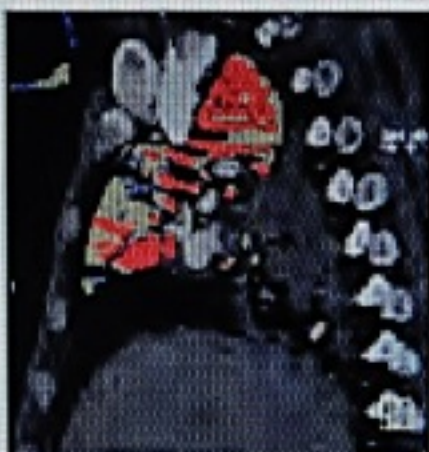
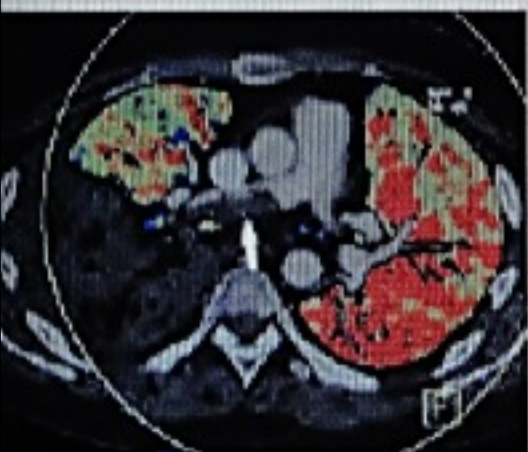
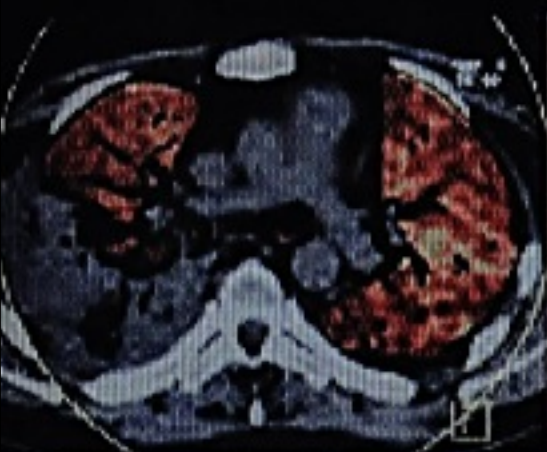


Mixed image + iodine overlay





# DECTV/Q to Monitor PE treatment



**Initial Diagnosis:** ventilation and perfusion defect in RLL, filling defect in R PA

**Post-tx:** almost complete resolution of clot, persistent ventilation and perfusion defect in RLL



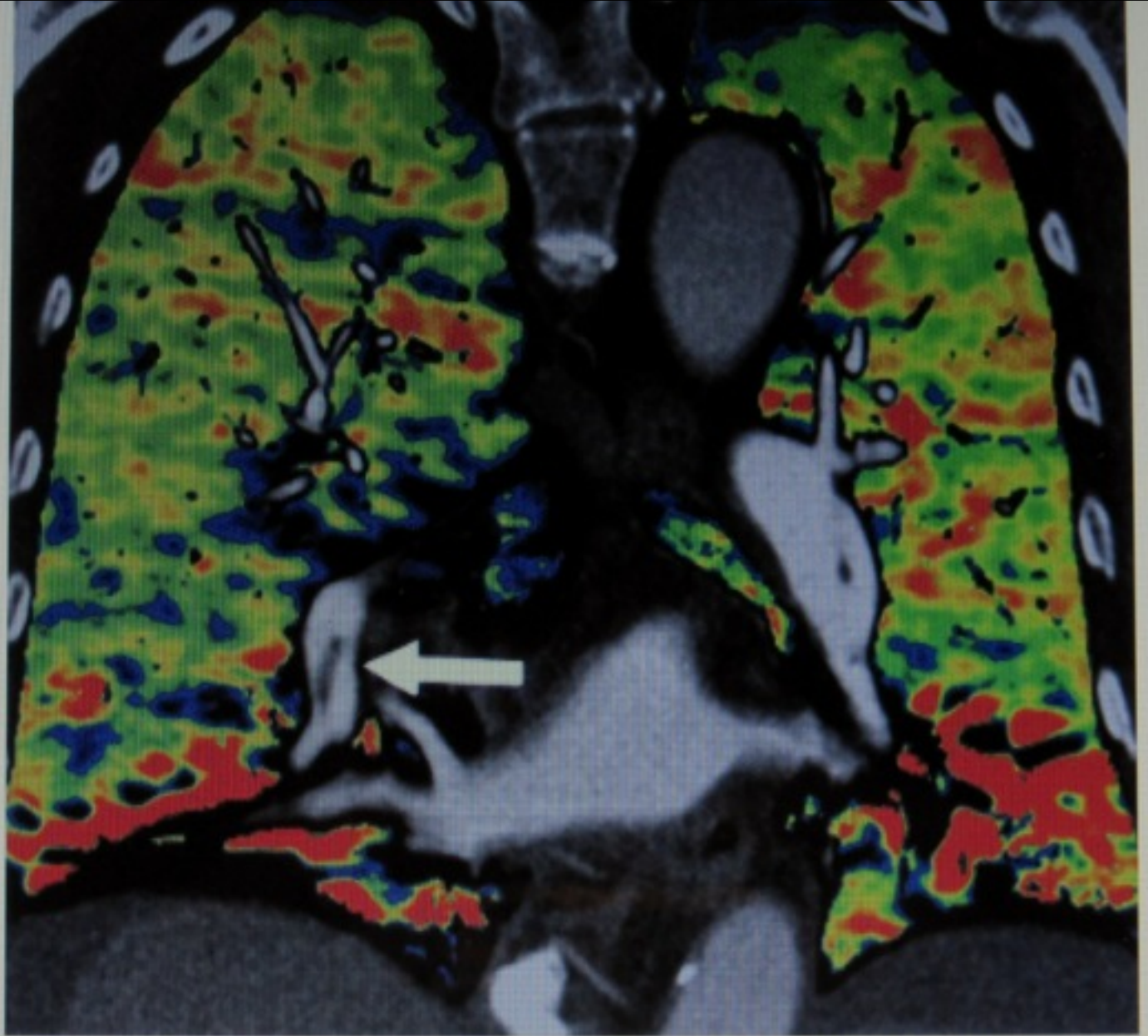


Fig. 6A—Negative findings on blood flow image of 68-year-old woman with right lower pulmonary artery embolus.

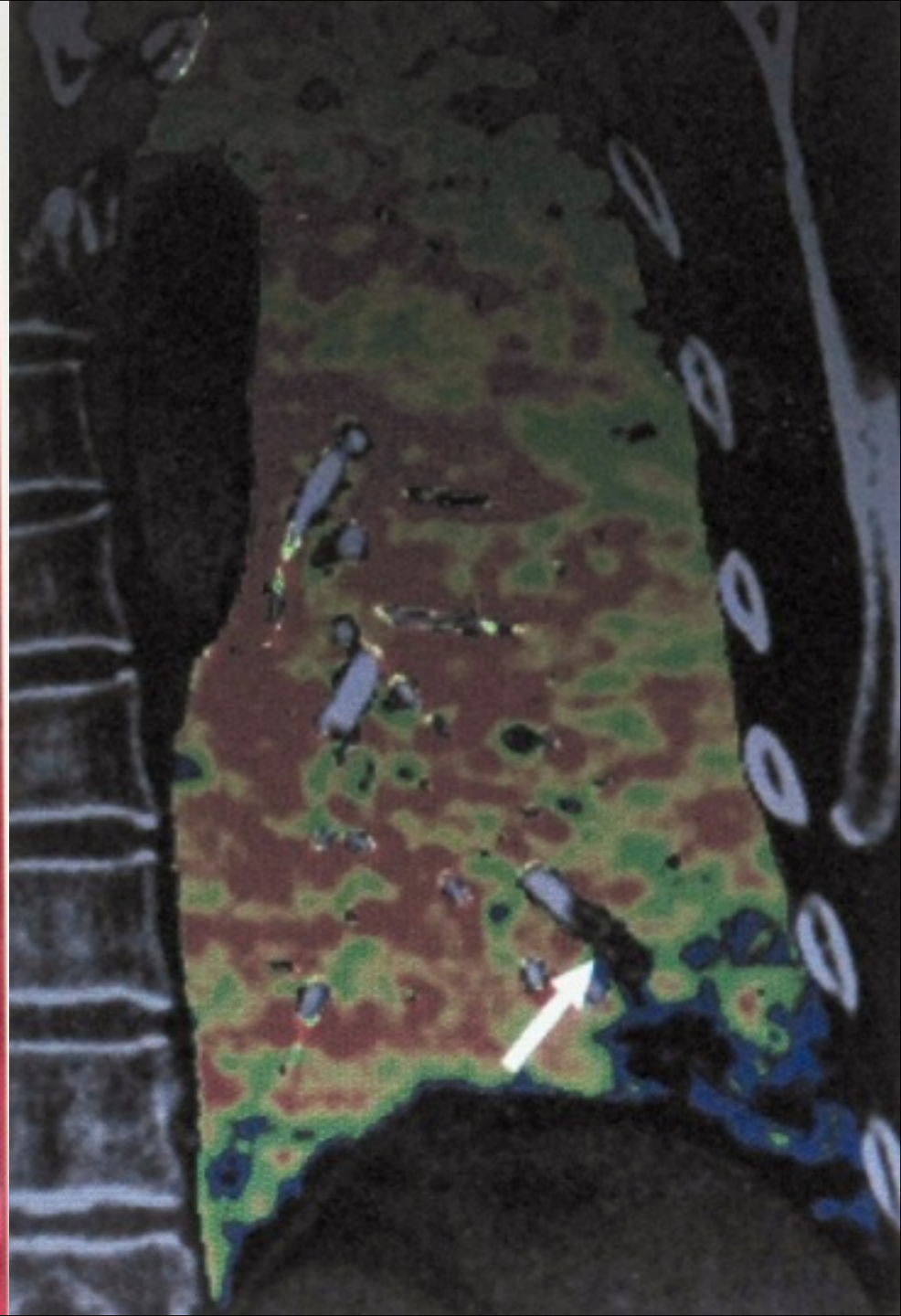
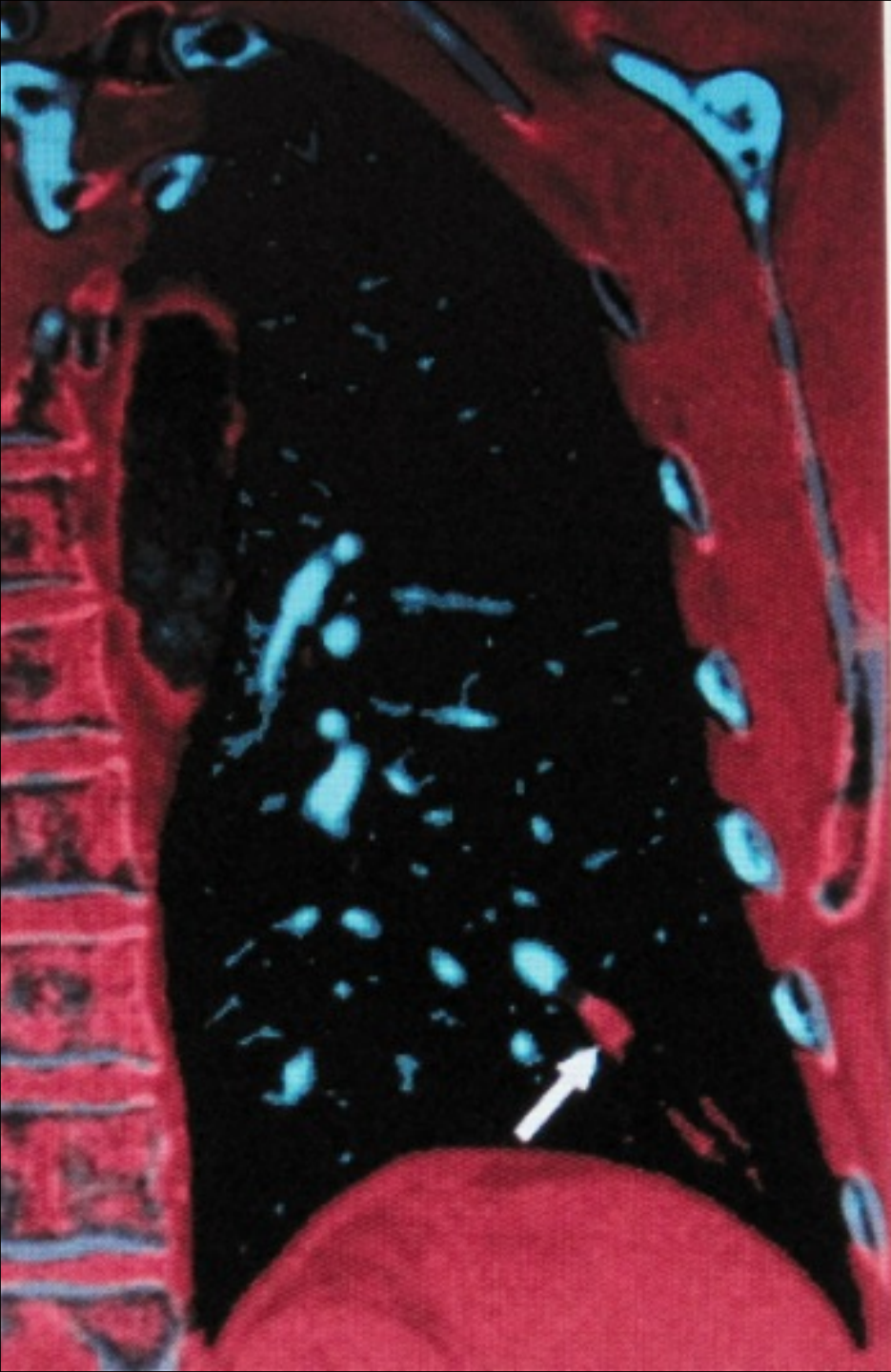




Fig. 7A—Acute pulmonary embolism in 42-year-old woman. Dual-source CT-based dual-energy CT (DECT) angiography images of lungs are shown as coronal reformations.

A, Pulmonary MDCT angiography reconstruction (A), tissue-specific thrombus analysis (B), and DECT blood pool map (C) show occlusive pulmonary embolus (arrows) in left inferior lobar segmental pulmonary artery and corresponding perfusion defect.



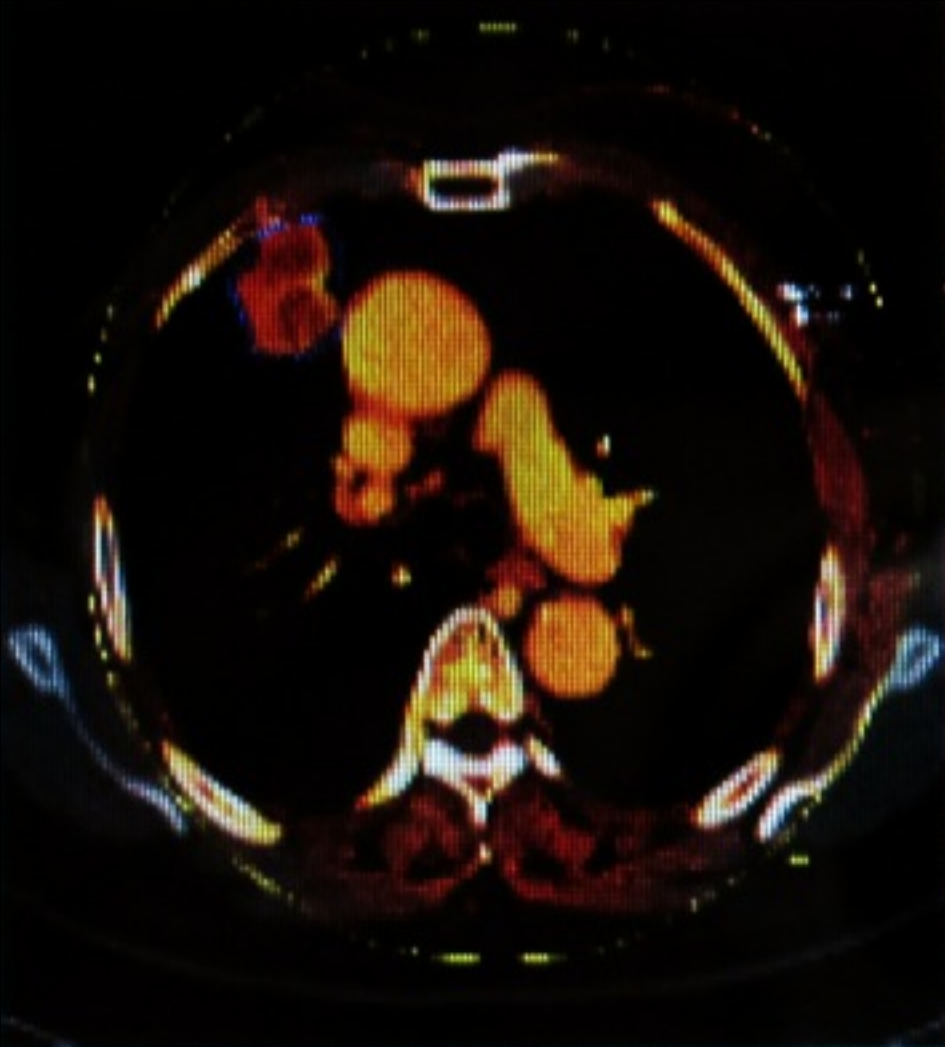




## Future Directions:

### Blood Perfused Volume Imaging

- DECT might better depict acute on chronic PE
- Promise for DECT pulmonary perfusion defect score on DECT likely better prognostic indices than traditional measures for patient outcomes
- DECT to monitor PE treatment



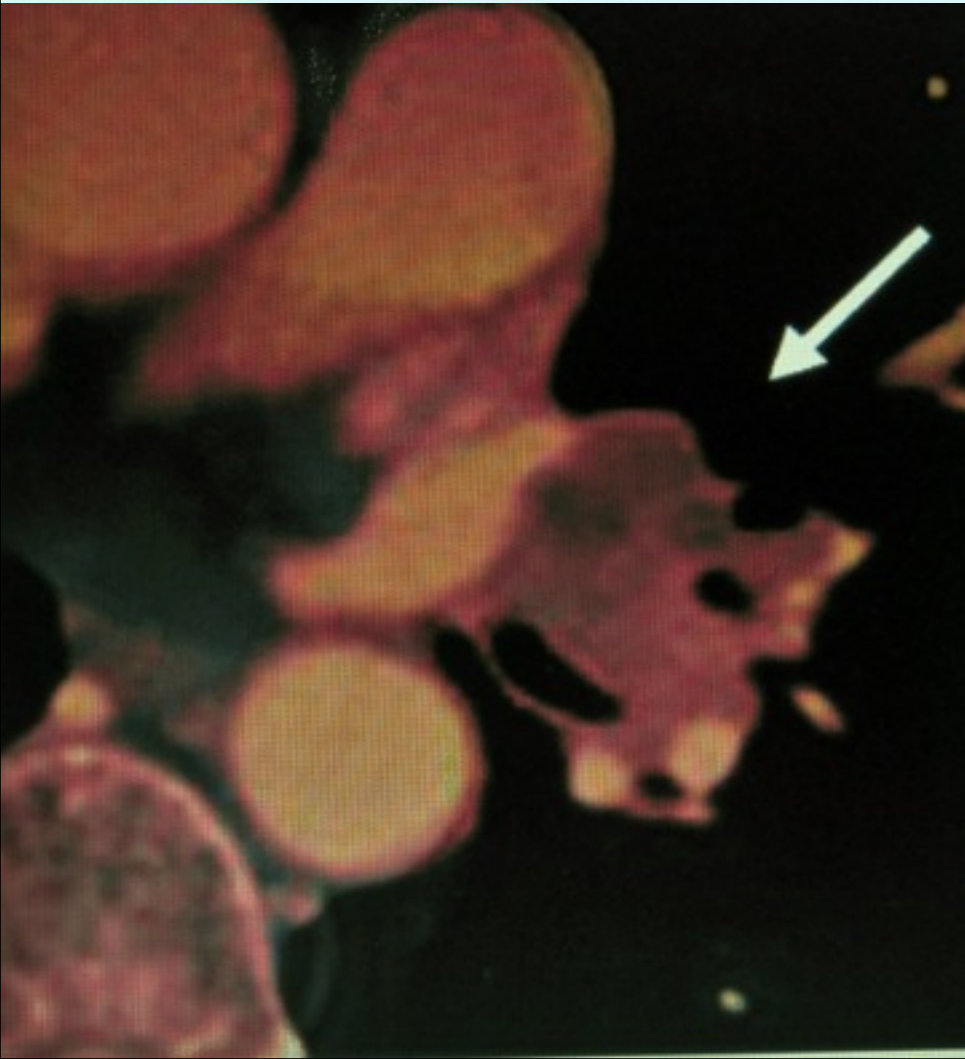
Measurement of  
Lung Nodule  
enhancement



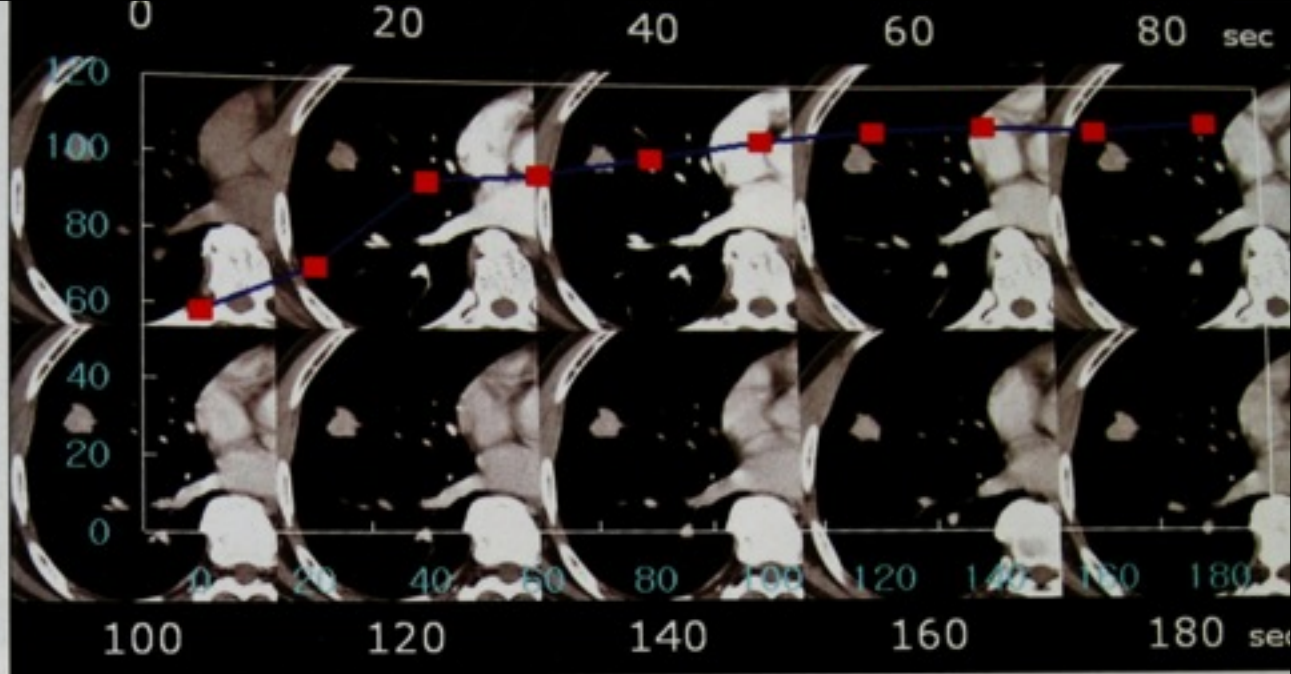
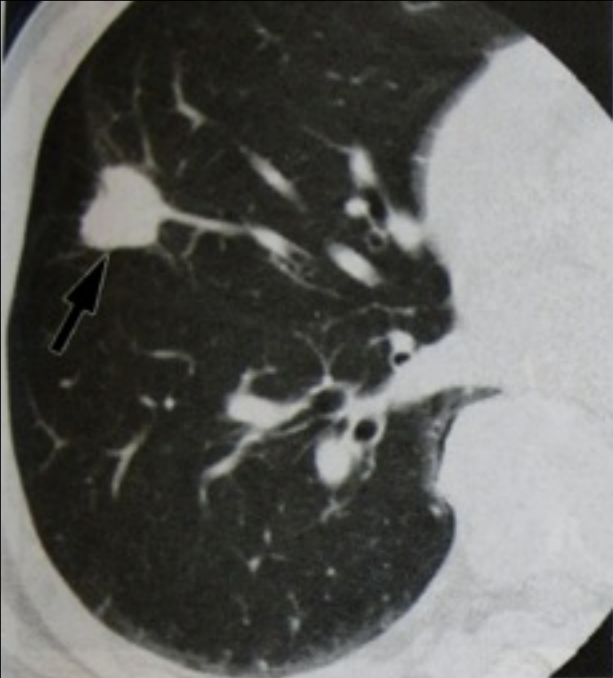
Measurement of  
Xenon Concentration  
courtesy of ASAN Medical  
Center, Seoul, Korea



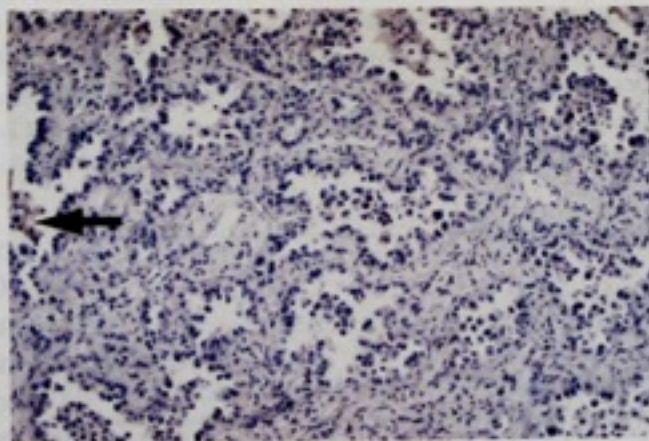
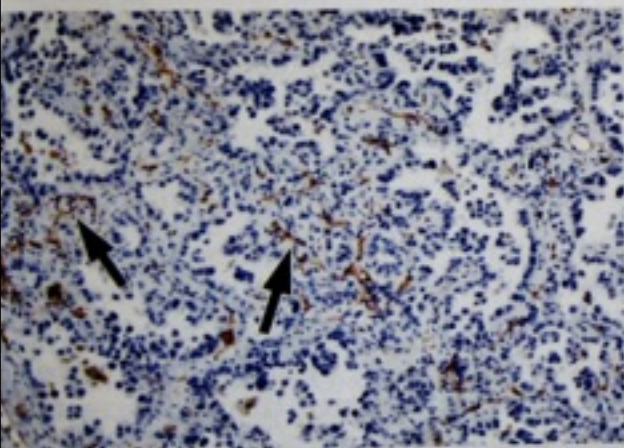
# CONTRAST ENHANCEMENT IODINE “SUV” BIOMARKER-DX/RX







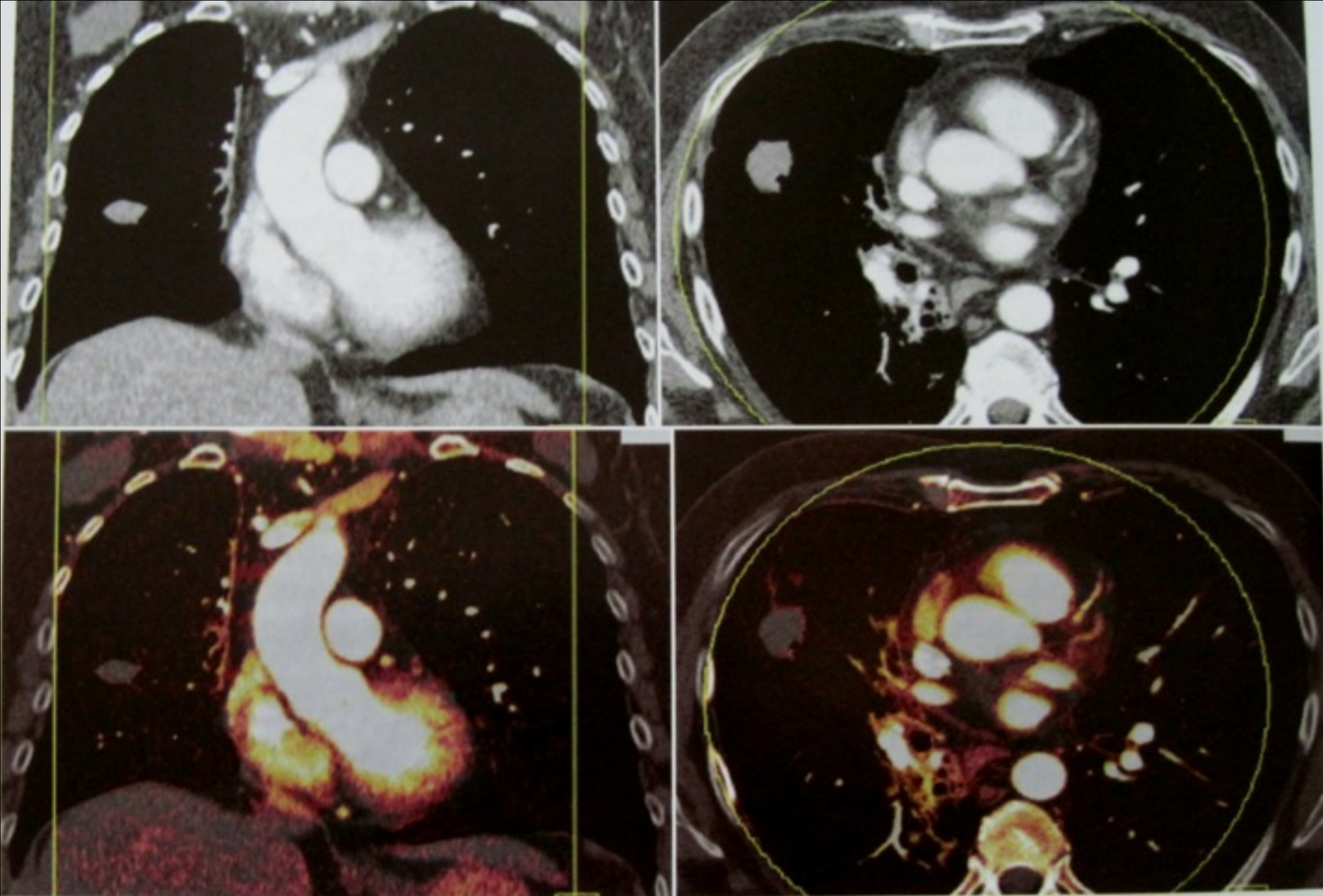
b.



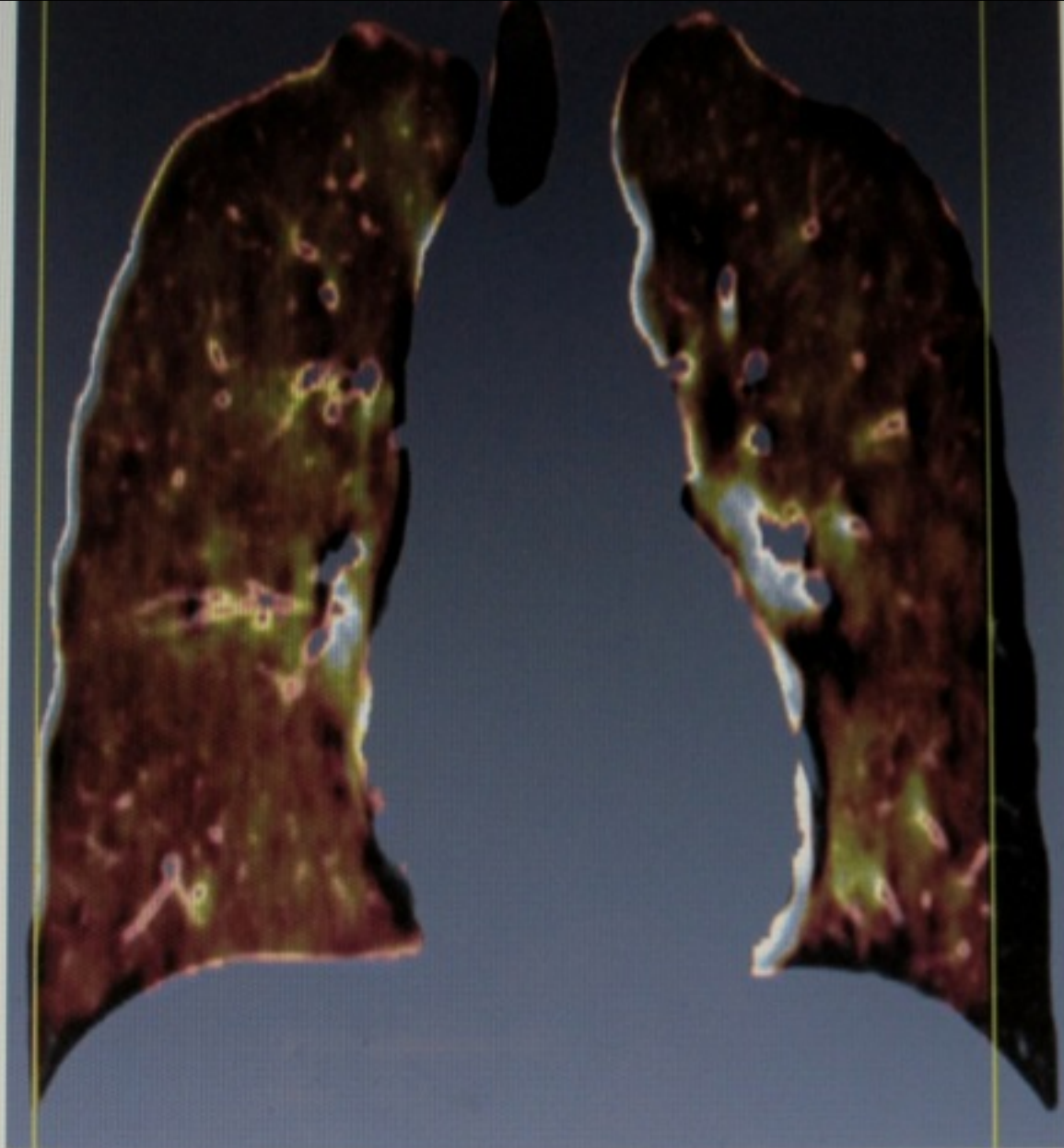
d.

Figure 2. Adenocarcinoma in a 64-year-old man. (a) Lung window of transverse thin-section (2.5-mm collimation) CT scan obtained at level of right inferior pulmonary vein shows 21-mm nodule (arrow) with lobulated and spiculated margin in right middle lobe. (b) Serial images obtained at 20-second intervals and at similar levels show enhancement dynamics of nodule. Peak enhancement is 110 HU; net enhancement, 52 HU; maximum enhancement ratio, 0.906; slope of enhancement, 0.005; and time to peak enhancement, 180 seconds. (c) Microvessel density with CD31 immunostaining is 67. Vessel wall (arrows) is stained dark brown. (Original magnification,  $\times 40$ .) (d) VEGF is 3. Intracytoplasmic brown pigment (arrow) indicate VEGF. (Original magnification,  $\times 40$ .)





**Fig. 2** DECT of a 63-year-old patient with an incidentally detected pulmonary nodule of soft tissue density and unclear dignity. DECT iodine maps (lower row) show only minor iodine uptake of the nodule indicating a benign lesion. CT guided biopsy revealed a hamartoma



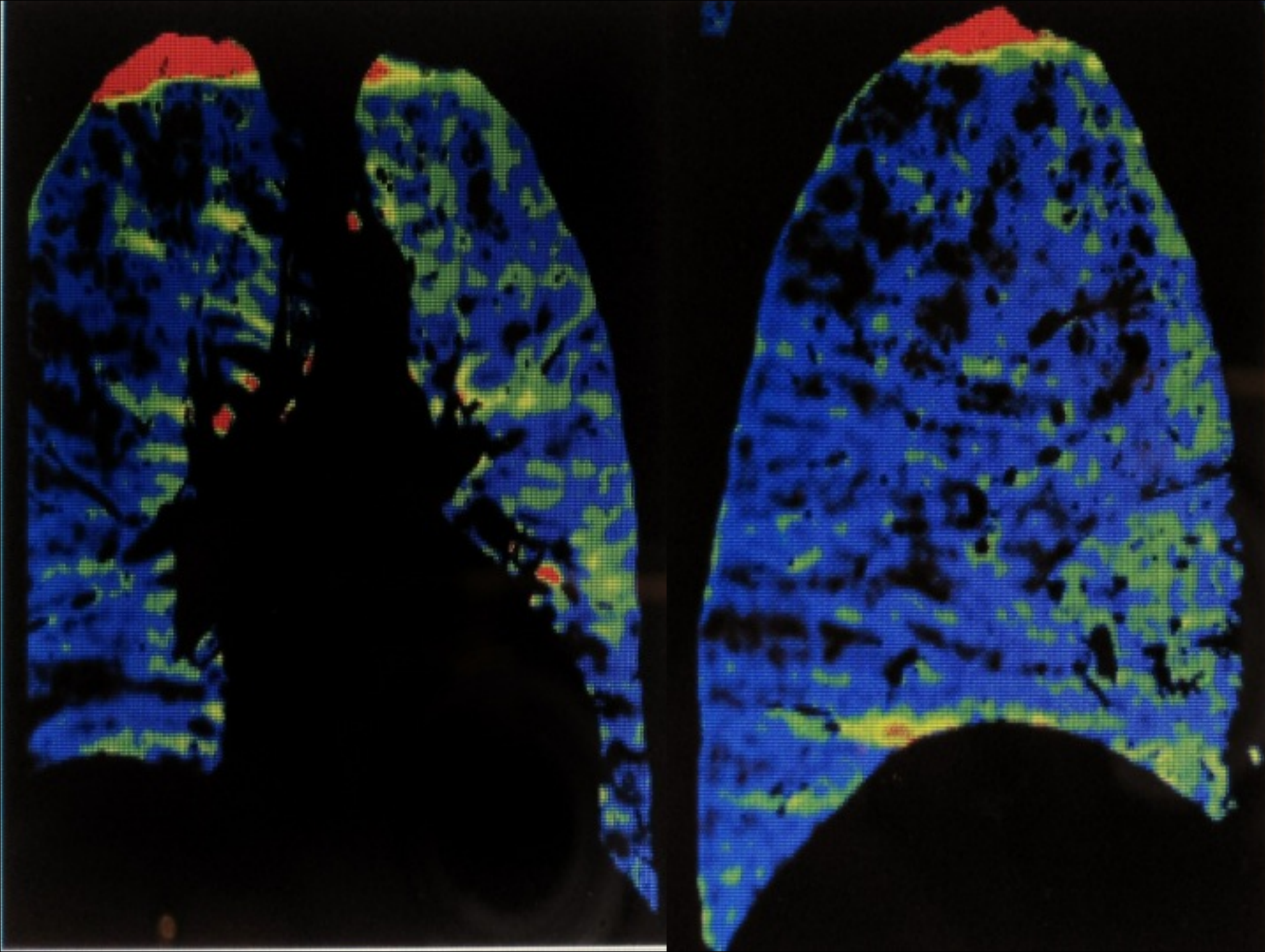
**Fig. 12B**—Xenon-enhanced dual-energy CT (DECT) lung ventilation study of 54-year-old man. DECT-based chest CT acquisition was performed while patient inhaled xenon gas.



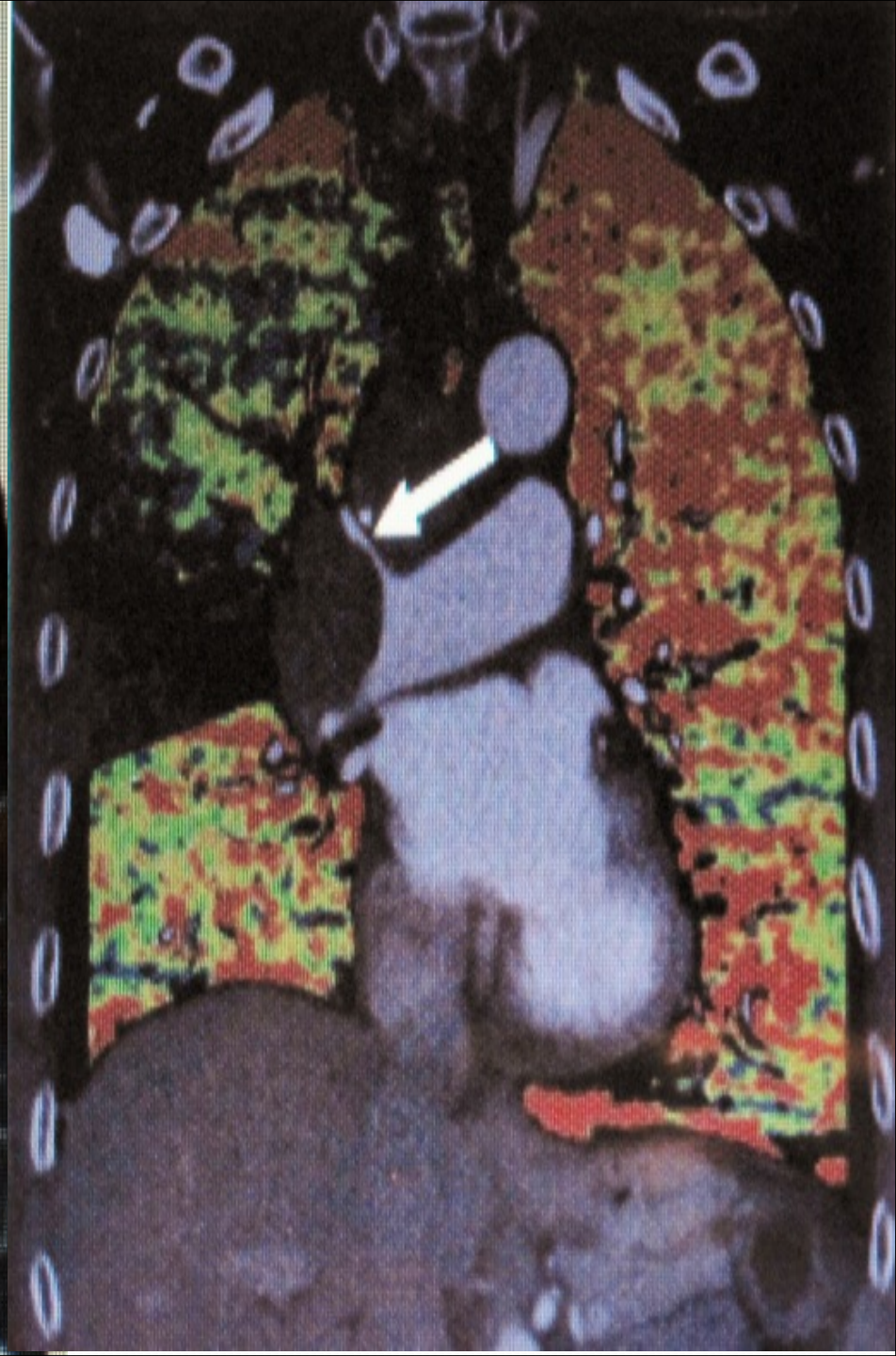


Fig. 3C—Blood pool defect on dual-source CT-based dual-energy CT blood pool study of lungs caused by emphysema in 67-year-old man.

C, Findings shown in A and B are readily seen on coronal multiplanar reformation displayed in lung window









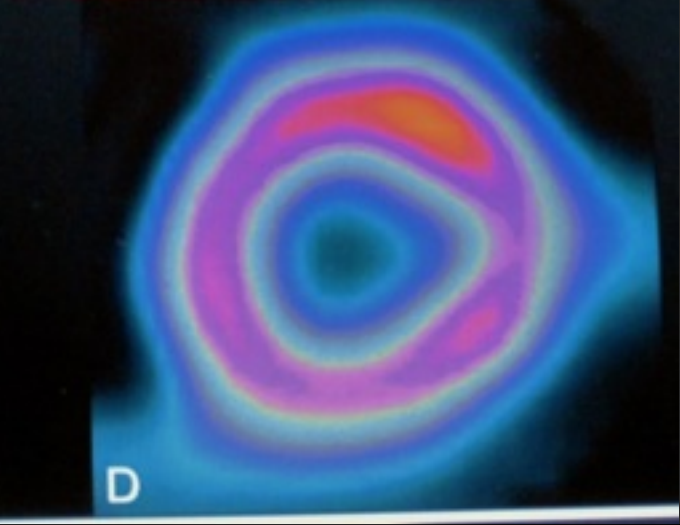
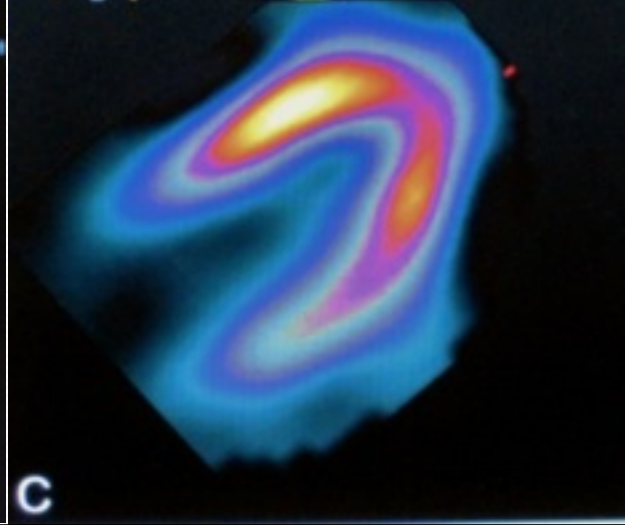
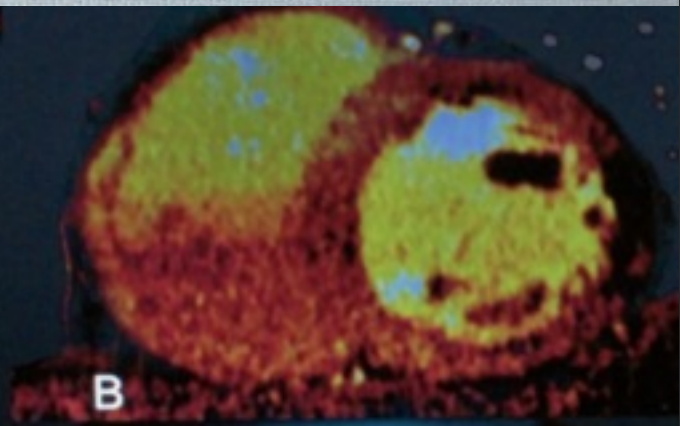
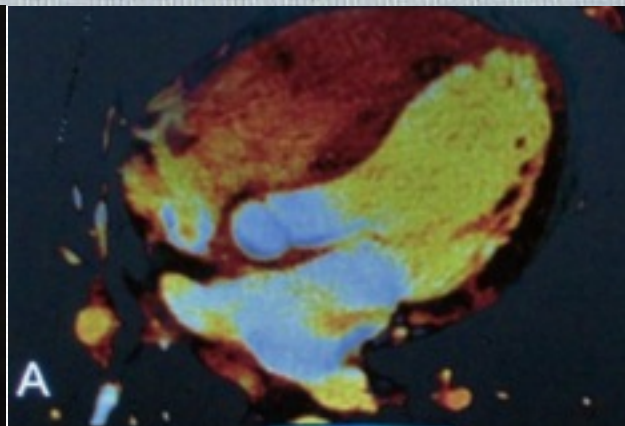
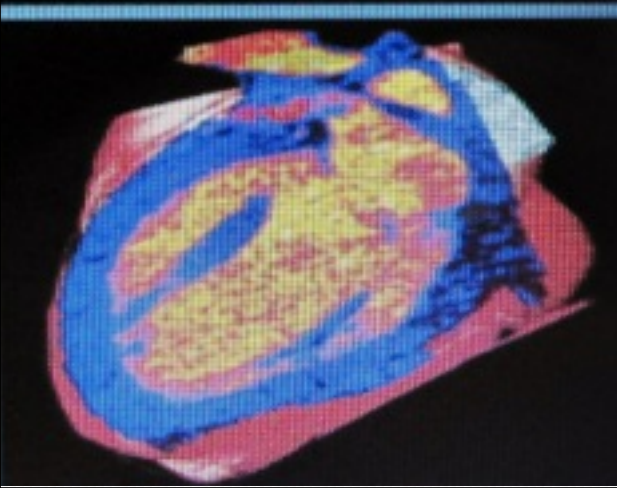
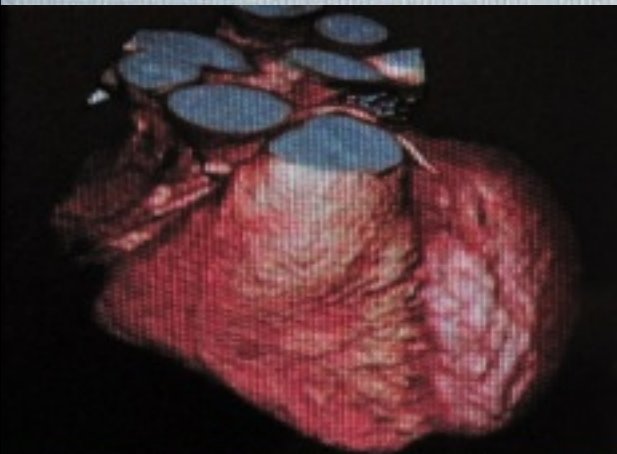
# DSCT Myocardial perfusion versus SPECT CT myocardial perfusion

posted by Balazs Ruzsics, M.D., PhD | Oct 22, 2009

The following question has been sent by Dr. Shrinivas Desai:

DSCT Myocardial perfusion versus SPECT CT myocardial perfusion:

Jaslok Hospital in mumbai, India is buying Siemens DSCT (Flash Definition Dual source Dual energy). We already have a SPECT on which thallium myocardial perfusion is done. The nuclear medicine department is considering acquiring SPECT-CT with rubidium to perform myocardial perfusion. Jaslok Hospital is a stand alone private hospital with 350 beds with moderate cardiac workload. In your opinion will it be viable for a hospital to possess both Siemens DSCT (Flash Definition Dual source Dual energy) and SPECT-CT for the purpose of myocardial perfusion. Will the myocardial perfusion done on the dual source CT give results comparable to SPECT-CT or are both needed?



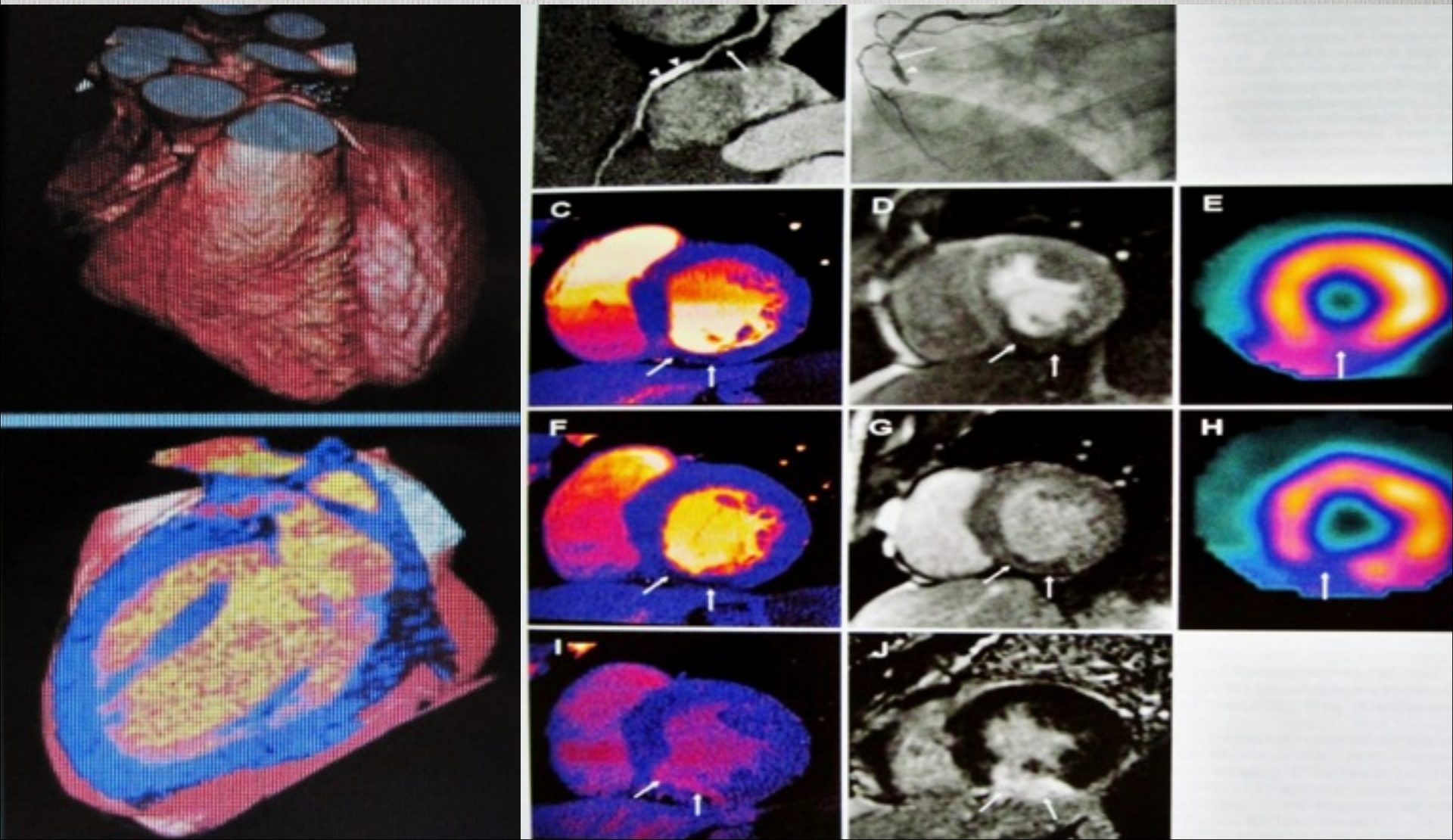


Balasz Ruzsics, M.D., Medical University of South Carolina:

Dear Dr. Shrinivas,

Thank you for the question and your interest in DSCT.com website.

Dual source CT technology in dual energy mode is a promising tool for detecting myocardial ischemia. To date initial experience studies established the potential role of dual energy CT (DECT) acquisitions for detecting not just the coronary stenosis but corresponding myocardial blood pool defect. DECT successfully combined anatomical (coronary artery) and functional (myocardium) imaging information.





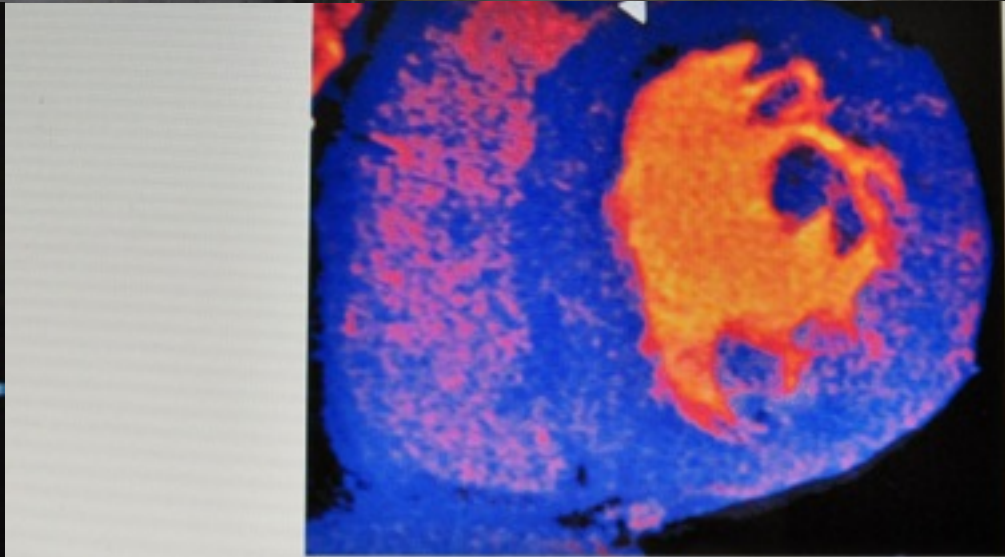
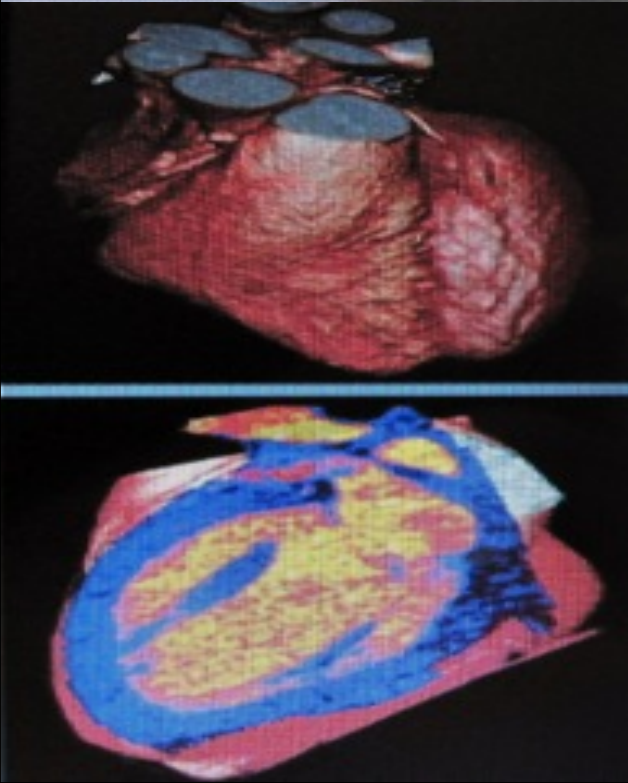
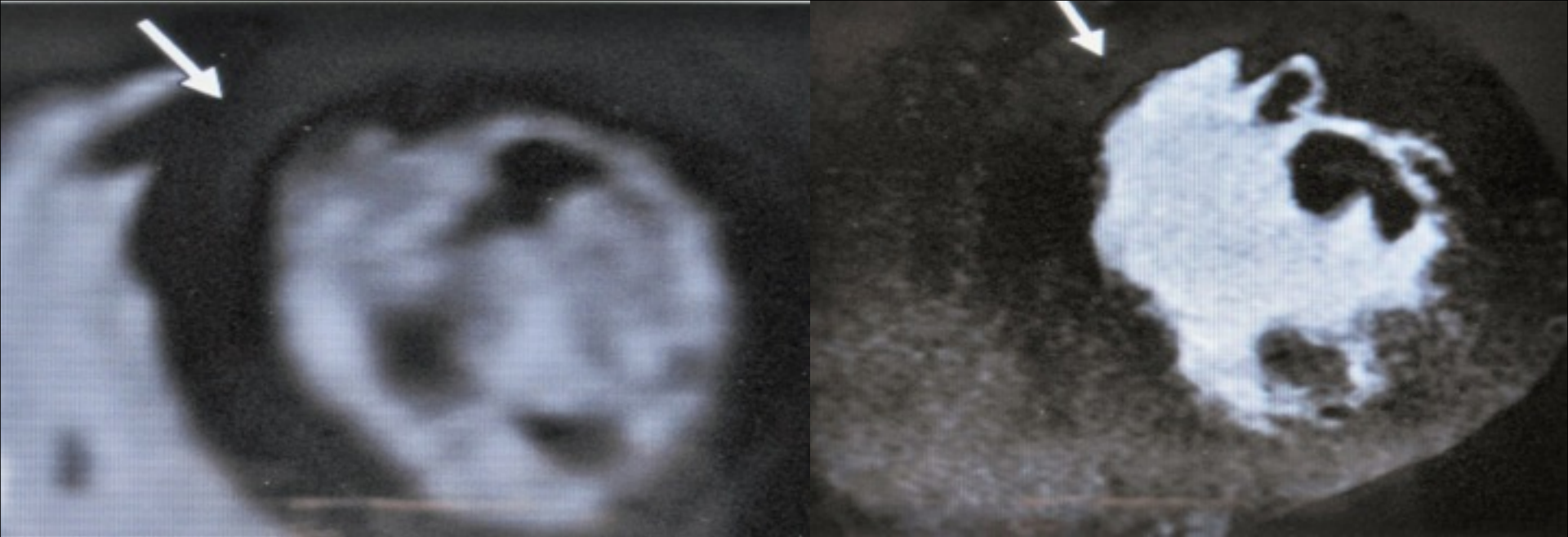


**Fig. 1D**—50-year-old man with recurrent chest pain after prior myocardial infarction in left anterior descending artery territory and surgical revascularization.

D, Corresponding short-axis cross-section of contrast-enhanced dual-energy CT study at rest, reconstructed as merged gray-scale image (C), with superimposed iodine distribution color map (D), and as single-energy image (E). Anteroseptal wall of left ventricle shows subendocardial perfusion defect (arrows, C–E), suggestive of infarction. This is also visible on merged gray-scale and especially iodine color map, but not on single-energy image.



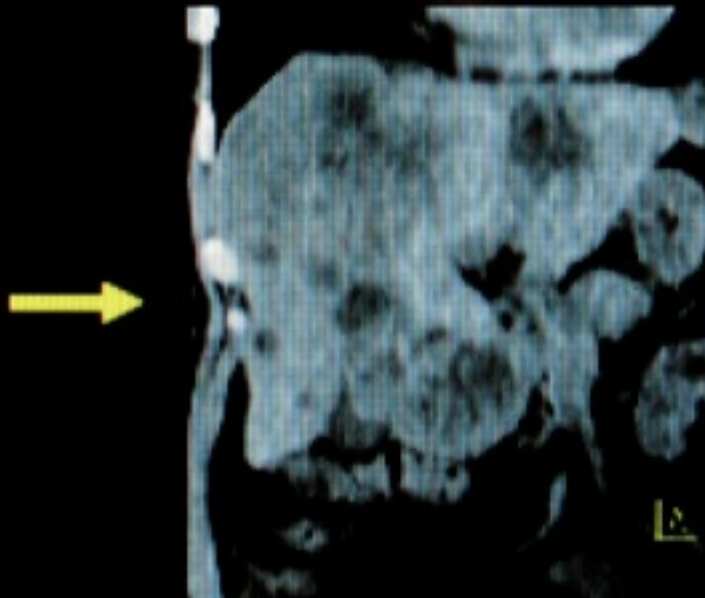
# ABDOMINAL DUAL ENERGY CT

- **Virtual non-contrast image and iodine image:**
- **Characterization of liver / kidney / lung tumors**
  - Solve ambiguity: low fat content or iodine-uptake
  - Quantify iodine-uptake in the tumor and at the tumor surface  
→ Differentiation benign - malignant
- **Monitoring of therapy response**

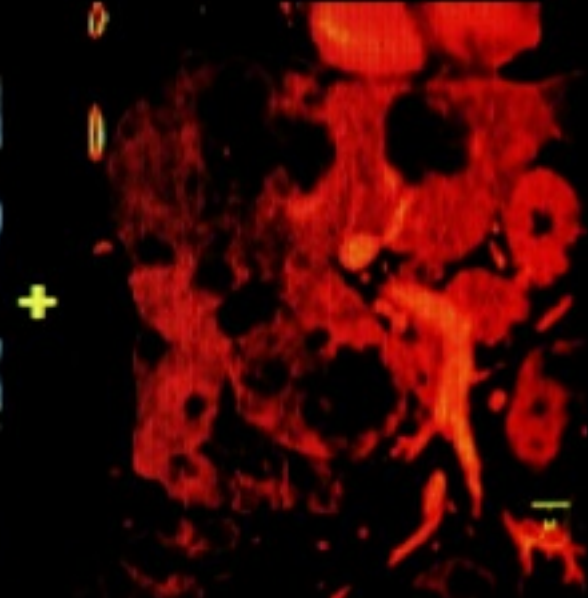
Mixed image



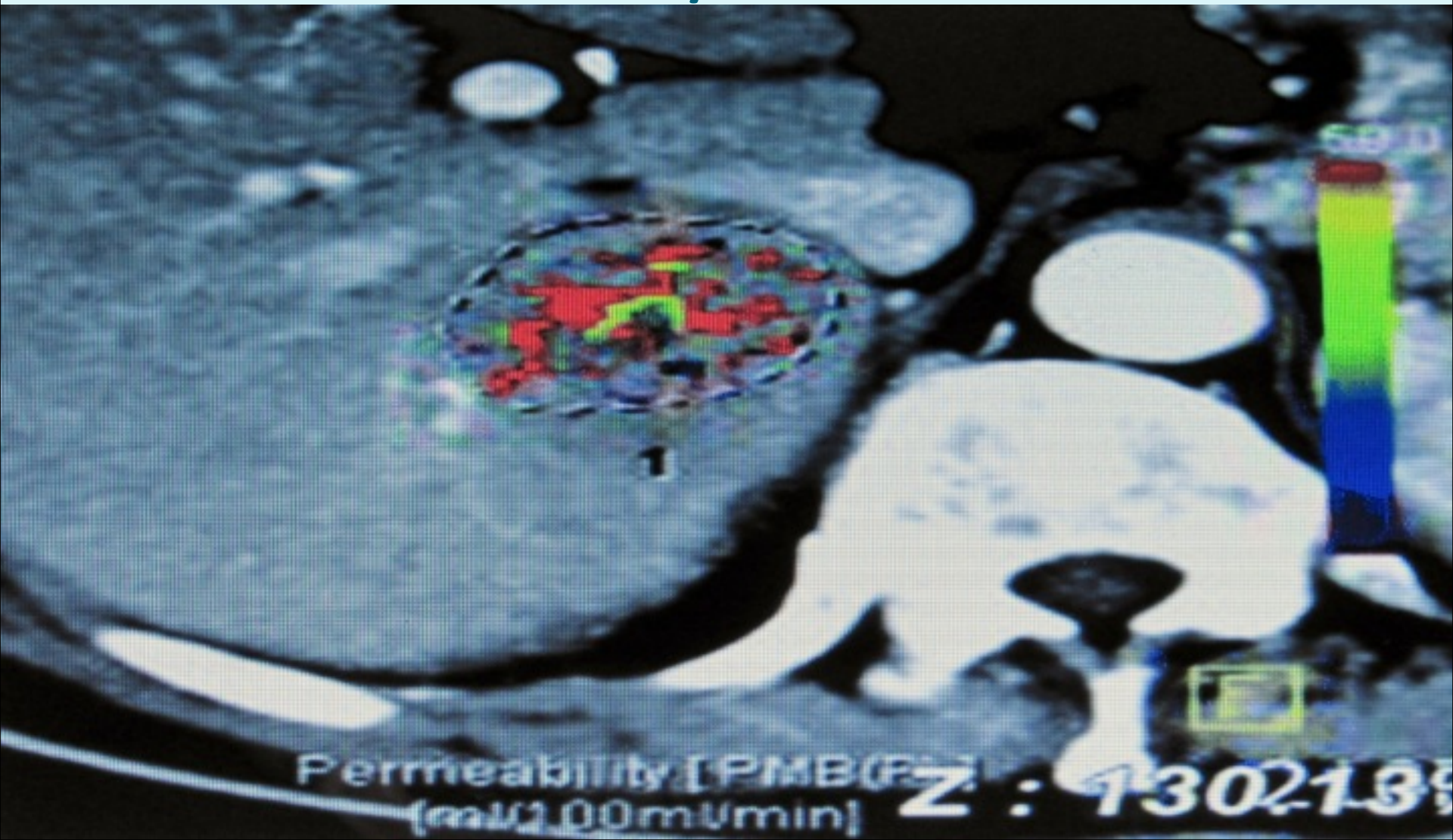
VNC image



Iodine image

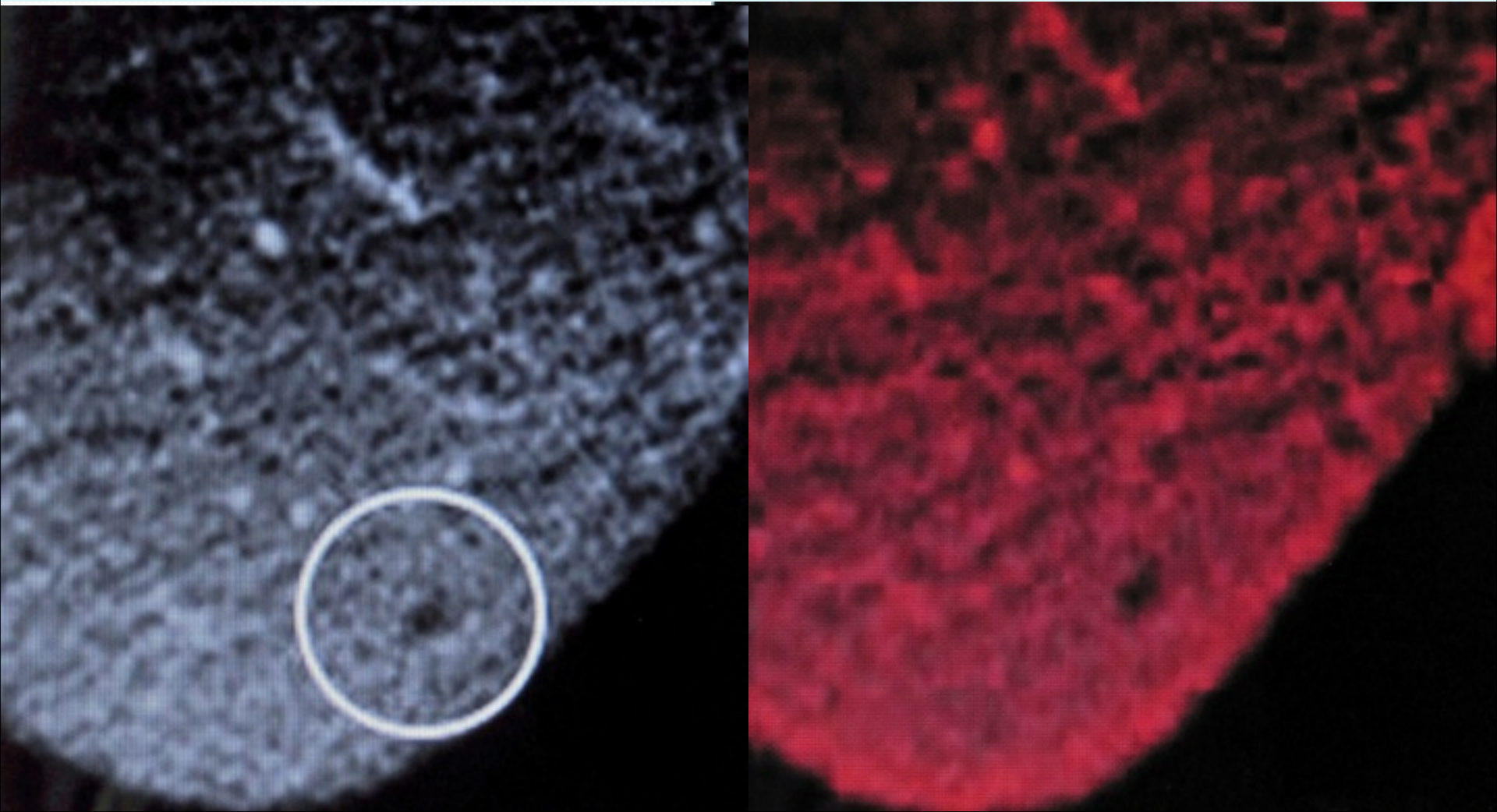


# ANGIOGENESIS/PERMEABILITY DIAGNOSIS/FOLLOW-UP

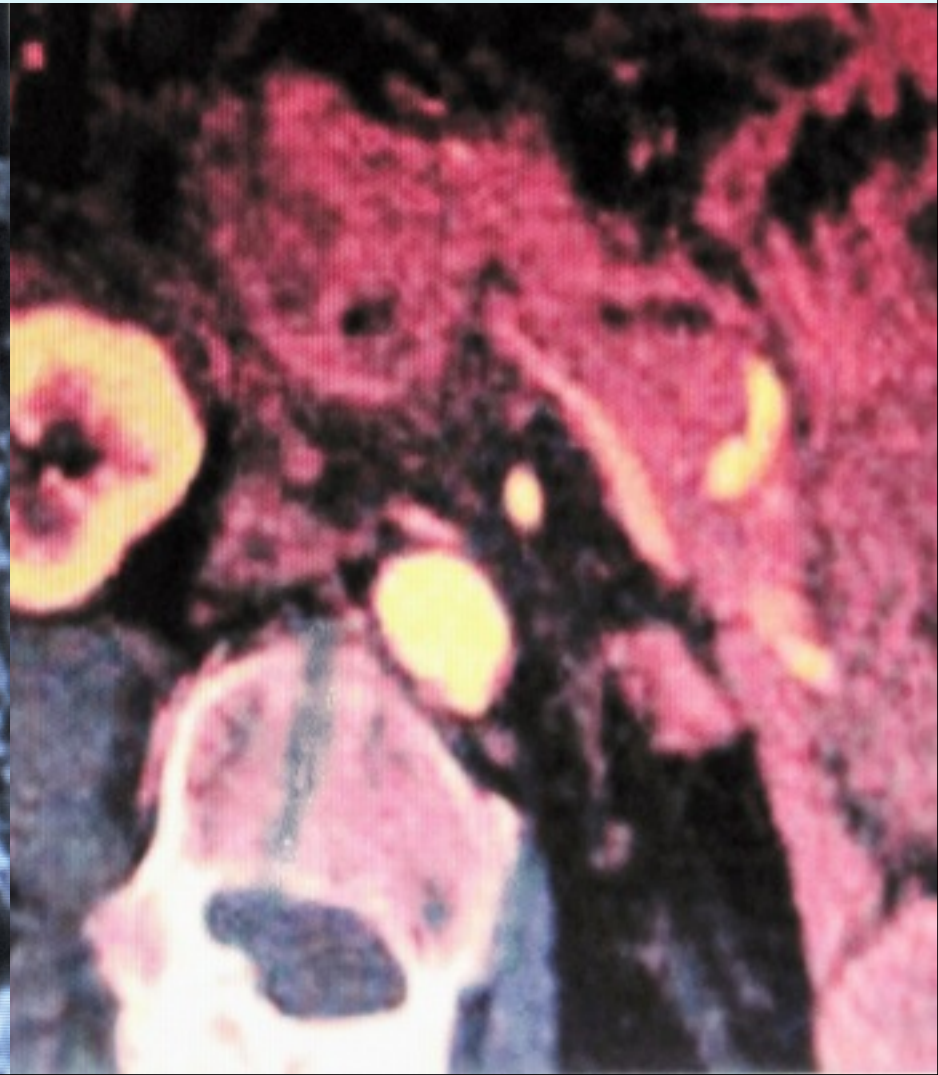




# LIVER LESION TOO SMALL TO CLASSIFY-IODINE “MAP”=CYST

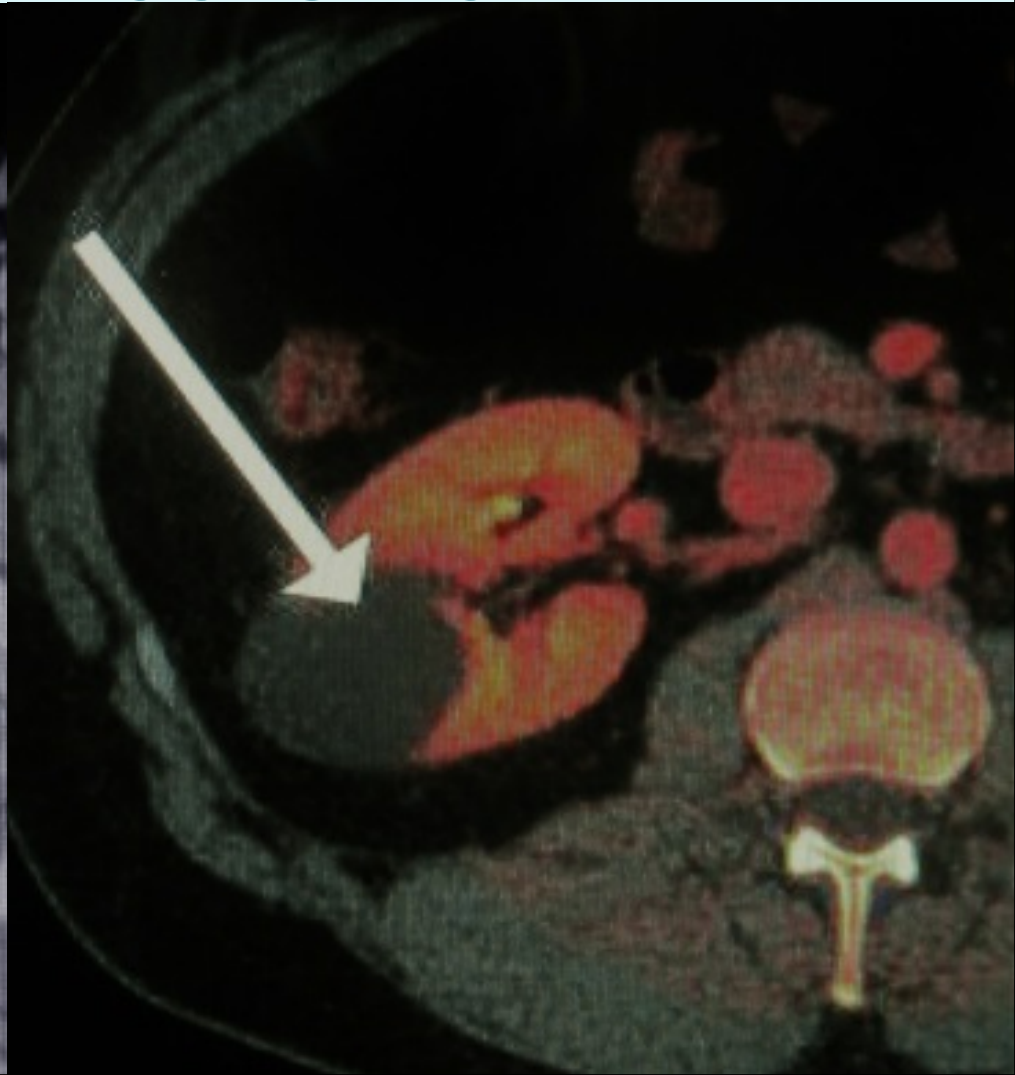
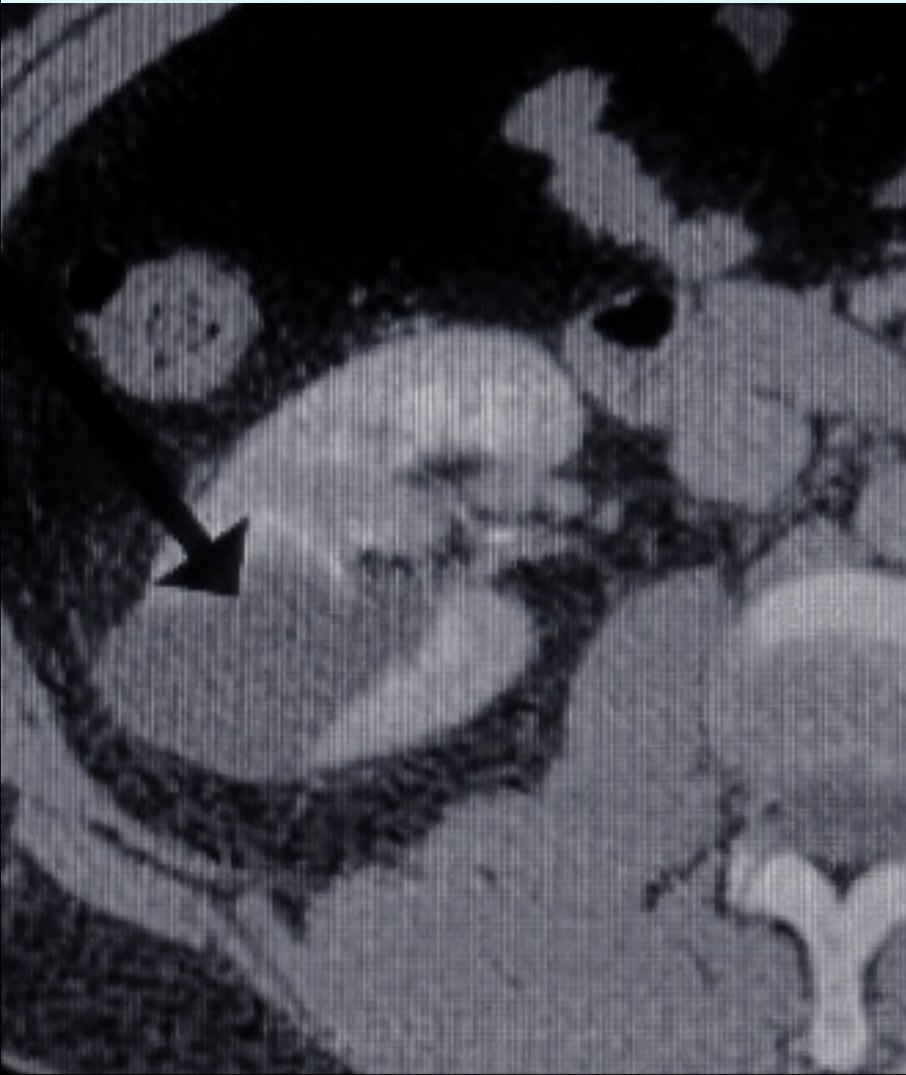


# IODINE “MAP” OUTLINES PANCREATIC TUMOR





# IODINE “MAP” DEFINES CYSTIC RENAL LESIONS





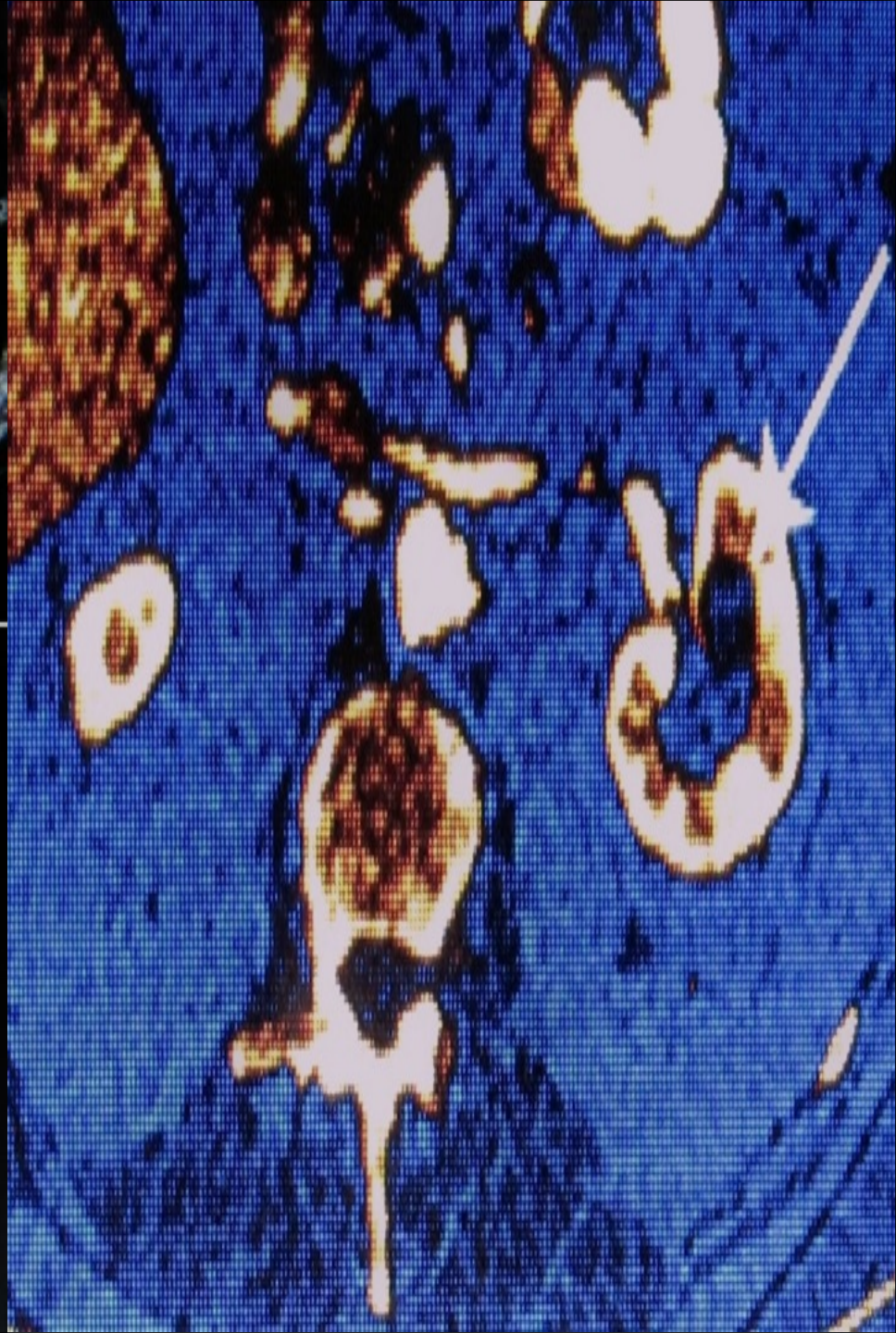


**Figure 2A. Hemorrhagic renal cyst.** (A) Conventional contrast-enhanced CT shows an indeterminate left renal lesion (arrow). (B) DECT virtual unenhanced image shows that the lesion is hyperdense compared with adjacent renal parenchyma. (C) DECT iodine image with color overlay (iodine-containing structures are depicted with an orange-yellow hue) shows no iodine (ie, enhancement) in the lesion. (D) A conventional, true, precontrast image. (E) A magnetic resonance subtraction image. Note that DECT can, in a single acquisition (B-C), provide the same information as that obtained from 2 acquisitions (A, D). However, the iodine image (C) is not a "true" subtraction image because bone (eg, vertebral body, ribs) is present on both the virtual noncontrast (B) and iodine (C) displays.



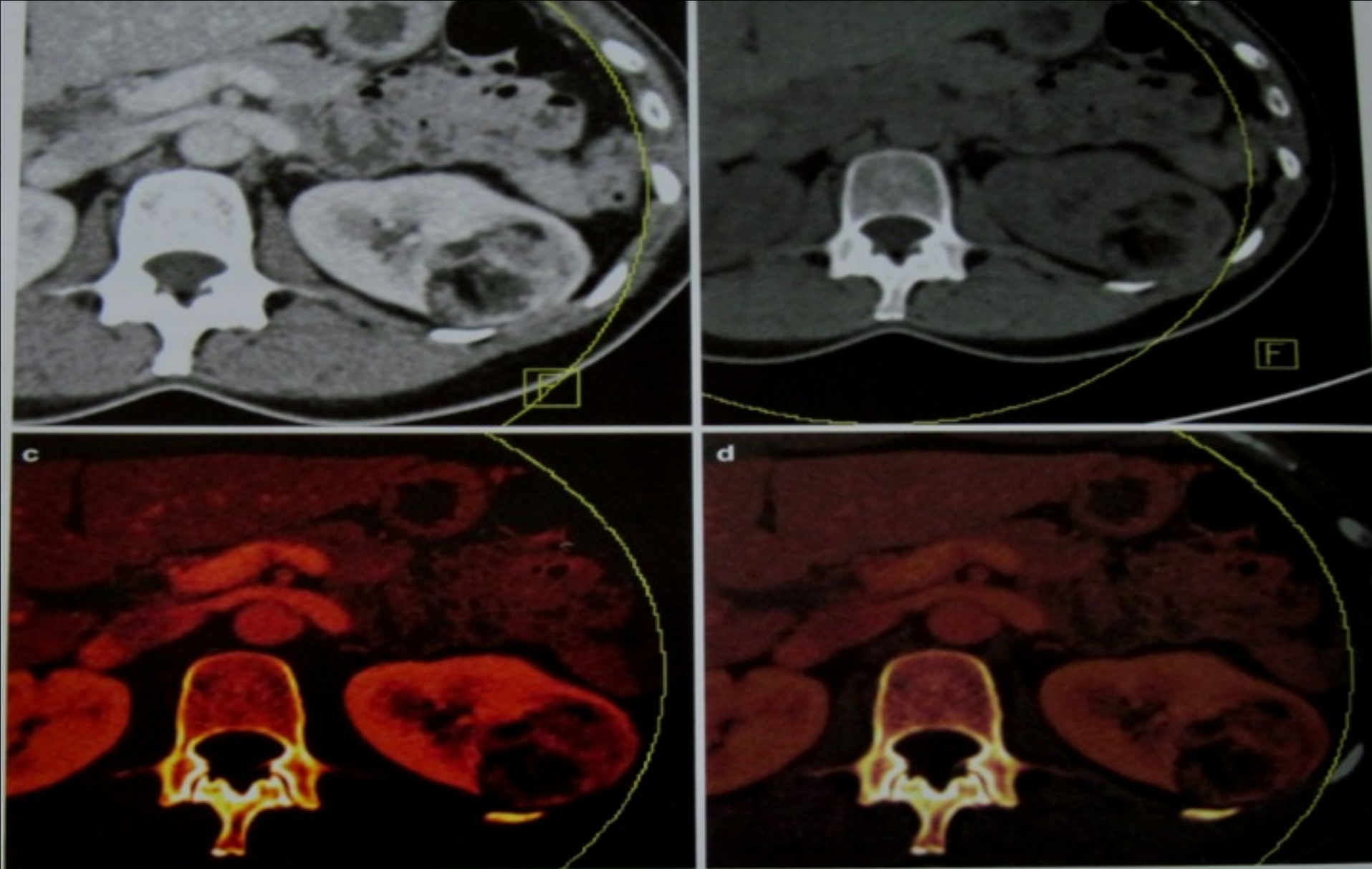


**Fig. 2** Images derived from a nephrographic phase dual-energy CT scan in a patient with a fat-containing, well-defined mass on the posterolateral aspect of the left kidney most consistent with an angiomyelolipoma (AML). The weighted average image (a) contains information on both the high and low kVp tube and approximates a standard 120 kVp single energy image. Image

(b) represents the virtual nonenhanced (VNE) image from which iodine has been subtracted; (c) shows an iodine-only image; and (d) shows a superimposition of (c) onto (b), allowing for simultaneous visualization of enhancement and high-resolution anatomical information.

# THE INCIDENTALOMA

Contrast-enhanced DECT

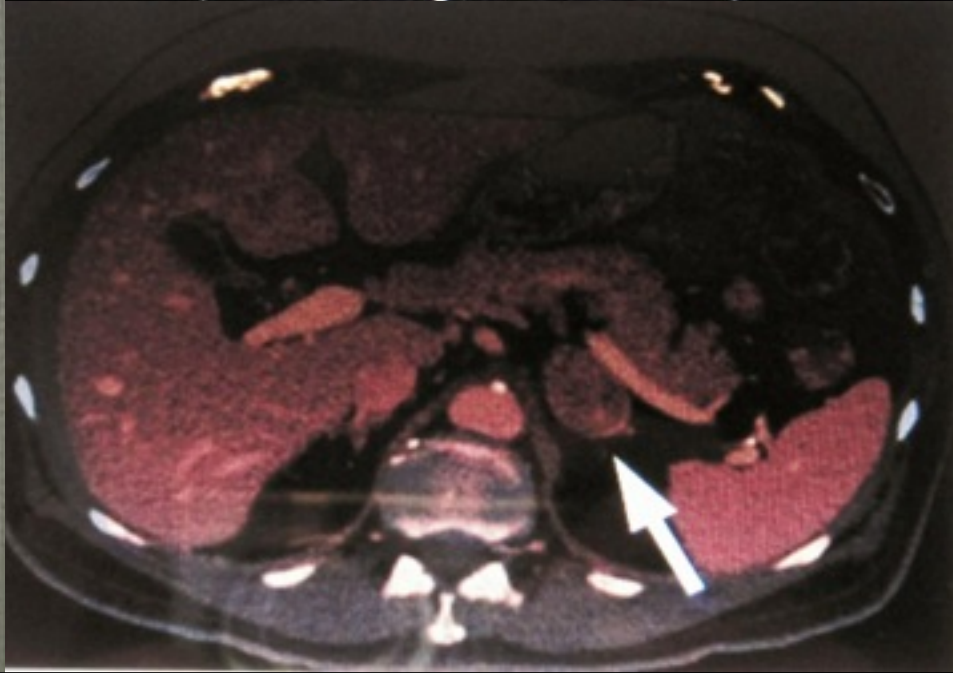
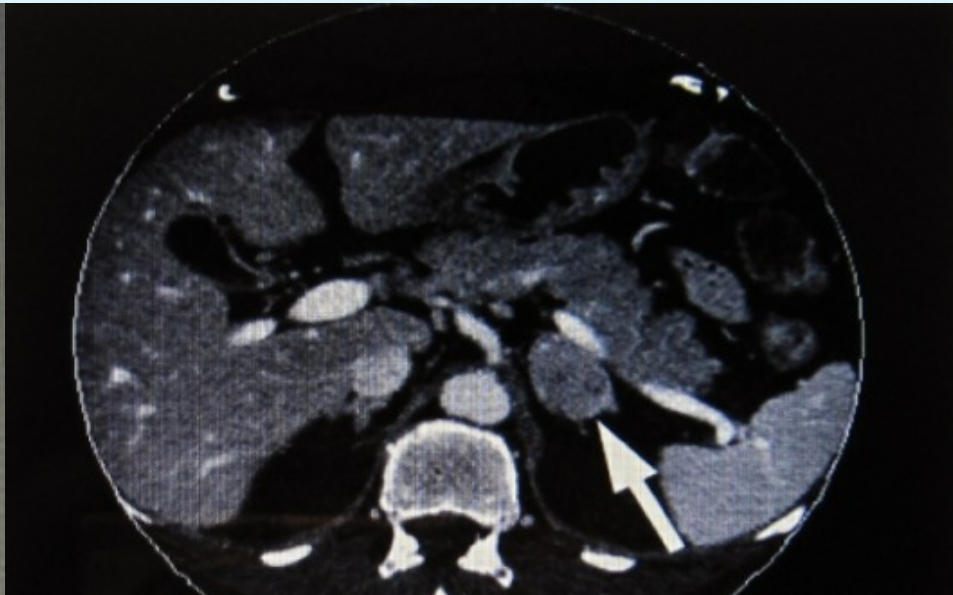
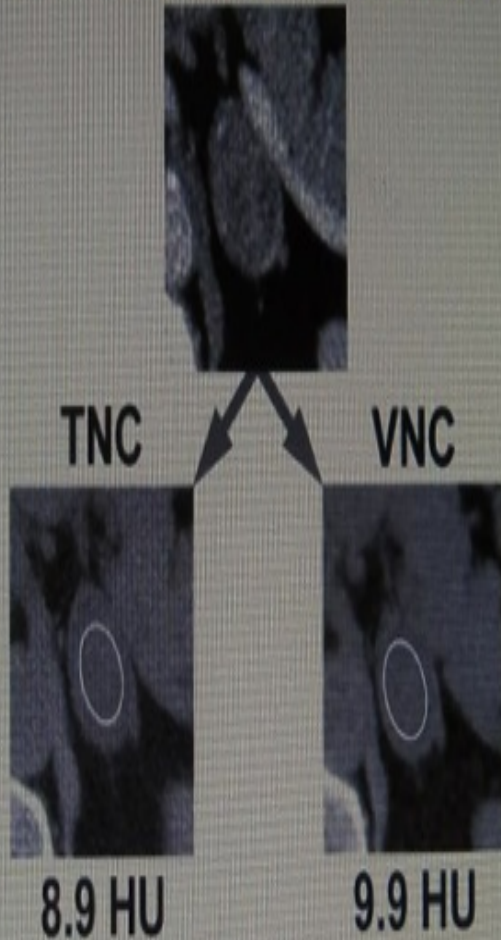
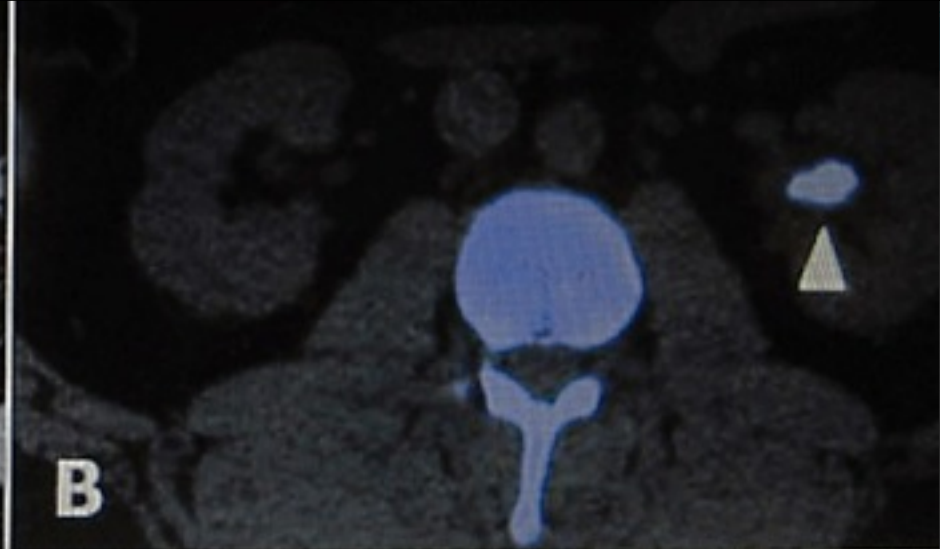
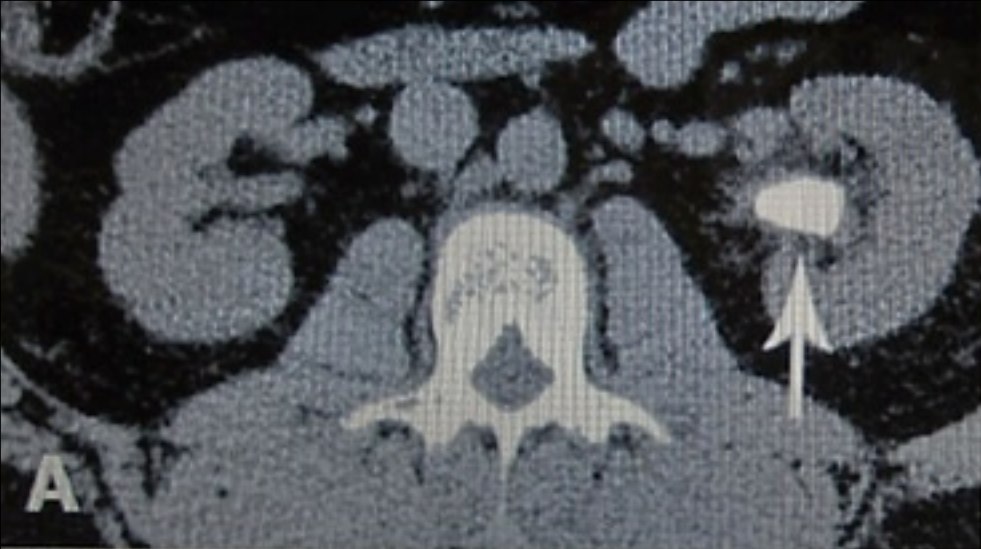


Fig. 4B—65-year-old man with hematuria

B, Nephrographic phase dual-energy CT (DECT) image (A) of abdomen reveals incidental nodule in left adrenal gland. True unenhanced





**Figure 2. (A)** Axial unenhanced abdominal CT scan in a 36 yr-old-man shows a large calculus in the left renal pelvis (arrow). **(B)** Corresponding color-coded dual energy image after post-processing shows the calculus coded as blue (arrowhead) indicating a non-uric acid stone.

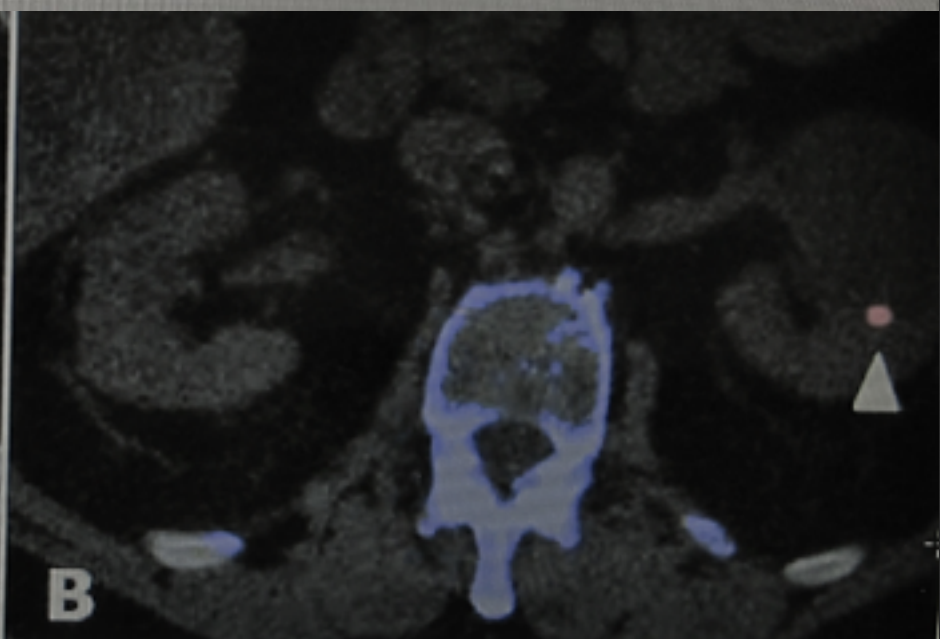
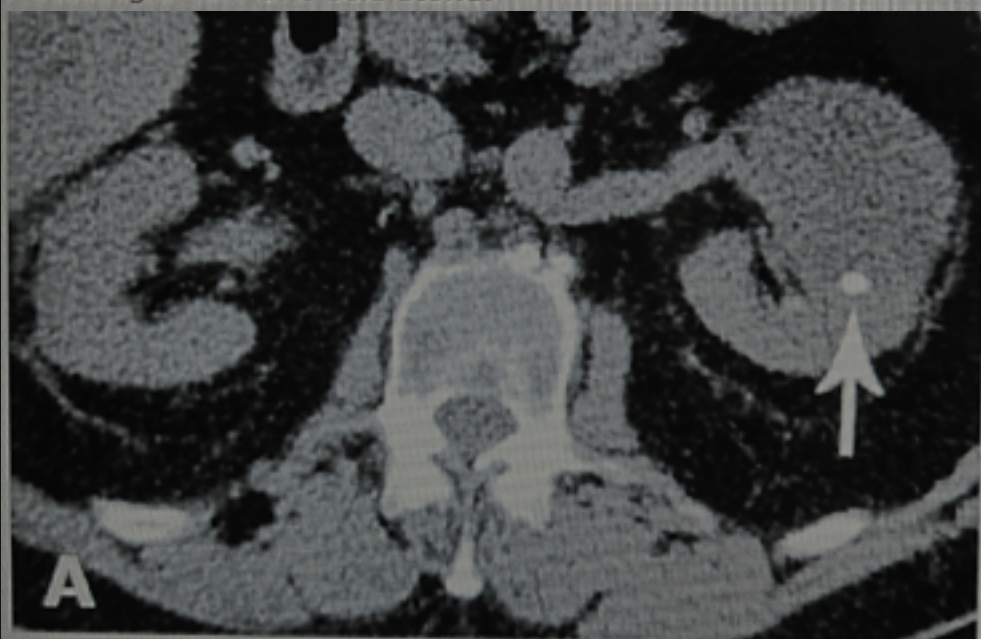
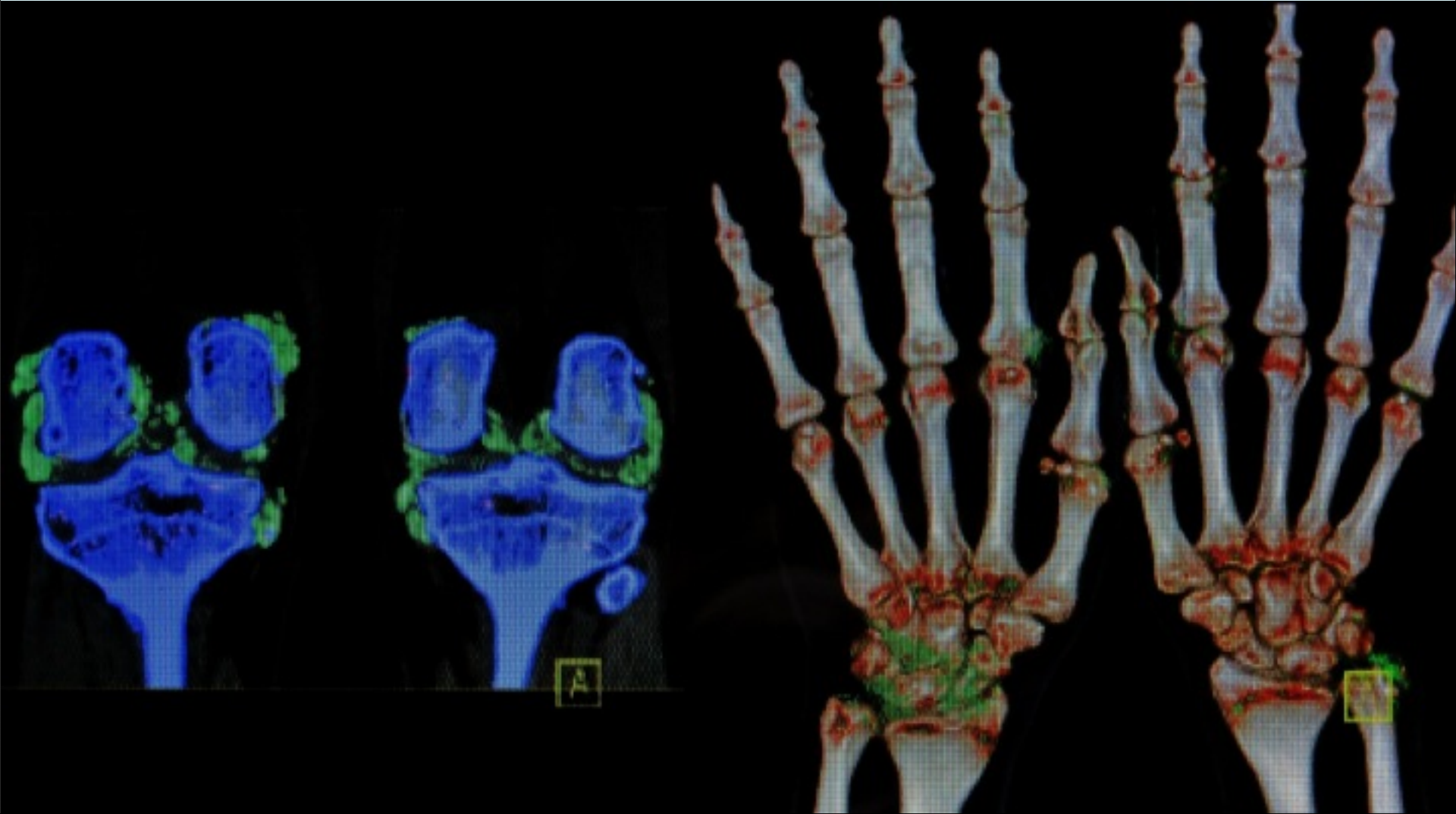


**Figure 1. (A)** Axial unenhanced abdominal CT scan in a 43 yr-old-man shows a calculus in the left mid pole (arrow). **(B)** Corresponding color-coded dual energy post processed image shows the calculus coded as red (arrowhead) indicating a uric acid stone.

# MUSCULOSKELETAL DUAL “E”CT

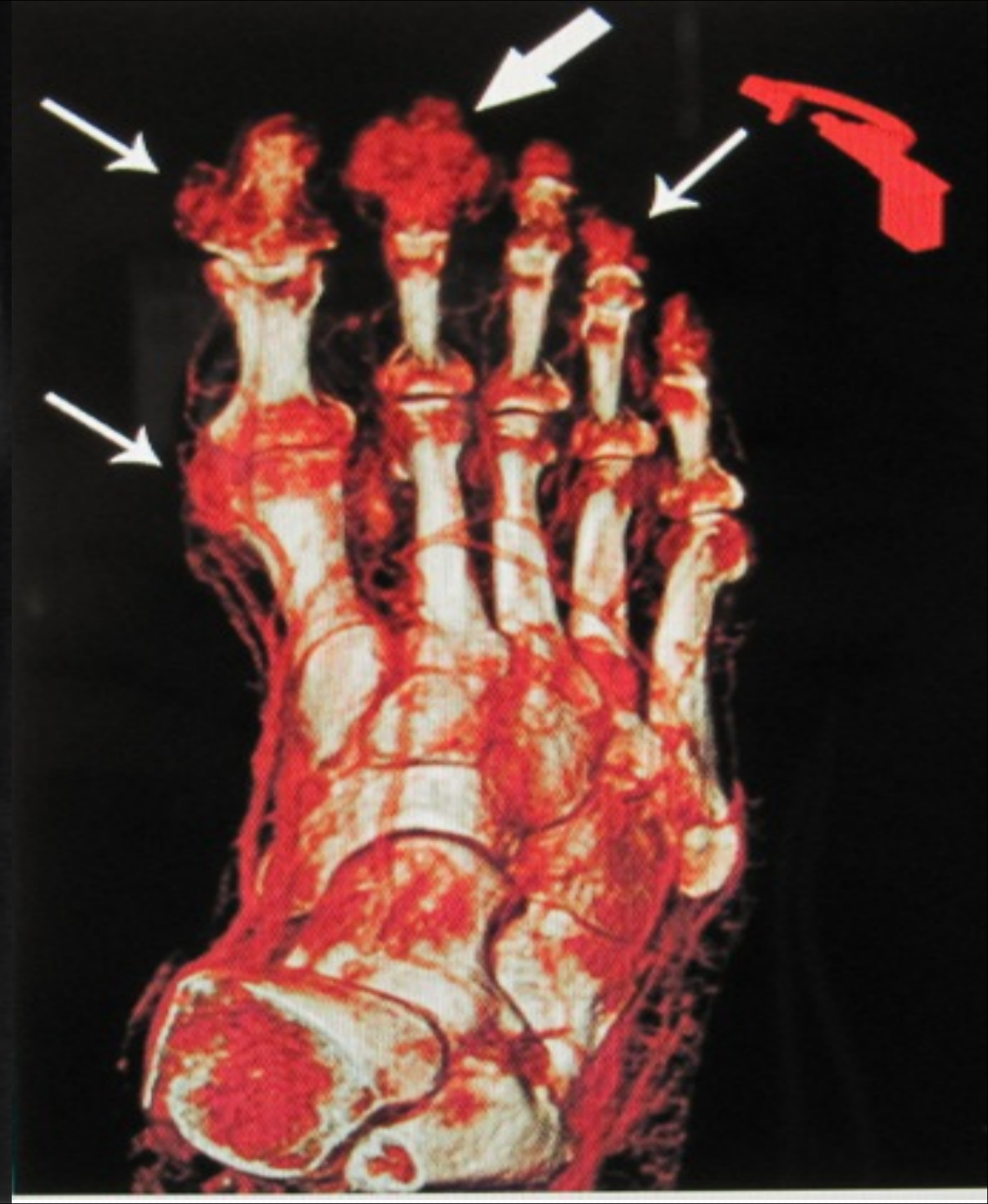




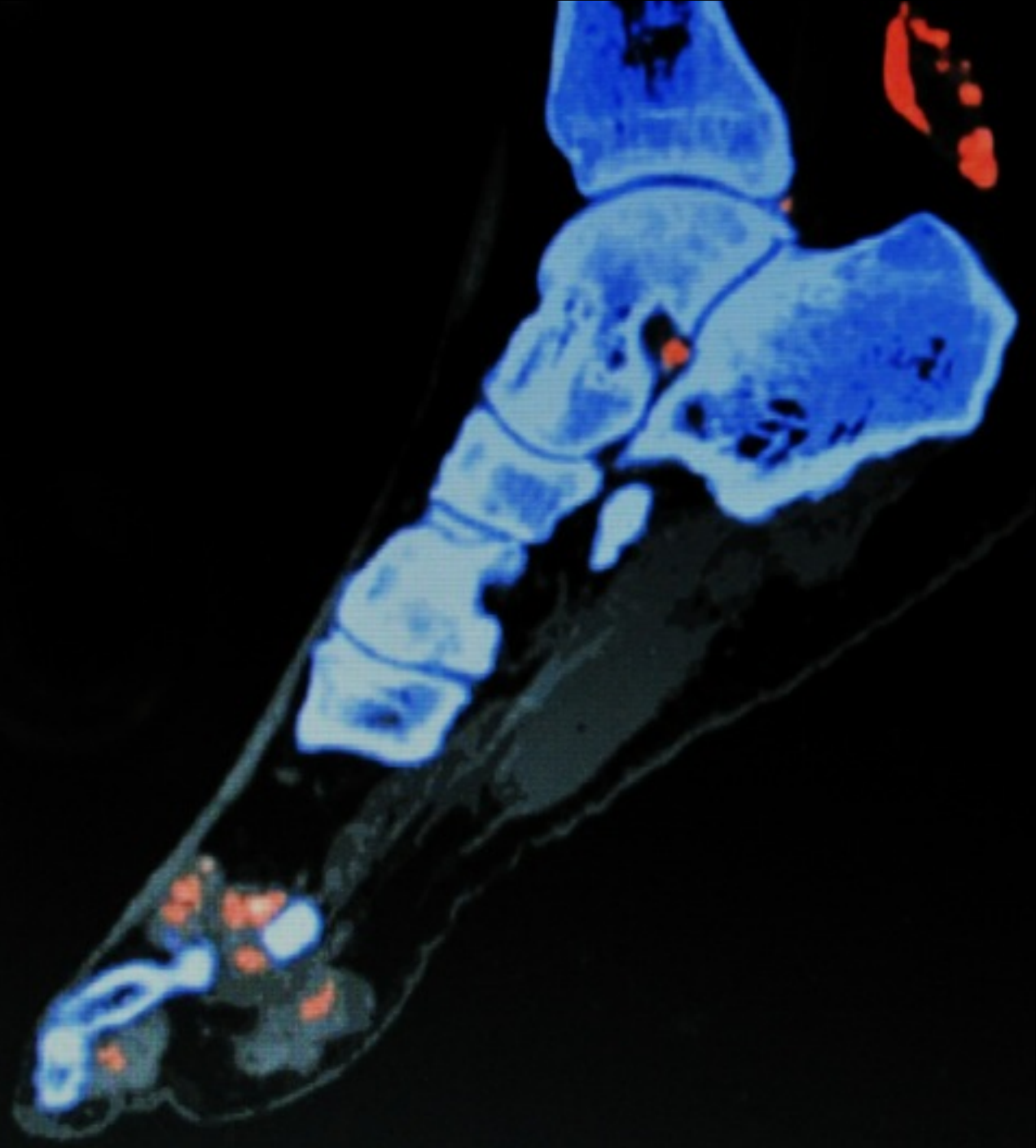


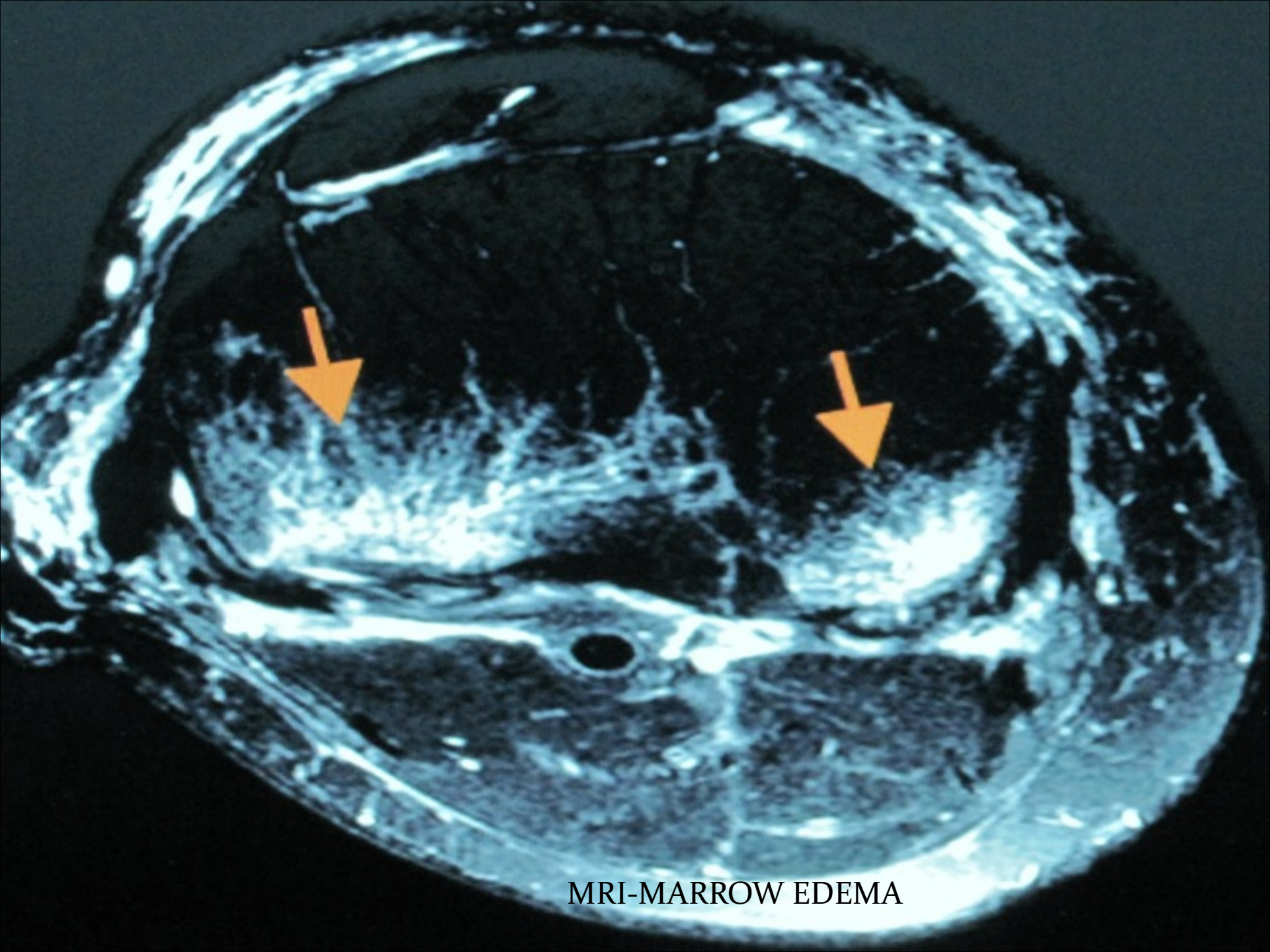
- 70 yo M
- ?Osteomyelitis vs. Gouty arthropathy in the DIP of the index finger?







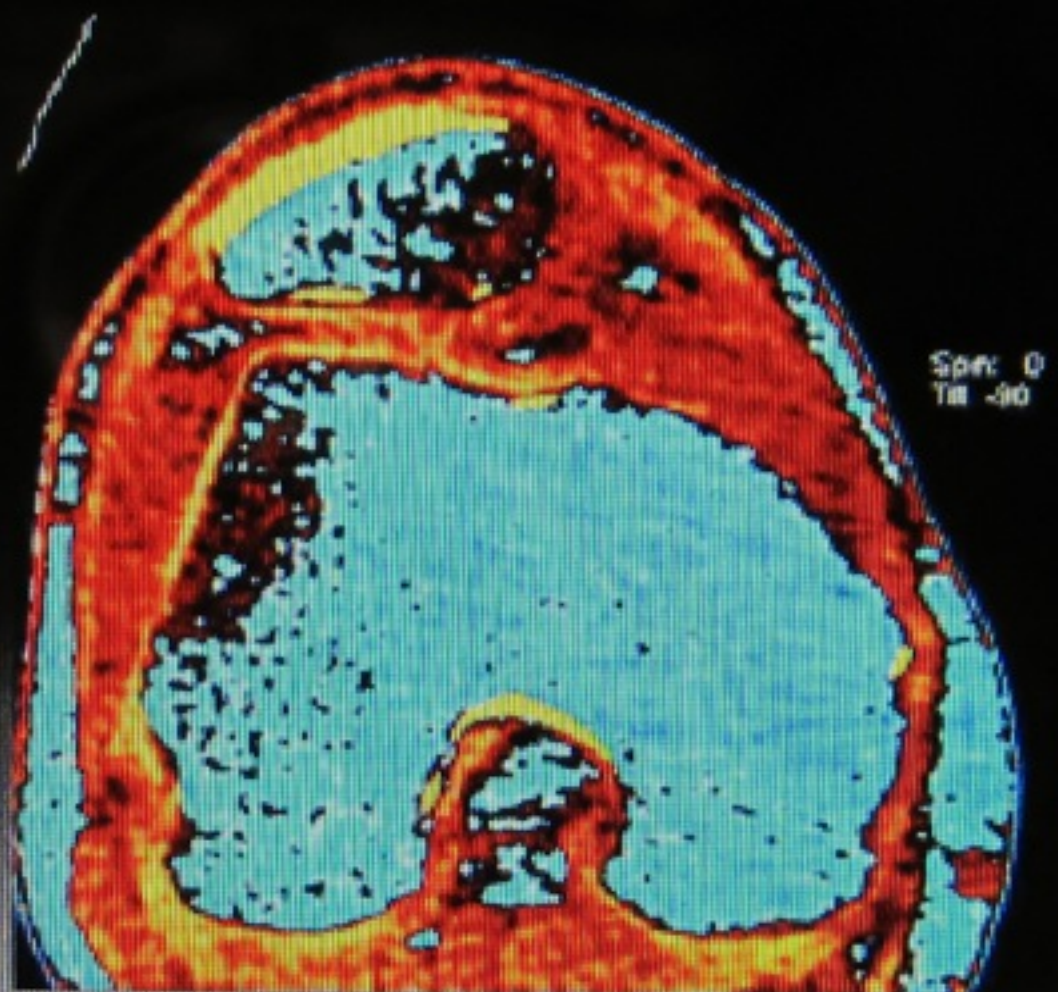


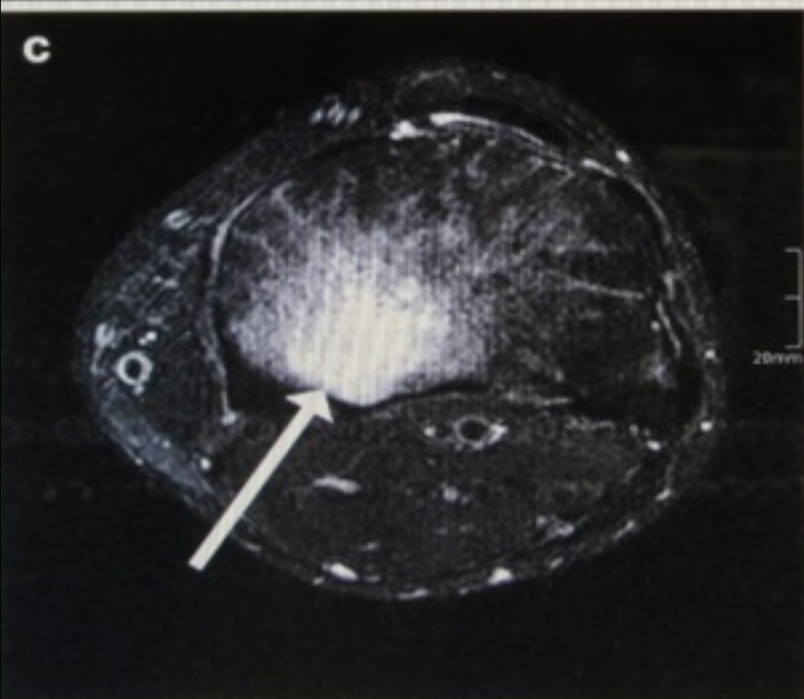
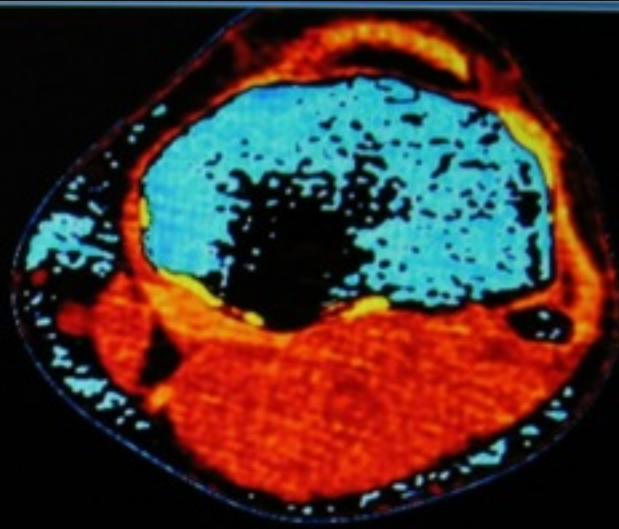
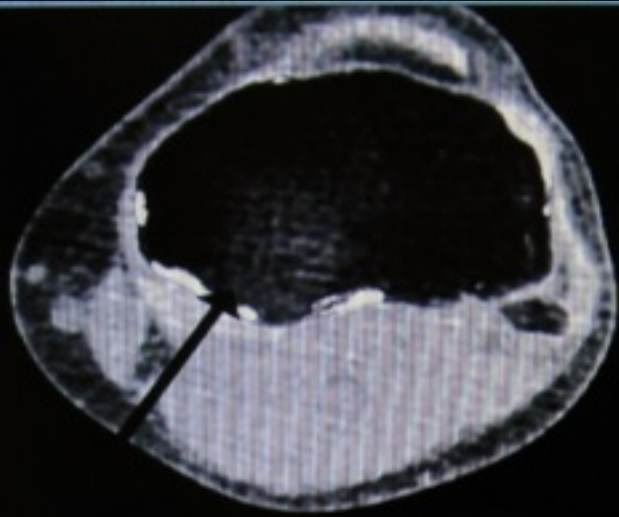


MRI-MARROW EDEMA



# CHARACTERIZING ACUTE BONE MARROW EDEMA WITH DECT

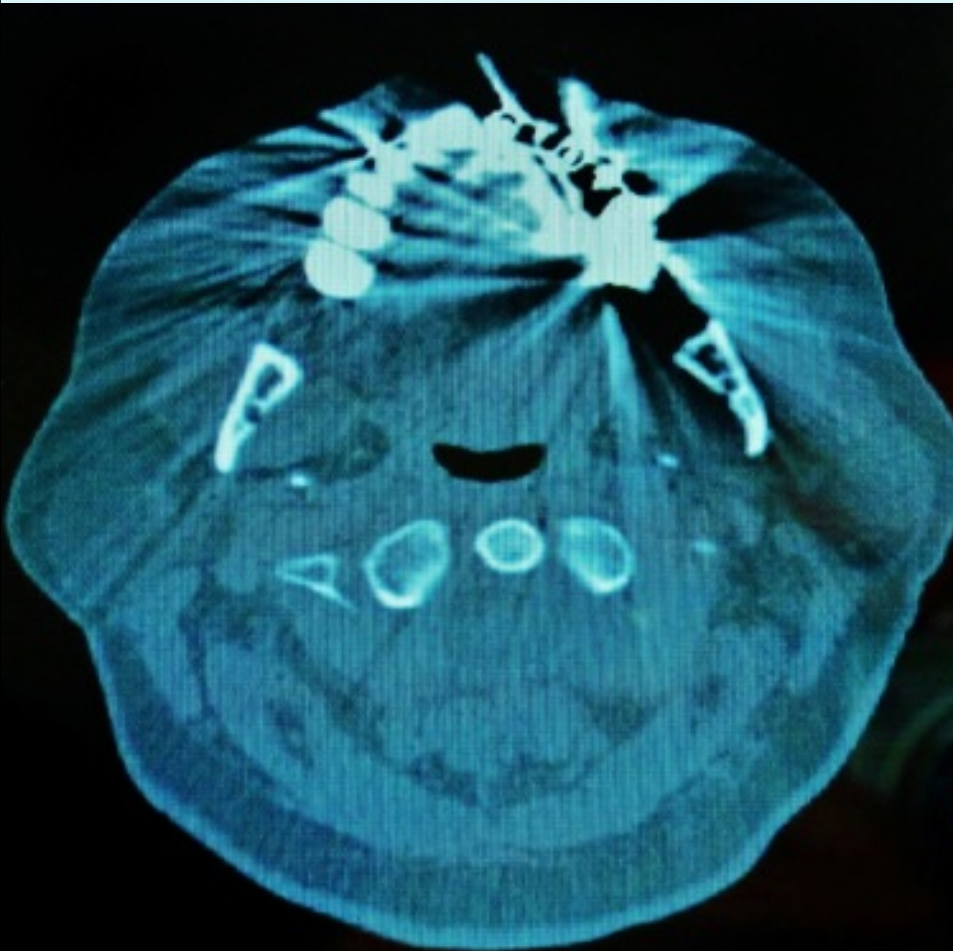




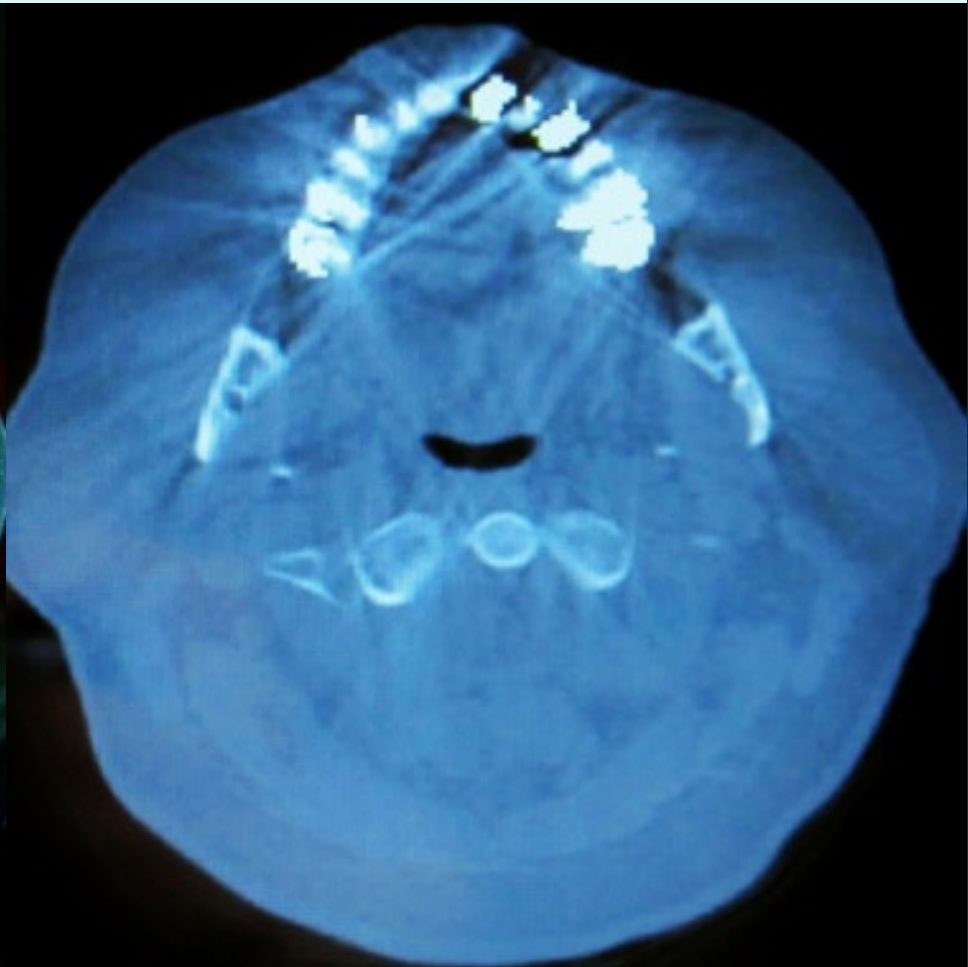
Dual-energy CT virtual non-calcium grey-scale (A) and colour-coded images (B) clearly demonstrate post-traumatic bone bruise as proven by T2-weighted magnetic resonance imaging (C). Note the intact osseous structures (D)



# BEAM HARDENING ARTIFACT



140 kVp



70 keV w/MAR

80kVp

Ex: Apr 04 2008

Acid Volume 2  
Ex: 9910  
Se: 202  
I: 308.8  
In: 381  
DFOV: 42.0cm  
BONE: 76.0%

A: 88

140kVp

VF: Model: 0810, All Series  
AW184721 3481880 8207534429  
Dc: 8  
Ex: Apr 04 2008

Acid Volume 4  
Ex: 9910  
Se: 1001  
I: 308.8  
In: 381  
Non GE Image  
DFOV: 42.0cm  
BONE

A: 100

80keV

P: 282

Q: 67  
Ex: 140  
mA: 114  
JCI  
Q: 6mm ACISep  
In: 0.0  
01:51:54 PM  
W: 450 L: 40

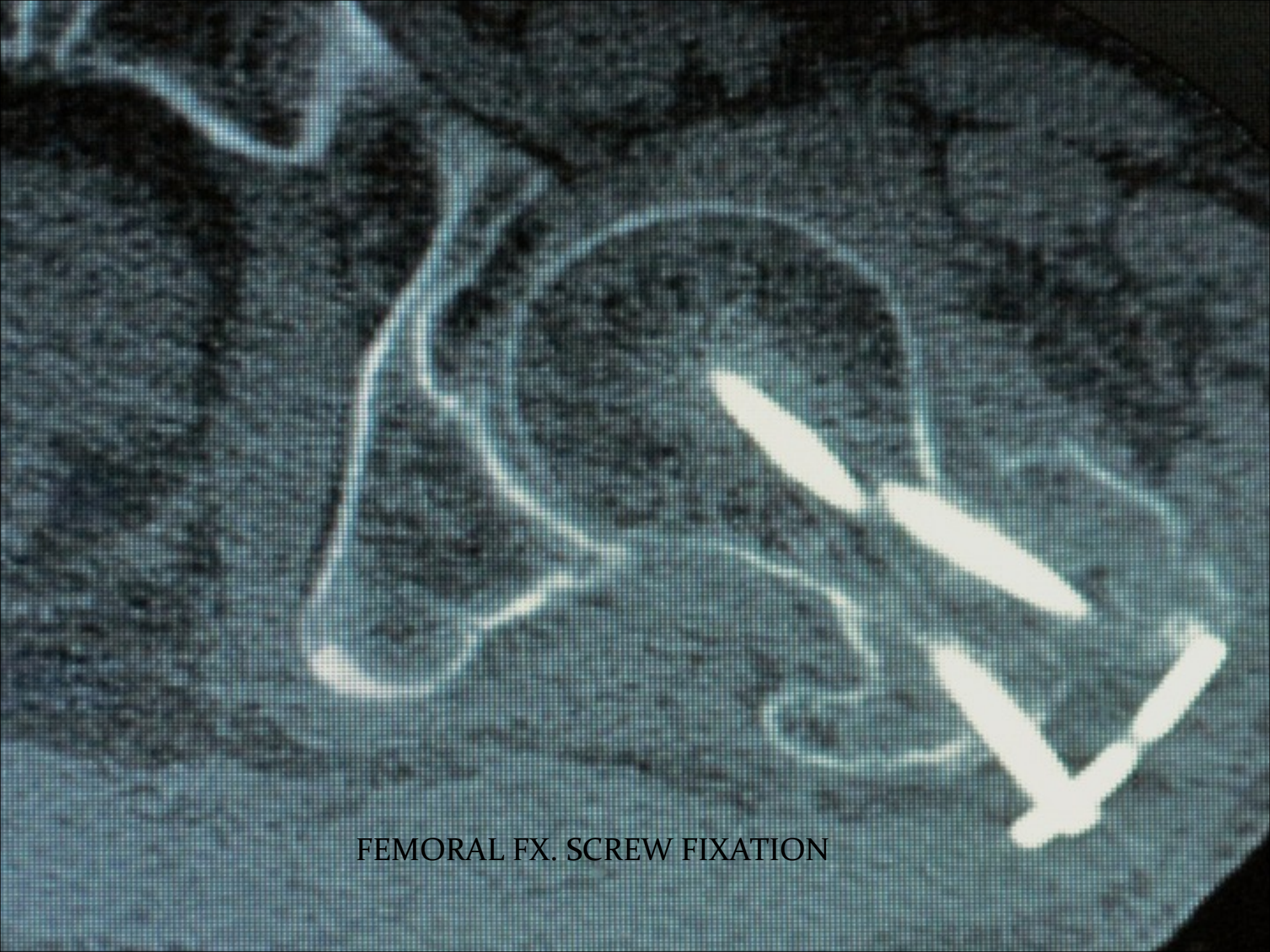
P: 232

R  
2  
0  
3

HIP ARTHROPLASTY







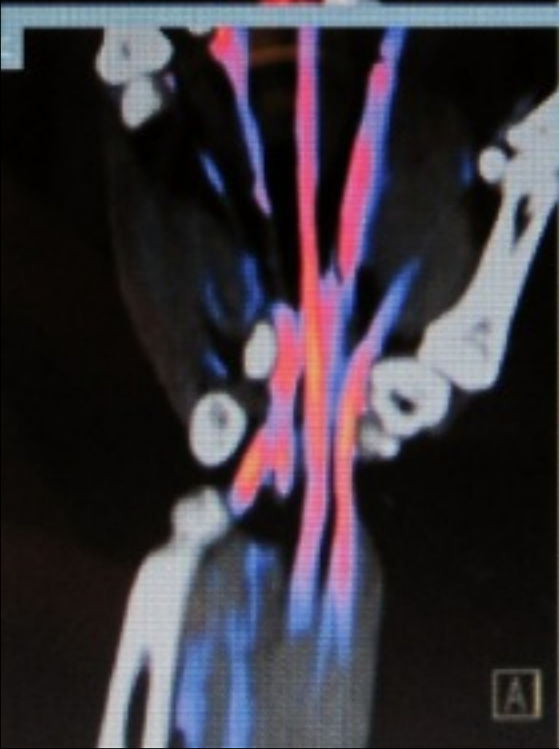
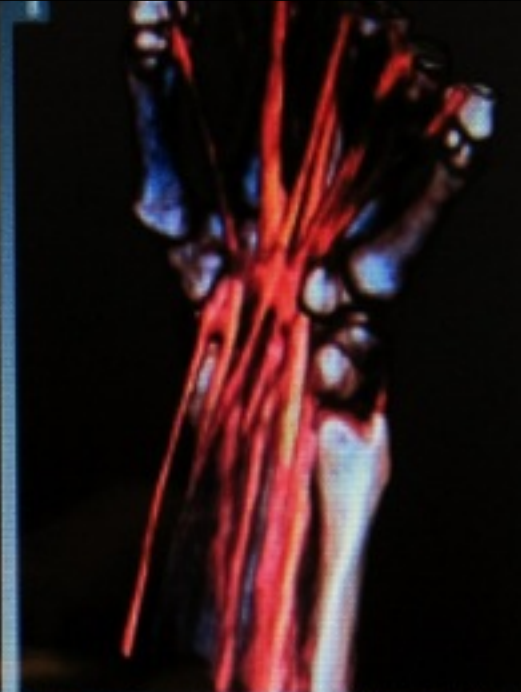
FEMORAL FX. SCREW FIXATION

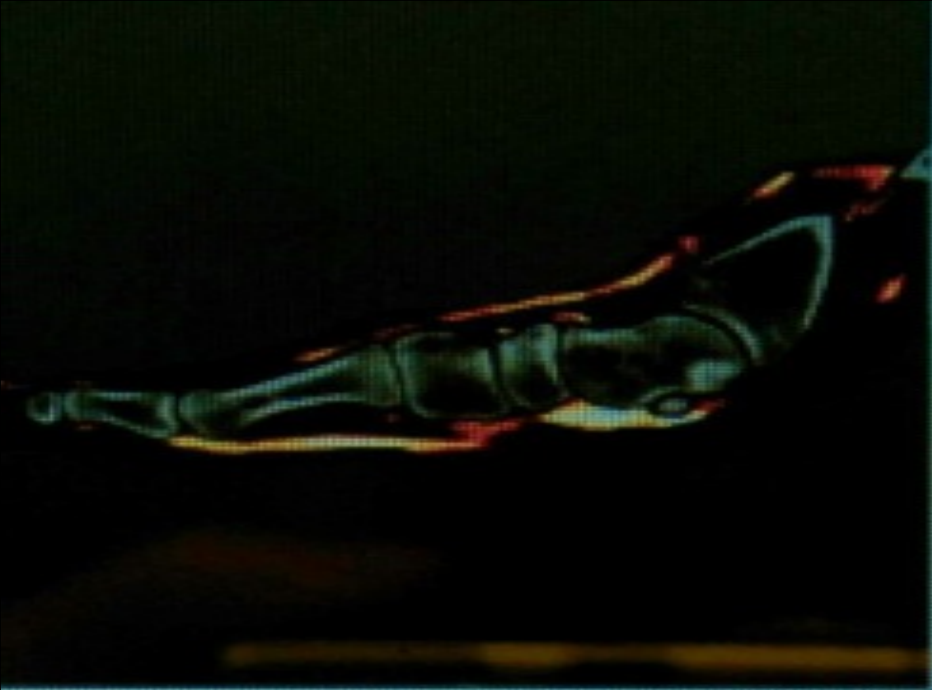


# DECT: Tendons and Ligaments

- Specific dual energy index value allows collagen to be decomposed from surrounding tissue
- Three material collagen decomposition algorithm (collagen, fat, soft tissue)
- Johnson et al: 3 material decomposition to differentiate tendons in unenhanced scan
- Persson et al: depicted tendons and ligaments using DECT for better visualization of wounds in ankle/wrist in post mortem analysis









# Dual energy CT accurately identifies ACL tears in emergency department

Dual energy CT is an effective way to evaluate emergency department patients with possible anterior cruciate ligament (ACL) tears, a new study shows. ACL tears are one of the most frequent ligamentous injuries of the knee; they are not commonly diagnosed in the emergency department because they are not seen on plain x-rays.

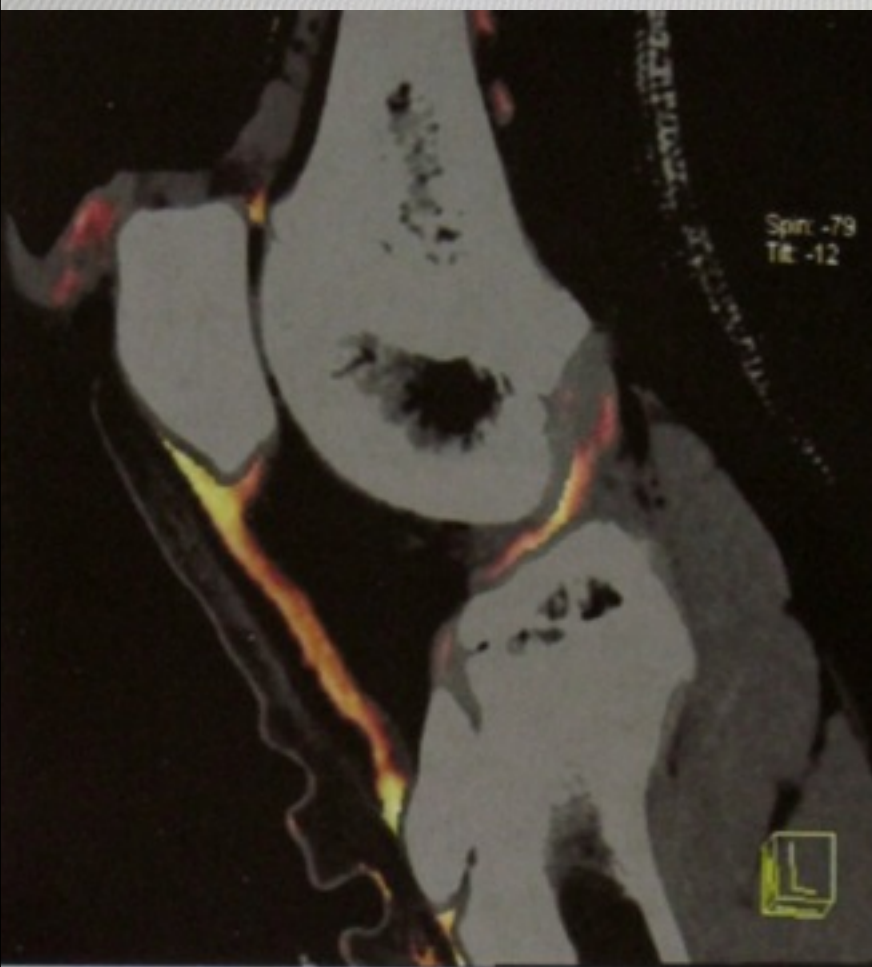


**Fig. 2** Good depiction of the anterior cruciate ligament and patella ligament in an animal model (swine), sagittal view



**Fig. 3** Good depiction of the patella ligament and the posterior cruciate ligament in the swine model. Regard the incomplete depiction of the anterior cruciate ligament at the dorsal apical part representing a proven complete rupture of this ligament (Sagittal view)

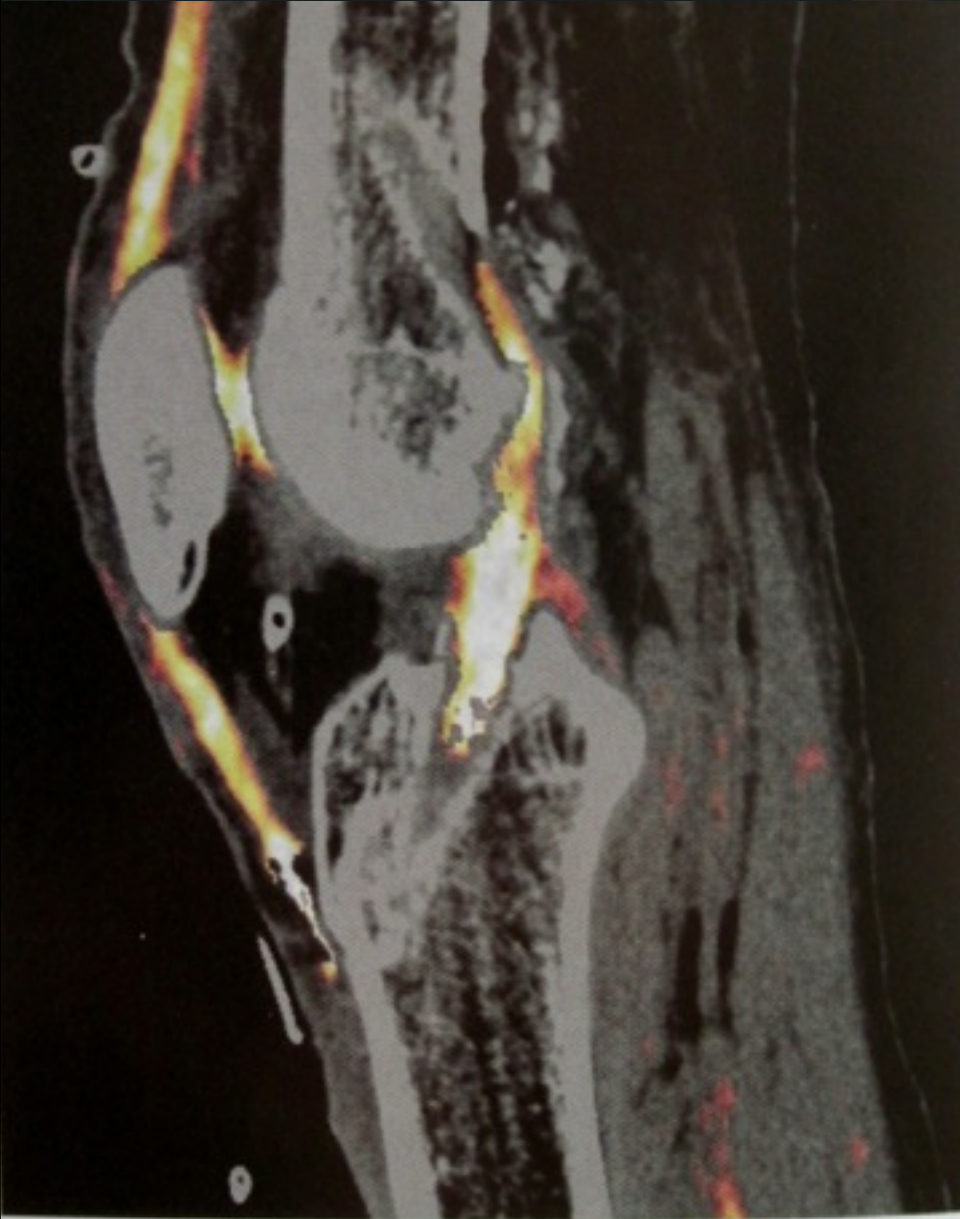


**Fig. 6** ACL autograft reconstruction with a good delineation in dual-energy CT, sagittal view. The circular structures within the knee and on the skin surface are drainages

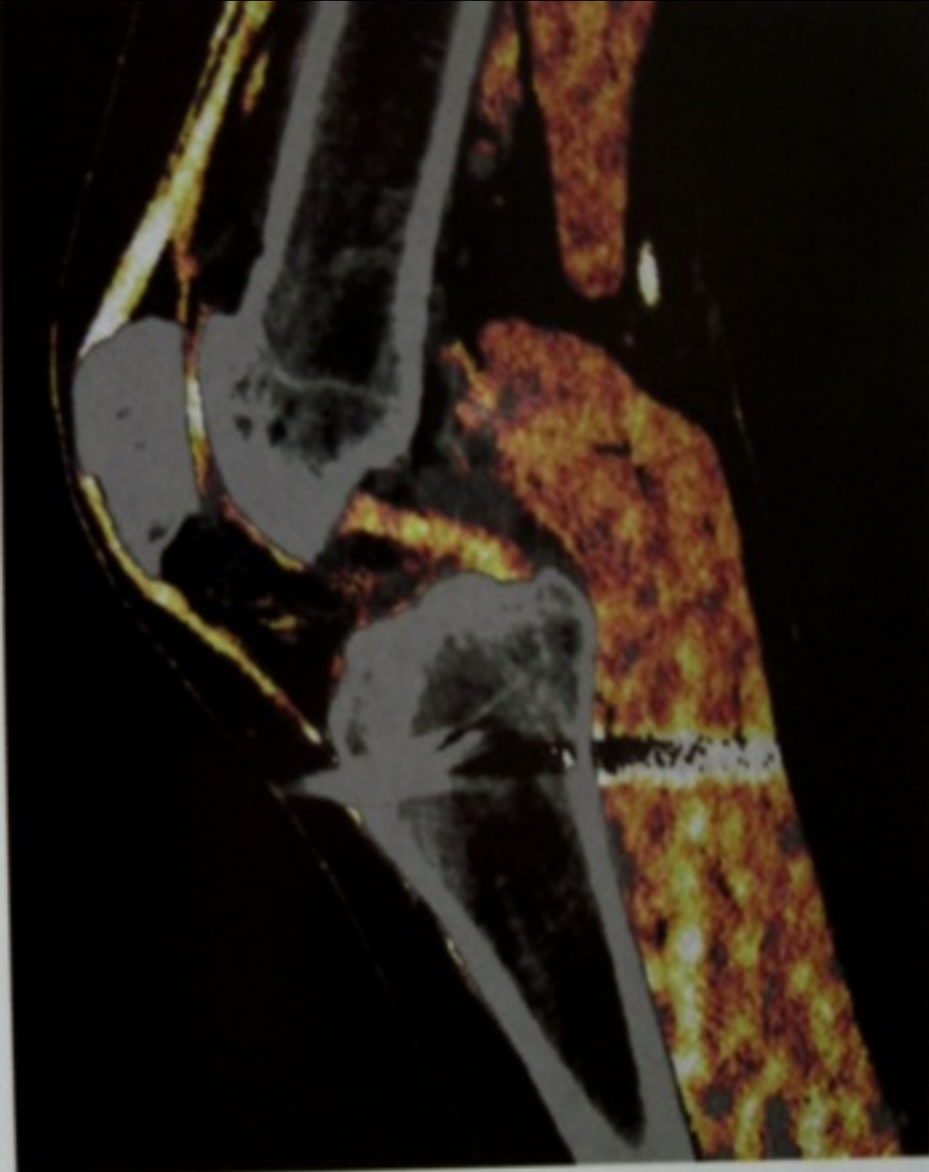


**Fig. 4** Sagittal view with a good depiction of the dorsal cruciate ligament in a patient. The basal artifact in the tibia is caused by metal fixation after reconstruction of the anterior cruciate ligament with an autograft



## VASCULAR DUAL ENERGY CT

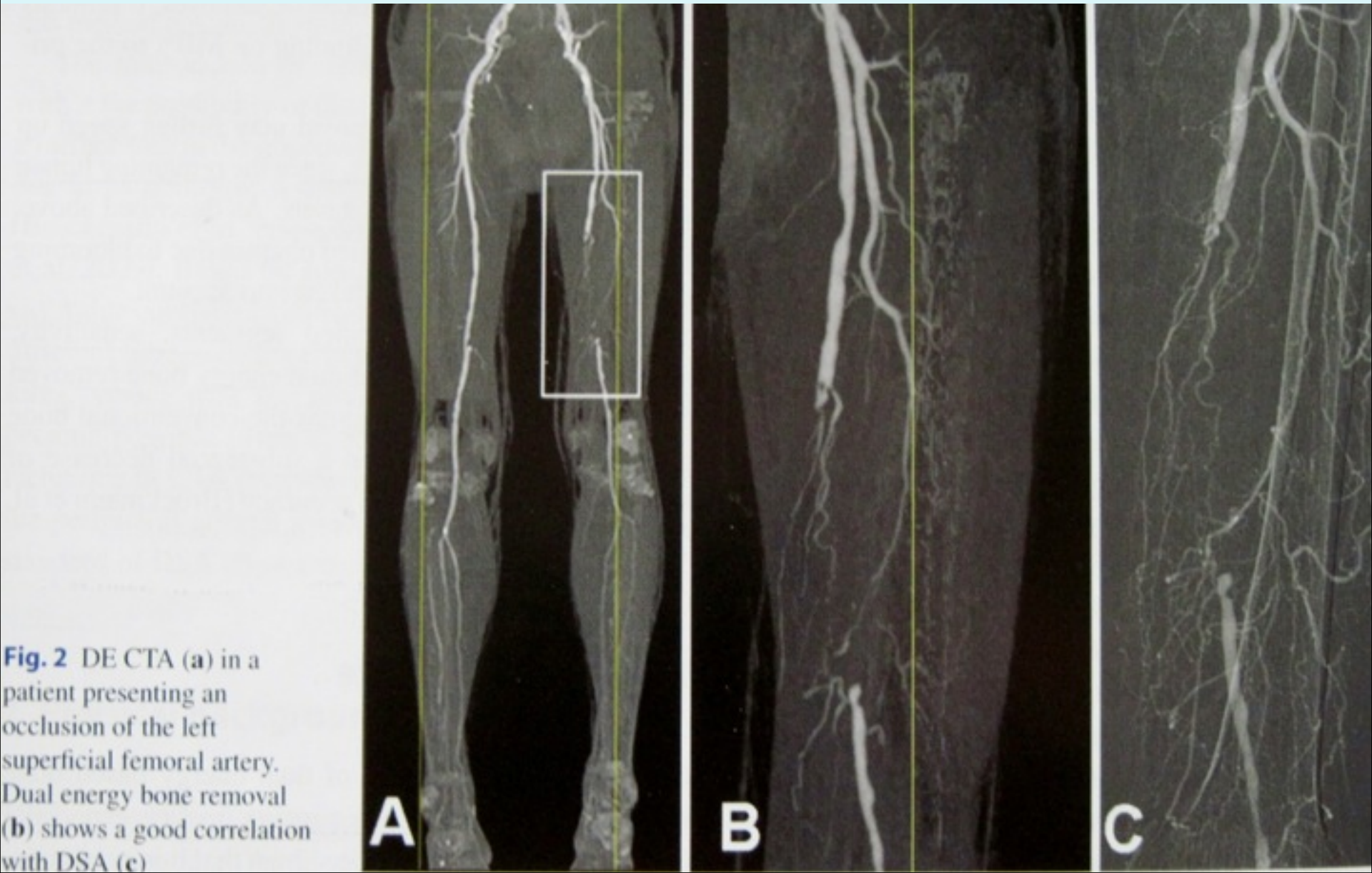


**Fig. 2** DE CTA (a) in a patient presenting an occlusion of the left superficial femoral artery. Dual energy bone removal (b) shows a good correlation with DSA (c)

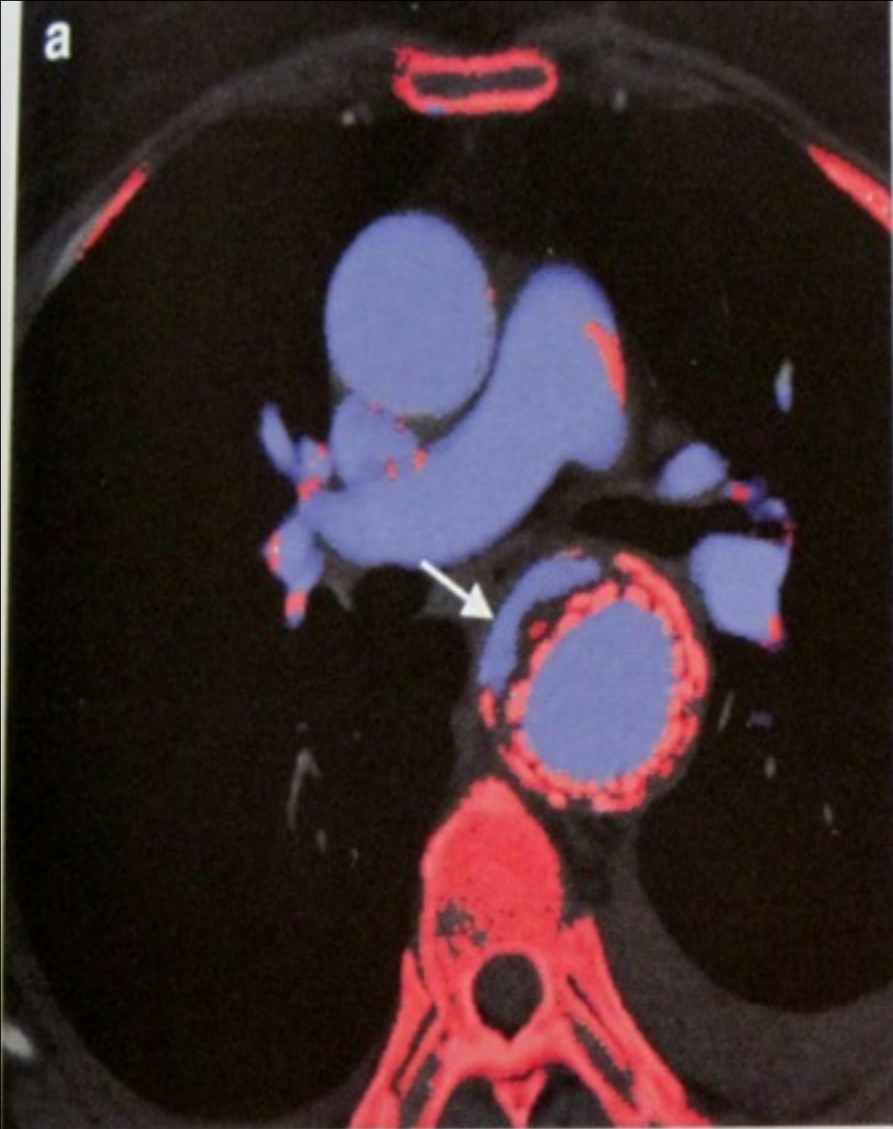


**Fig. 3** Application of the “hard plaque” algorithm to a dual-energy dataset. Iodine is colored in *blue*, while calcium and also the stentgraft are colored in *red*. In axial (**a**) and coronal slices (**b**) of this 53-year-old male patient, iodine is detected in

the excluded aneurysm sac outside the stentgraft. This corresponds to a type I endoleak, supplied from the distal end of the stentgraft



# TUCSON WINTER SKY









Thus endeth the lesson.

Thank you very much  
for your attention.

Storks and Egrets at Sunset